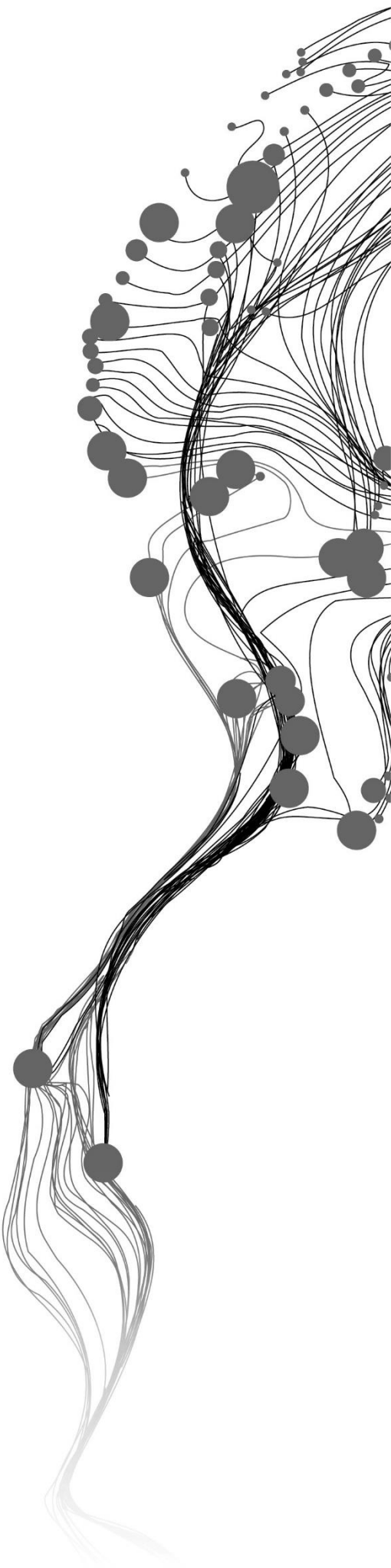# ASSESSING THE EFFECT OF UAV OBLIQUE IMAGING ON TREE PARAMETER ACCURACY – A STUDY IN HAAGSE BOS, THE NETHERLANDS.

SRILAKSHMI GNANASEKARAN
JUNE, 2021

SUPERVISORS:
ir. L.M van Leeuwen – de Leeuw
drs. ing. M. Huesca Martinez

# ASSESSING THE EFFECT OF UAV OBLIQUE IMAGING ON TREE PARAMETER ACCURACY – A STUDY IN HAAGSE BOS, THE NETHERLANDS.

SRILAKSHMI GNANASEKARAN
Enschede, The Netherlands, June, 2021

SUPERVISORS:
ir. L.M van Leeuwen – de Leeuw
drs. ing. M. Huesca Martinez

THESIS ASSESSMENT BOARD:
dr. R Darvish (Chair)
dr. Tuomo Kauranne (External Examiner, Lappeenranta University of Technology, Finland)

# ABSTRACT

As forest can sequester carbon, it plays a crucial role in regulating carbon dioxide in the atmosphere, thus mitigating the effects of climate change. The sequestered carbon is found in different pools in forests, and aboveground biomass (AGB) is one of the main pools. In order to monitor and report the forest carbon stock, it is essential to estimate the AGB. AGB can be estimated using allometric equations that use the structural information of trees like the diameter at breast height (DBH) and tree heights as input parameters. This tree structural information can be extracted from remote sensing data. The latest development in remote sensing is the advent of Unmanned Aerial Vehicle (UAV). UAVs are flexible, time and cost-efficient means of data collection. Using photogrammetric techniques like Structure from Motion (SfM), it is possible to generate a 3D point cloud from over-lapping 2D images acquired by UAV, thereby enabling tree parameter retrieval. However, the digital camera onboard the UAV lacks penetration capability, which subsequently affects the accuracy of the retrieved tree parameter. Several studies have incorporated oblique images in the SfM model and reported improvement in the density and accuracy of the generated 3D point cloud. However, how incorporating oblique images to build a dense 3D point cloud and surface models for the forests is affected by different canopy structures has not been well documented in the literature.

This study was done in the Haagse Bos in The Netherlands. It was aimed to assess and compare the accuracy of DTM, tree height, and DBH retrieved from UAV nadir and UAV oblique datasets under dense and medium dense canopy. This study also assesses the effect of tree height estimation error on the AGB estimates. UAV images used in this study were acquired at nadir and 75 degrees east-facing oblique view angle using DJI Phantom 4. The UAV nadir dataset comprises the DTM, DSM, and orthophoto generated from the nadir images acquired in the double grid. The UAV oblique dataset comprises the DTM, DSM, and orthophoto generated from the combination of nadir images acquired in the double grid and oblique images acquired in a single grid. The accuracies of UAV DTMs and tree heights extracted from UAV CHMs were assessed by comparing to LiDAR DTM and tree heights extracted from LiDAR CHM. The DBH modeled using UAV-derived tree parameters were compared with field-measured DBH.

The study's statistical analysis revealed no significant difference between the means of elevation from UAV nadir and UAV oblique DTM in both dense and medium dense canopy. Similarly, there was no significant difference between the means of tree height extracted from UAV nadir and UAV oblique CHMs in both the dense and medium dense canopy blocks. In addition to that, the DBH models using tree parameters retrieved from the UAV nadir dataset and UAV oblique dataset did not differ significantly in both the dense and medium dense blocks. The sensitivity analysis of tree height uncertainties on the accuracy AGB estimation revealed that in the dense block, the errors in tree height affected the AGB accuracy. Whereas in the medium dense block, the tree height errors did not significantly affect the AGB estimates.

**Keywords:** UAV oblique, SfM, DTM, Tree height, DBH, AGB, canopy density

# ACKNOWLEDGEMENTS

# TABLE OF CONTENTS

# LIST OF FIGURES

# LIST OF TABLES

# LIST OF ACRONYMS

| | |
|---|---|
| AGB | Above Ground Biomass |
| AHN | Actueel Hoogtebestand Nederland |
| ALS | Airborne Laser Scanning |
| AT | Aerial Triangulation |
| CD | Crown Diameter |
| CHM | Canopy Height Model |
| $CO_2$ | Carbon dioxide |
| CPA | Crown Projection Area |
| DBH | Diameter at Breast Height |
| DSM | Digital Surface Model |
| DTM | Digital Terrain Model |
| EU | European Union |
| GCP | Ground Control Point |
| GHG | Green House Gas |
| IPCC | Intergovernmental Panel on Climate Change |
| GNSS | Global Navigation Satellite System |
| LiDAR | Light Detection and Ranging |
| LULUCF | Land Use, Land-Use Change and Forestry |
| Mg | Megagram |
| RADAR | Radio Detection And Ranging |
| RMSE | Root Mean Square Error |
| SAR | Synthetic Aperture Radar |
| SEEA EEA | System of Environmental-Economic Accounting – Experimental Ecosystem Accounting |
| SfM | Structure from Motion |
| TH | Tree Height |
| UAV | Unmanned Aerial Vehicle |
| UNFCCC | United Nations Framework Convention on Climate Change |

# 1. INTRODUCTION

## 1.1. Background

Forest covers 31% of the land area on earth, and it is distributed globally (FAO & UNEP, 2020). It stabilizes climate change and mitigates its effect by regulating atmospheric carbon dioxide ($CO_2$). Forest sequesters approximately 2.6 billion tonnes of $CO_2$ every year, which is 7% of the global carbon emitted (IUCN, 2017). When managed sustainably, it has the potential to sequester 10% of the global carbon emitted (FAO, 2012). The sequestered carbon is found in the forest in different pools, such as vegetation biomass, deadwood, litter, and soil organic matter (IPCC, 2014b).

The forest ecosystems are under enormous pressure due to human activities and natural factors, such as land-use change, overgrazing, deforestation, and fire. Deforestation and degradation of forests threaten their potential to sequester carbon and affect the carbon sinks (IPCC, 2007). When a forest is cleared or degraded, it becomes a source of emission as it emits its stored carbon. Forest degradation and deforestation accounted for 12% of $CO_2$ emissions globally between 2000 and 2009 (IPCC, 2014a). Given the role of global forests in climate change mitigation, maintaining them and increasing the carbon sinks is of utmost importance.

The United Nations Framework Convention on Climate Change (UNFCCC) is a United Nations entity with 197 member countries aimed to stabilize Greenhouse Gas (GHG) concentration in the atmosphere and prevent dangerous human interference with the climate system (UNFCCC, 2021). The UNFCCC devised a GHG inventory that records the GHG emission and removal from land use, land-use change, and forestry (LULUCF). In 2018, the European Union (EU) adopted the LULUCF as part of its regulation to reduce GHG emissions (Eric & Mart-Jan, 2019). The Netherlands implemented the 'System of Environmental-Economic Accounts – Experimental Ecosystem Accounting' (SEEA EEA) to comply with the EU regulations. This carbon reporting system measures and accounts for all the relevant carbon stocks and flows in various reservoirs (Lof et al., 2017). Aboveground biomass (AGB) is one of the major forest carbon pools and an indicator of the amount of carbon sequestered by the forest (Bombelli et al., 2009). As 50% of the forest AGB is sequestered carbon (Brown, 1997), it is required to estimate the forest biomass in order to measure its carbon stock.

AGB can be estimated through direct destructive method or indirect non-destructive method (Wakawa, 2016). Estimating biomass through destructive methods is accurate, but it is expensive, time-consuming, and practically not possible at a national scale to cut, dry, and weigh all the trees (Vashum & Jayakumar, 2012). A non-destructive method of estimating biomass uses allometric equations. These equations use field-measured tree biometrics like the Diameter at Breast Height (DBH), tree height, and tree wood density as input parameters in the mathematical equations to estimate AGB (Kebede & Soromessa, 2018; Shi & Liu, 2017). The process of collecting tree biometric data at the national level poses its challenges like 1) inaccessible areas, 2) time-consuming process, 3) difficulty in assembling a large workforce for operations, and 4) risk of measurement bias. Hence, Intergovernmental Panel on Climate Change (IPCC) and UNFCCC recommend using a combination of field measurements and remote sensing methods to monitor and estimate biomass (IPCC, 2006).

Remote sensing is an indirect non-destructive method of AGB estimation. Tree height and DBH, the two important input parameters in the allometric equation to estimate AGB, can be extracted or modeled using

remote sensing data (Roy & Ravan, 1996; Vashum & Jayakumar, 2012). The tree DBH, however, can only be indirectly extracted from remote sensing data. Several studies have explored the relationship between remotely sensed forest parameters like crown projection area (CPA), crown diameter (CD), and tree height, and tree DBH (González-Jaramillo et al., 2018; Jucker et al., 2017; Popescu, 2007; Priedītis, Šmits, Arhipova, Daǎis, & Dubrovskis, 2012; Shimano, 1997; Verma, Lamb, Reid, & Wilson, 2014). The studies proved that there is a strong relationship between remotely sensed forest parameters and DBH, and statistical regression models can be used to predict the DBH of trees by establishing relationships between remotely sensed forest parameters like CPA, CD, tree height, or their combinations and field sampled DBH. The tree parameters predicted by the model are then used in allometric equations, leading to AGB estimation (Pizaña, Hernández, & Romero, 2016).

AGB estimation using remote sensing is time and cost-efficient (Lu, 2006). It provides biophysical information of the forest on various scales ranging from local to global scale (Mohren, Hasenauer, Köhl, & Nabuurs, 2012). Various sensors and data sets can be employed depending on the type of forest and scale of study to acquire forest parameters (Mitchell, Rosenqvist, & Mora, 2017). The datasets used in forestry applications include 1) optical remote sensing data like medium and low spatial resolution multispectral broadband images, 2) high spatial resolution optical data from satellite, manned aerial vehicles, and unmanned aerial vehicle (UAV), 3) Hyperspectral data, 4) Radio Detection And Ranging (RADAR)/Synthetic Aperture Radar (SAR) data and 5) Light Detection and Ranging (LiDAR) data (Pandey, Srivastava, Chetri, Choudhary, & Kumar, 2019; Timothy, Onisimo, Cletah, Adelabu, & Tsitsi, 2016). Each of these data sets has its advantages and disadvantages with the data availability, temporal characteristics, the accuracy of biophysical information, and acquisition cost (Kumar & Mutanga, 2017).

Medium and low spatial resolution optical remote sensing data from satellites like LANDSAT and MODIS were used to estimate AGB (Halperin, LeMay, Chidumayo, Verchot, & Marshall, 2016; Yin et al., 2015). However, these data have limitations in biomass estimation accuracy because of their low spatial resolution and mixed pixels (Avitabile, Baccini, Friedl, & Schmullius, 2012; Lu, 2006). High spatial resolution satellite data from satellites like IKONOS and Quickbird provide better accuracy when compared to moderate or low spatial resolution data (Sousa, Gonçalves, Mesquita, & Marques da Silva, 2015). Hyperspectral data like data from Hyperion are also used to estimate AGB (Thenkabail, Enclona, Ashton, Legg, & De Dieu, 2004). However, all these data do not provide details of the forest's vertical structure and are very sensitive to weather phenomena like clouds (Lu, 2005). Holopainen, Vastaranta, and Hyyppä (2014) found that, due to lack of information about the vertical structure, the accuracy of AGB estimated is lower than the accuracy of AGB estimated using 3D data from LiDAR or RADAR. Additionally, fit-for-purpose high spatial resolution satellite data and hyperspectral data are costly to acquire and difficult to process (Timothy et al., 2016; Vastaranta et al., 2018).

RADAR/SAR is an active remote sensing method that uses microwave radiation as its source. Longwave microwave radiations like the L-band and P-band can penetrate through the tree canopy leading to a dense 3D point cloud (Mitchell et al., 2017). However, low spatial resolution, saturation, and complex corner reflection properties lead to AGB estimation uncertainties, and data acquisition is also expensive (Sinha, Jeganathan, Sharma, & Nathawat, 2015). LiDAR is also an active remote sensing method; it uses a laser beam as the source. LiDAR data also provides a 3D point cloud with information on the vertical forest structure in all types of forest (Means et al., 1999; Sterεńczak, Zasada, & Brach, 2013). Though LiDAR data products are accurate in estimating AGB, the acquisition cost is high. Therefore multiple flights are practically not feasible due to financial constraints (Dayamit, Pedro, Ernesto, & Fernando, 2015; Mlambo, Woodhouse, Gerard, & Anderson, 2017; Timothy et al., 2016).

The UAVs are the latest development in remote sensing, where a digital camera onboard the drones acquires high spatial resolution optical images. UAVs are easy to operate, and they are flexible. Therefore, custom missions can be planned to collect fit-for-purpose data proving to be time and cost-effective (Banu, Borlea, & Banu, 2016; Lu et al., 2020). With UAVs, optical images with overlap can be acquired. Photogrammetric algorithms and software models like Aerial Triangulation (AT), Structure from Motion (SfM), or stereo-matching enable accurate 3D reconstruction of the scene from overlapping 2D optical images (Gatziolis, Lienard, Vogs, & Strigul, 2015).

The widely employed SfM model is a computer vision algorithm that uses stereophotogrammetry principles to create 3D information from multiple overlapping 2D images. SfM model automatically identifies similar points called key points in multiple images. The model then performs key point matching in multiple images to compute the camera position and produces a sparse 3D point cloud in relative image space. Using Ground control points (GCP), intense bundle block adjustment is done to georeference the 3D point cloud to real object space. The quality of the 3D point cloud depends on the number of images, the overlap between images, and the flying height. More images with high overlap and lower flying height increase the 3D point cloud density (Iglhaut et al., 2019; Micheletti, Chandler, & Lane, 2015; Mlambo et al., 2017; Westoby, Brasington, Glasser, Hambrey, & Reynolds, 2012).

The 3D point cloud obtained from the SfM model is classified into ground and non-ground points. These points are used to generate elevation models like the Digital Terrain Model (DTM) representing the bare ground surface or terrain surface and the Digital Surface Model (DSM) representing the ground surface including objects. The DTM and DSM's arithmetic difference is the Canopy Height Model (CHM) from which tree heights can be extracted (Birdal, Avdan, & Türk, 2017; Mlambo et al., 2017; Moe, Owari, Furuya, & Hiroshima, 2020). High spatial resolution true orthophoto can be generated from UAV images by the orthorectification process. The orthorectification process uses DSM to eliminate the vertical distortion of surface objects, thus retaining their geometric accuracy (Amhar, Jansa, & Ries, 1998; Barazzetti, Brumana, Oreni, Previtali, & Roncoroni, 2014; Liu, Zheng, Ai, Zhang, & Zuo, 2018). The high spatial resolution orthophoto enables individual tree crown segmentation leading to the accurate measurement of crown parameters like CPA and CD from which DBH can be modeled (Berie & Burud, 2018). UAV data products provide both horizontal and vertical structural information of a forest needed for AGB estimation, thus making UAVs the most sought-after data acquisition method for forest monitoring projects. Several studies have used forest parameters extracted from the UAV dataset to estimate aboveground biomass (Fernandes et al., 2020; Kachamba, Ørka, Gobakken, Eid, & Mwase, 2016; Lin, Wang, Ma, & Lin, 2018; Ota et al., 2015; Wahyuni, Jaya, & Puspaningsih, 2016).

## 1.2.   Problem statement

In order to successfully implement carbon accounting, reliable, accurate, and cost-efficient methods of forest carbon monitoring and AGB estimation should be used. In their study, Chave et al. (2014) found that the AGB model that used an allometric equation with DBH and tree height as parameters performed better than the model that used just DBH as a parameter. Though UAV data products are time and cost-effective, the AGB estimation accuracy depends on the accuracy of extracted forest parameters like tree height derived from CHM and CPA, and CD derived from orthophoto (Berhe, 2018; Kachamba, Ørka, Næsset, Eid, & Gobakken, 2017).

The accuracy of tree heights extracted from the CHM is influenced by the quality of DTM (Kachamba et al., 2017; Krause, Sanders, Mund, & Greve, 2019; Moe et al., 2020). A significant shortcoming with UAV data is the accuracy of DTM. DTM is generated by spatial interpolation of ground points from UAV 3D point cloud data (Fawcett et al., 2019). The accuracy of DTM is influenced by the number of points considered during interpolation. Optical sensors onboard UAVs do not penetrate the forest canopy. Therefore, when the forest canopy is dense or when there is dense understory vegetation, they do not penetrate to the actual forest floor. As a result, fewer points are created that represent the ground (Mlambo et al., 2017). The limitation in the number of points reaching the actual ground affects the accuracy of DTM generated based on interpolation of ground points, subsequently affecting the quality of CHM generated and the accuracy of extracted tree height.

Also, in the forest with interlocking tree crowns, delineation of CPA and extraction of CD from UAV orthophoto is challenging as the edges of tree crowns are not captured accurately. Some crown edges are hidden under the other interlocking crowns. This inaccurate CPA subsequently affects the accuracy of modeled DBH.

Nesbit and Hugenholtz (2019) researched on improving the density and accuracy of the 3D point cloud generated from the UAV SfM model by incorporating nadir and off-nadir obliques images in the workflow. Meinen and Robinson (2020) studied the effect of incorporating oblique images in the UAV SfM model on the accuracy of surface models. Both the studies have concluded that the UAV-SfM model that uses both nadir images and oblique images in combination results in a 3D point cloud with more points and improved the accuracy of surface models. This method of incorporating images acquired at different imaging angles to build a dense 3D point cloud and surface models for the forests with different canopy structures has not been well documented in the literature. In forests with dense and medium dense canopy, using an oblique camera view may image the forest's actual ground and tree crown structure, which otherwise would have been hidden in nadir view due to adjacent trees and interlocking tree crowns. Thus, subsequently influencing the accuracy of extracted tree parameters. *Figure 1-1* shows the schematic illustration of the field of view of UAV nadir and oblique angles. Thereby, this study aims to assess the accuracy of tree parameters extracted from the UAV-SfM 3D model that incorporates images acquired at different imaging angles and assess the effect of tree height estimation errors on AGB estimation accuracy.
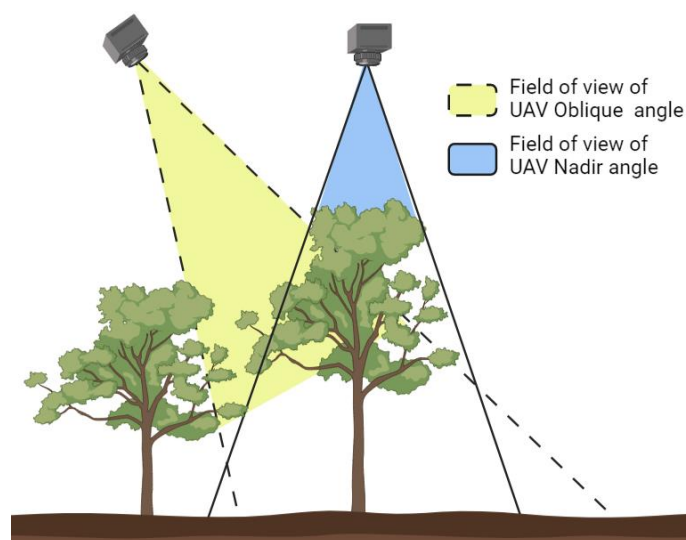


*Figure 1-1. Schematic illustration of the field of view of different UAV view angle*

## 1.3. Research objective

To assess the accuracy of tree parameters generated from the UAV-SfM 3D model that incorporates images acquired at different imaging angles under different canopy densities and assess the effect of tree height estimation errors on AGB estimation accuracy in Haagse Bos, The Netherlands.

### 1.3.1. Specific objective

1) Assess the accuracy of DTM generated from UAV-Nadir images and UAV-Oblique images under dense and medium dense canopy.
2) Assess the accuracy of tree heights derived from UAV-Nadir CHM and UAV-Oblique CHM under dense and medium dense canopy.
3) Assess the accuracy of DBH modeled using tree parameters derived from UAV-Nadir images and UAV-Oblique images under dense and medium dense canopy.
4) Assess the effect of tree height estimation errors on the accuracy of AGB estimates under dense and medium dense canopy

### 1.3.2. Research question

1) What is the accuracy of DTM generated from UAV-Nadir images and UAV-Oblique images under dense and medium dense canopy compared to LiDAR DTM?
2) How accurate are the tree heights derived from UAV-Nadir CHM and UAV-Oblique CHM under dense and medium dense canopy compared to LiDAR CHM?
3) How accurate is the DBH modeled using tree parameters extracted from UAV-Nadir images and UAV-Oblique images under dense and medium dense canopy compared to field-measured DBH?
4) What is the effect of tree height estimation errors on AGB estimation under dense and medium dense canopy?

### 1.3.3. Hypothesis

1) $H_0$: There is no significant difference between the UAV-Nadir, UAV-Oblique, and LiDAR DTM.

   $H_1$: There is a significant difference between the UAV-Nadir, UAV-Oblique, and LiDAR DTM.

2) $H_0$: There is no significant difference between the tree heights derived from UAV-Nadir, UAV-Oblique, and LiDAR CHMs.

   $H_1$: There is a significant difference between the tree heights derived from UAV-Nadir, UAV-Oblique, and LiDAR CHMs

3) $H_0$: There is no significant difference between the DBH modeled from UAV-Nadir and UAV-Oblique-derived tree parameters and field-measured DBH.

   $H_1$: There is a significant difference between the DBH modeled from UAV-Nadir and UAV-Oblique-derived tree parameters and field-measured DBH.

4) $H_0$: Tree height estimation errors do not have a significant effect on AGB estimation

   $H_1$: Tree height estimation errors do have a significant effect on AGB estimation

## 1.4. Conceptual diagram

The conceptual diagram given in *Figure 1-2* shows the important systems identified in this study and their interactions. The central system in this study is the Haagse Bos forest in Enschede, Netherlands, which consists of deciduous and coniferous trees (subsystem). The sun interacts with the subsystem trees by emitting radiation, thus enabling photosynthesis in trees. The trees interact with the atmosphere by

absorbing $CO_2$ during photosynthesis, thus regulating the carbon in the atmosphere. The problem arises when this interaction between trees and the atmosphere is affected due to deforestation and degradation.

The other essential systems relevant to this study are the remote sensing sensors and platforms like UAV and Airborne LiDAR. These platforms and sensors are used to collect the necessary data required to monitor and estimate the AGB of the Haagse Bose forest. The researchers also play a crucial role in building the models to estimate the AGB. The primary interaction of the researchers and the forest is during the field sampling process when they collect representative ground samples to build the AGB estimation models.
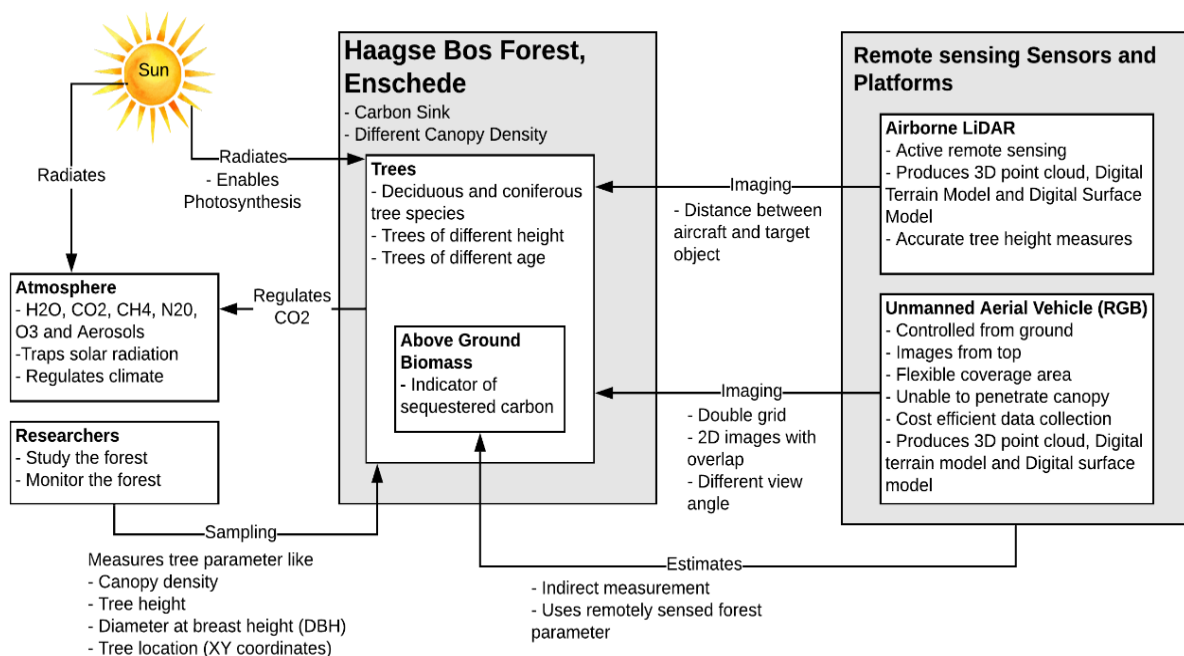


*Figure 1-2. Conceptual diagram*

# 2. MATERIAL AND METHOD

## 2.1. Study area

The study is conducted in the Haagse Bos forest in The Netherlands. It is located in the province of Overijssel between 52°16'10" N - 52°16'50" N and 6°57'00" E - 6°57'40" E. Haagse Bos was once a privately owned plantation forest used for timber production, and a part of it was later converted to a natural forest managed by Natuurmonumenten. Bureau Takkenkamp manages the privately-owned plantation forest. The study area has a mix of deciduous and evergreen trees. The common deciduous tree species found include Oak (*Quercus robur*), European Beech (*Fagus sylvatica*), European White Birch (*Betula pendula*), European larch (*Larix decidua*), Maple *(Acer pseudoplatanus),* and Alder *(Alnus glutinosa).* The common evergreen coniferous tree species found include Douglas Fir (*Pseudotsuga menziesii*), Scots Pine (*Pinus sylvestris*), and Norway Spruce (*Picea abies*). *Figure 2-1* shows the study area's location, which includes the dense and medium dense canopy blocks used in the study. The dense canopy block covers an area of 10.10ha with a canopy closure of 76%, and the medium dense canopy block covers an area of 9.84ha with a canopy closure of 64%.
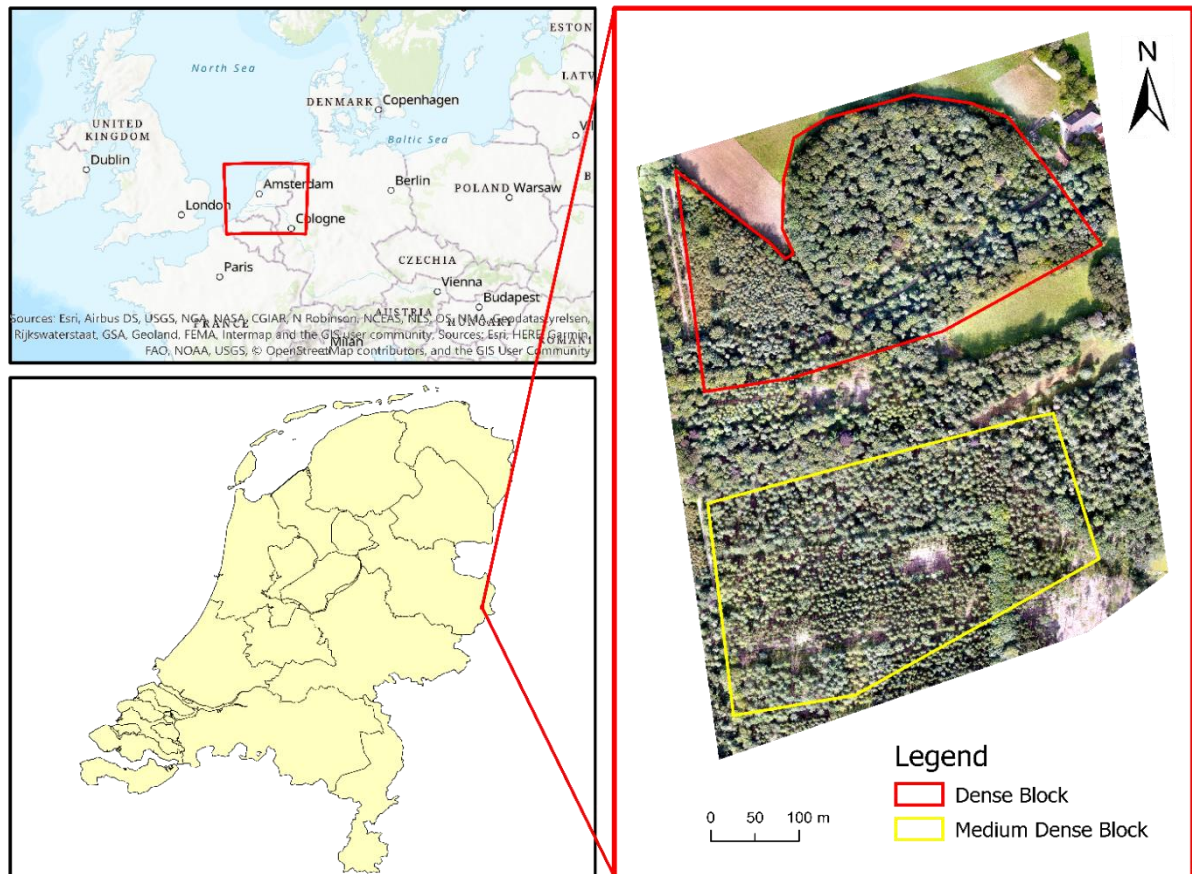


*Figure 2-1. Location of the study area*

## 2.2. Material

This section includes a brief description of the various data sets, the types of equipment used to collect the data, and the various software used to process the data in this study.

### 2.2.1. Data

The data used for this study include UAV images acquired at different viewing angles, LiDAR point cloud data, and tree biometric data. The UAV data and the tree biometric data were collected from the field, and the LiDAR point cloud was downloaded from the Actueel Hoogtebestand Netherlands (AHN). The list of data and its sources are given in *Table 2-1*.

*Table 2-1. List of data and sources*

| Data | Source |
| --- | --- |
| UAV Images | DJI Phantom 4 |
| LiDAR point cloud | Actueel Hoogtebestand Netherlands |
| Tree location | Fieldwork |
| Tree DBH | Fieldwork |
| Tree Species | Fieldwork |
| Ground control points (GCP) | Fieldwork |

### 2.2.2. Equipment

Different types of equipment were used to collect data from the field for the study. The equipment list and its purposes are given in *Table 2-2*.

*Table 2-2. List of equipment used and purpose*

| Data | Purpose |
| --- | --- |
| Diameter tape | DBH measurement |
| Measurement tape 30m | Sample plot radius measurement |
| | Distance measurement of the tree from the plot center |
| Tree tag | Tree numbering |
| Compass Suunto | Tree bearing measurement |
| GNSS LEICA C15 | GCP and 3D ground data measurement |
| GCP markers | Mark GCPs |
| Datasheet | Record data |
| DJI Phantom 4 | Acquire UAV RGB images |

### 2.2.3. Software

The data processing, data analysis, interpretation, and documentation for this study were made using various software. The list of software used and its purposes are listed in *Table 2-3*.

*Table 2-3. List of software used and purpose*

| Data | Purpose |
| --- | --- |
| Pix4DMapper | UAV image processing |
| LAZ tools in ArcGIS | LiDAR data processing |
| ArcMap 10.7.1 | Spatial data analysis and visualization |
| Microsoft Excel | Data storage and analysis |
| RStudio | Data analysis |
| SPSS | Data analysis |
| Google Earth Pro | UAV flight block selection |
| Avenza Map | Navigation in field and recording field notes |
| Gap Light Analysis Mobile Application (GLAMA) | Canopy closure estimation |

## 2.3. Workflow

The method followed to complete the study includes five main processes, and they include
1) UAV flight planning and UAV image acquisition
2) UAV data processing to generate orthophoto, DSM, DTM and CHM
3) Fieldwork planning, ground truth data collection, and processing
4) LiDAR point cloud download and processing to generate DSM, DTM, and CHM.
5) Data analysis to answer the study's research questions

Sections 2.5 to 2.7 describes the five main processes, and *Figure 2-2* shows the study's overall workflow indicating the five main processes.



*Figure 2-2. The overall workflow of the study*

## 2.4. Canopy density classes

An initial reconnaissance survey of the study area was done before the UAV flight to identify different canopy density blocks. During ground truth data collection, the percentage canopy closure was measured in each of the chosen blocks. Canopy closure was measured using the Gap Light Analysis Mobile Application (GLAMA) at the sample plot center and in four directions. The GLAMA estimates the canopy cover using hemispherical, wide-angle, and standard photographs (Tichý, 2016). In the field, the mobile camera with a wide-angle setting was used to capture the canopy image. The image was used as input in the GLAMA to calculate the percentage canopy closure. The average canopy closure percentage of the different blocks is given in *Table 2-4*, and they comply with different international forest canopy density classification standards (Barber, Bush, & Berglund, 2011; Brohman & Bryant, 2005; FAO, 2003; "Scheme of classification: Forest Survey of India," 2018; Vandendriesche, 2013).

*Table 2-4. Percentage canopy closure in the study area*

| Canopy Density Block | Canopy Closure (%) |
|---|---|
| Dense Canopy | 76% |
| Medium Dense Canopy | 64% |

## 2.5. Data collection

### 2.5.1. UAV flight planning and data collection

Visual interpretation of Google earth images and Planet scope images was done to select flight blocks and ensure enough open space to establish a well-distributed GCP placement. UAV RGB images were acquired in September 2020 for the study. UAV RGB images were acquired with a camera view angle set at 90 degrees (nadir) and 75 degrees (15 degrees off-nadir and east facing). Pepe, Fregonese, and Scaioni (2018) and Wenzel, Rothermel, Fritsch, and Haala (2013), in their studies, quoted that finding an optimal oblique angle of view is challenging, and it should be found by experiments and trials. However, that was beyond the scope of this study. Meinen and Robinson (2020) analyzed 150 scenarios with multiple angles and combinations. The study concluded that 15-degree tilt resulted in increased point cloud density with accurate and precise points. Also, in their study, Meinen and Robinson (2020) used 15-degree off-nadir images and proved that it improved the accuracy of surface models. Therefore 75 degrees (15-degree tilt off-nadir) was chosen for the study. The flight parameter settings are provided in *Table 2-5*. UgCS, the drone control software, was used to set the flight parameter, and it was also used to track the drone in real-time while acquiring images. The GCPs were measured using GNSS LEICA C15. The distribution of GCP and images acquired at nadir are shown in *Figure 2-3*.

*Table 2-5. UAV flight parameters of dense and medium dense canopy blocks*

| Parameter | Value (RGB-Nadir) | Value (RGB-Oblique) |
|---|---|---|
| Flight Pattern | Double grid | Single grid |
| Camera Angle | $90^0$ | $75^0$ |
| Camera Orientation | Nadir | East facing oblique |
| Forward Overlap | 90% | 90% |
| Side Overlap | 80% | 80% |
| Speed | Slow | Slow |
| Altitude | 100-110m | 100-110m |
| Ground control points | 9 | 9 |
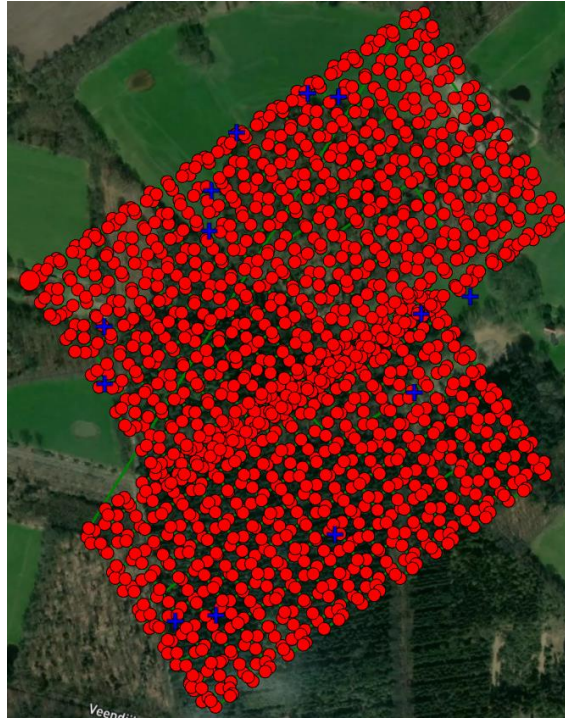
*Figure 2-3. Distribution of GCP (blue check) and images (red dots) acquired at nadir*

### 2.5.2. Field data sampling design

The study area was stratified based on canopy density, and then sample plots were purposively selected in each stratum due to accessibility, time, and weather constraints. Circular sample plots were established, with a radius of 12.60m, which makes an area of 500m². For biomass estimation studies, the sample plot size of 500m² is efficient because a larger plot size does not increase the accuracy of results but increases the fieldwork cost and time (Kachamba et al., 2017; Ruiz, Hermosilla, Mauro, & Godino, 2014). Circular sample plots were chosen because it is easy to establish with single control point and efficient in forest inventory (Kershaw, Ducey, Beers, & Husch, 2017; Köhl, Magnussen, & Marchetti, 2006; Maniatis & Mollicone, 2010; Paudel & Mandal, 2019). A total of 13 plots were sampled in dense canopy block, and 10 plots were sampled in medium dense canopy block. *Figure 2-4* shows the location of sample plots in dense and medium dense canopy density blocks.
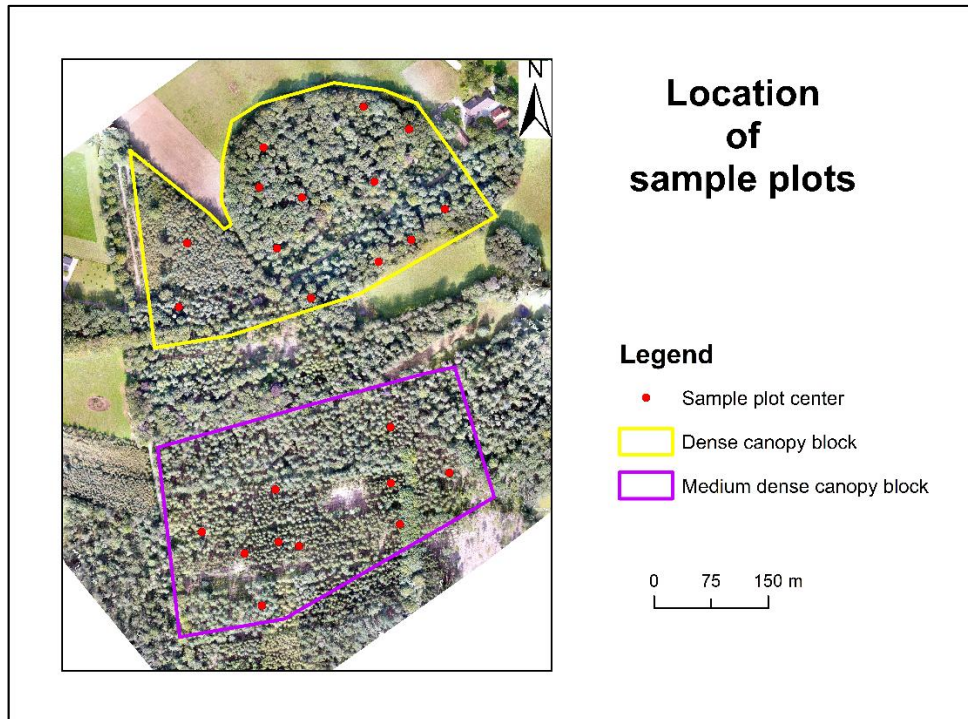
*Figure 2-4. Map showing the location of sample plots in dense and medium dense canopy blocks*

### 2.5.3. Ground truth data collection

Ground truth data were collected between September 2020 and November 2020 for the study. In the blocks, mostly big trees easily identifiable on orthophoto were made as plot centers. These sample plots center were marked on UAV orthophoto loaded in Avenza Map mobile application. Tree species, DBH, and the location of all trees with respect to the plot center within the established sample plot were recorded. Only the biometrics of trees within the sample plot that were visible on orthophoto were recorded. The data entry sheet used in the field is given in *Appendix 1*. Biometric data of 113 trees were recorded in the dense block, and 171 trees were recorded in the medium dense block.

### 2.5.4. LiDAR data

LiDAR point cloud data was downloaded from AHN. The AHN produces LiDAR data products for the whole of the Netherlands, and it is open-source data owned by Rijkswaterstaat. Though the AHN provides DTM as grids at 50cm resolution, they had voids. Therefore, the LiDAR point cloud from AHN was used in the study to generate the DTM, DSM, and CHM, which are considered reference data for accuracy assessment. The tile 29CZ1 of the AHN3 dataset covers the study area, and it was acquired in February 2019 ("Voortgang AHN 2019," 2019). In AHN 3 dataset, 99.70% of points have a vertical accuracy of 20cm and a systematic and standard deviation of not more than 5cm. The 3D point cloud was downloaded in LAZ format, which has a point density of 6 to 10 points/m2 ("Quality description | AHN," 2019).

## 2.6. Data processing

This study's data processing includes processing ground truth data, UAV images, and LiDAR point cloud data, explained in the following sections.

### 2.6.1. Ground truth data processing

The ground truth data collected from the field were entered in Microsoft Excel for digital storage and further processing. The XY coordinates of the plot centers were used as a reference to identify the location of the sampled trees. The field measured distance and bearing of each tree within the sample plot were converted to departure and latitude using *Eq (1) and (2)*. The schematic illustration of departure and latitude is shown in *Figure 2-5*. The X and Y coordinates of the tree were calculated by adding the departure and latitude to the X and Y coordinate of the plot center, respectively *(Eq 3 and 4)* (Harvey, 2012; Wilson, 2000). The sampled trees were identified in the orthophoto by importing the calculated XY coordinates to ArcMap. Then the individual tree crowns were manually digitized for further data analysis.

$$Departure = Distance * \sin \theta \qquad \text{Eq (1)}$$
$$Latitude = Distance * \cos \theta \qquad \text{Eq (2)}$$
$$X\ Coordinate\ of\ tree = Departure + X\ coordinate\ of\ plot\ center \qquad \text{Eq (3)}$$
$$Y\ Coordinate\ of\ tree = Latitude + Y\ coordinate\ of\ plot\ center \qquad \text{Eq (4)}$$
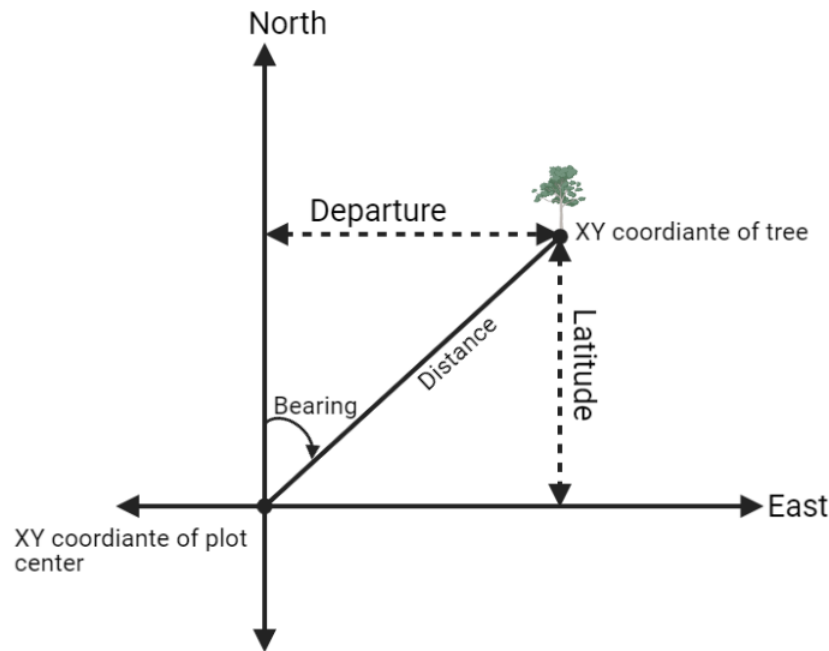


*Figure 2-5. Schematic illustration of departure and latitude*

### 2.6.2. UAV data processing

The UAV images were processed in photogrammetry software Pix4Dmapper to produce a 3D point cloud, DSM, DTM, and orthophoto. The Pix4Dmapper uses a three-step processing procedure to generate a 3D point cloud and orthophoto ("Processing steps – Support," 2021). First, the camera parameters are optimized, followed by keypoint extraction and matching in the initial processing step using SfM photogrammetric algorithm. The SfM model identifies matching key points from overlapping input 2D images to create a sparse point cloud (Iglhaut et al., 2019; Micheletti et al., 2015; Mlambo et al., 2017; Westoby et al., 2012). The 3D point cloud is georeferenced using the imported GCP marks measured in the field with GNSS LEICA C15. In the second step, it runs the bundle block adjustment to create a dense 3D point cloud. Finally, in the third step, the software generates the DSM using the Inverse Distance Weighting method and performs orthorectification to generate a true orthophoto ("Photo stitching vs orthomosaic

generation – Pix4D," 2021). The dense 3D point cloud is classified to generate the DTM. The Pix4Dmapper uses machine learning to classify the point cloud into five different classes: Ground, Road Surface, High Vegetation, Building, and Human-Made object based on geometry and color ("Automatic point cloud classification for construction | Pix4D," 2017; "How to generate the point cloud classification – Support," 2021). Only the points in the class ground and road surfaces are used to build the DTM in Pix4Dmapper.

The UAV images acquired for dense and medium dense canopy blocks were processed in two sets. For the first dataset (UAV nadir), the images acquired at nadir in the double grid were used for processing in Pix4Dmapper. For the second dataset (UAV oblique), images acquired at 75 degrees single grid and images acquired at the nadir in double grid were used in combination for processing. A total of 9 GCPs and 4 checkpoints were used in the processing of both datasets. *Figure 2-6* shows the schematic illustration of camera orientation of image sets used in both processing. The specifications of the 3D point cloud, DSM, Orthophoto, and DTM generated from SfM processing are given in *Appendix 2*.
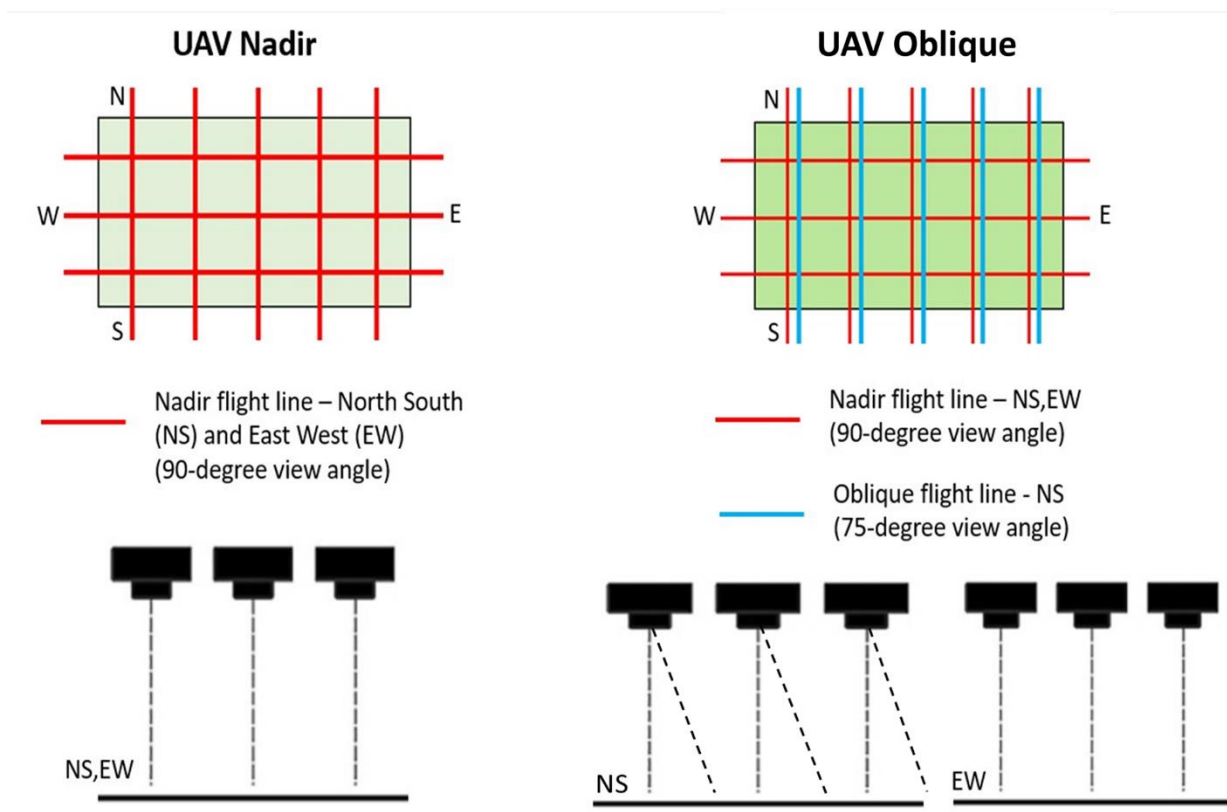


*Figure 2-6. Schematic illustration of camera orientation for image sets used for processing*

### 2.6.3. LiDAR data processing

The LiDAR point cloud was processed to generate the DTM and DSM using the LAStools in ArcGIS. The first returns were used to generate the DSM LAS dataset layer. The ground returns were used to generate the DTM LAS dataset layer. Both the LAS dataset layers were converted to raster layers of 50cm resolution (Bazezew, Hussin, & Kloosterman, 2018; Thapa Magar, 2014). Since AHN provides DSM and DTM (with voids) as grids at 50cm resolution, the same resolution was maintained in this study for the point cloud generated DTM and DSM, and it was not reduced to lower fine resolution.

### 2.6.4. Canopy height model

The CHM was used to extract the individual tree height. The UAV CHMs and LiDAR CHMs were generated by subtracting the DTM from DSM (Jayathunga, Owari, & Tsuyuki, 2018; Krause et al., 2019; Mohan et al., 2017; Reder, Waßermann, & Mund, 2019). The UAV nadir and oblique CHMs were generated at three different resolutions (22cm, 50cm, and 1m). LiDAR CHMs were generated at two different resolutions (50cm and 1m). The DSM and DTM from both the UAV nadir and oblique datasets were first resampled, and then the Raster Calculator tool in ArcGIS was used to generate the CHMs. The different CHMs generated, the layers used, and their resolutions are indicated in the flowchart shown in *Figure 2-7*.
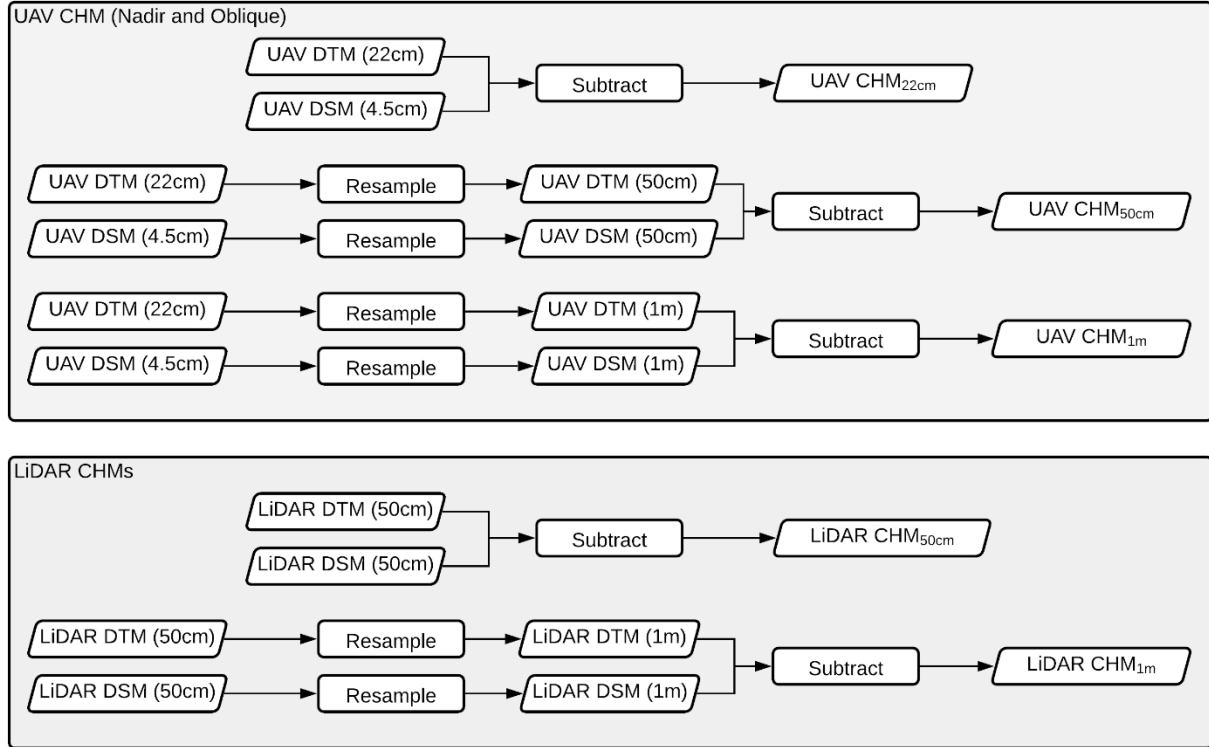


*Figure 2-7. CHMs generated and their resolutions*

### 2.6.5. Crown delineation and tree height extraction

Tree crown delineation is essential to create the CPA and CD of each tree. Using CPA, tree height can be extracted from CHM and both CPA and CD can be used to model DBH (Iizuka, Yonehara, Itoh, & Kosugi, 2017; Kattenborn, Hernández, Lopatin, Kattenborn, & Fassnacht, 2018; Moe, Owari, Furuya, Hiroshima, & Morimoto, 2020). The trees sampled in the field were identified in orthophoto, and their crowns were delineated by manual on-screen digitization. Manual digitization is considered the most accurate method as the crown edges can be identified without error (Pouliot, King, Bell, & Pitt, 2002). In addition, manual digitization was used in this study because of the small study area (Wagner et al., 2018). The Zonal Statistics tool in ArcGIS was used to extract the highest value from the generated UAV and LiDAR CHMs within the digitized tree crown. The extracted highest CHM value was considered the tree height. (Lim et al., 2015; Moe et al., 2020).

## 2.7. Data analysis

This research's data analysis includes the DTM accuracy assessment, tree height accuracy assessment, DBH model development, DBH model validation, and AGB estimation and sensitivity analysis. In addition, various statistical analysis and testing methods were used to analyze the data and draw conclusions in this study. They are described in the following sections.

### 2.7.1. DTM accuracy assessment

The LiDAR DTM generated at 50cm resolution was used as a reference to assess the accuracy of the UAV DTMs and answer research question 1. The resolution of UAV DTMs generated using nadir only images and a combination of nadir and oblique images were 22cm. They were resampled using bilinear interpolation to 50cm resolution so that all comparable DTMs are in the same resolution and values of similar areas are extracted for comparison. A total of 100 random points were generated in each of the canopy density blocks using the Create Random Points tool in ArcGIS. Elevation values from each of the DTMs were extracted for the 100 points. A linear relationship was established between the UAV DTM elevation and LiDAR DTM elevation using the simple linear regression model. The coefficient of determination ($R^2$) and Pearson's correlation coefficient (r) were used to determine the relationship's strength (Kahyani, Hosseini, & Basiri, 2011). The Root Mean Square Error (RMSE) was used to quantify the error associated with the elevation values from UAV DTM, and Bias was used to determine the direction of error (Harwell, 2018). RMSE and Bias were calculated using *Eq (5) – (8)*. One-way ANOVA and Tukey's Honest Significant Difference (HSD) test were used to assess the significance of the difference between the means at 95% confidence level ($\alpha = 0.05$). Tucky HSD test can compare multiple means simultaneously and thus can reduce the experiment-wise error rate. Since this study involves comparison of more than two sample sets, the Tucky HSD post hoc test was used in order to reduce the chances of false-positive (Frost, 2021; Stoll, 2017).

$$RMSE = \sqrt{\frac{\sum(\hat{y}_i - y_i)^2}{n}}$$

Eq (5)

$$RMSE \% = \frac{RMSE}{\overline{y_i}} \times 100$$

Eq (6)

$$Bias = \frac{\sum(\hat{y}_i - y_i)}{n}$$

Eq (7)

$$Bias \% = \frac{Bias}{\overline{y_i}} \times 100$$

Eq (8)

Where,
$\hat{y}_i$ is the estimated value
$y_i$ is the reference value
$\overline{y_i}$ is the average reference value and
$n$ is the number of observations.

### 2.7.2. Tree height accuracy assessment

Tree heights extracted from LiDAR CHMs were used as a reference to assess the accuracy of tree heights extracted from UAV CHMs, as it is proved to be more accurate than field-measured tree heights in several studies (Ke & Quackenbush, 2011; Sadadi, 2016; Wallace, Lucieer, Malenovskỳ, Turner, & Vopěnka, 2016; Wang et al., 2019). A linear relationship was established between the tree heights from UAV CHM and LiDAR CHM using the simple linear regression model. The coefficient of determination ($R^2$) and Pearson's correlation coefficient (r) were used to assess tree height accuracy. RMSE and bias were used to quantify the error in the tree heights extracted (Yin & Wang, 2016). *Eq (5) - (8)* were used to quantify error. One-way ANOVA and Tukey's Honest Significant Difference (HSD) test were used to assess the significance of the difference between the tree height means at a 95% confidence level ($\alpha = 0.05$), thus answering the research question 2.

### 2.7.3. DBH model development and validation

DBH can be modeled from tree parameters derived from remote sensing data using various regression models (Priedītis et al., 2012). Linear, quadratic, logarithmic, and power models were used in this study. Different UAV derived tree parameters like tree height (TH), CD, CPA, and product of tree height and crown diameter (TH*CD) were used as dependant variables to predict the DBH (Dalponte et al., 2018; Gaden, 2020; Jucker et al., 2017; Kattenborn et al., 2018; Verma et al., 2014). In this study, the product of TH and CD was used in order to avoid the problem of collinearity (Jucker et al., 2017). TH from UAV nadir and oblique $CHM_{50cm}$ were used. The CD was calculated using the formula given in *Eq (9)*.

$$Crown\ diameter\ (m) = \sqrt{\frac{CPA}{\pi}}$$

Eq (9)

$where\ \pi = 3.14159$.

The ground sampled data were split into 60% for model building and 40% for validation. From the different regression models built, the best model with lower RMSE and higher $R^2$ was chosen to predict the DBH of 40% of the trees for model validation. A simple linear relationship was established between the model predicted DBH and field measured ground truth DBH to validate the model. The coefficient of determination ($R^2$) and Pearson's correlation coefficient (r) were used to assess the predicted and field-measured DBH relationship. RMSE and bias were used to quantify the error in the model predicted DBH. *Eq (5) – (8)* were used to quantify error. One-way ANOVA was used to assess the significance of the difference between the predicted DBH and field measured DBH at a 95% confidence level ($\alpha = 0.05$).

### 2.7.4. AGB estimation

Allometric equations that use DBH and tree height as input parameters were used to calculate AGB. The allometric equations used in this study were species-specific developed for the Netherlands, taken from Zianis, Muukkonen, Mäkipää, and Mencuccini (2005). The equations used are given in *Table 2-6*. Three sets of AGB were calculated using field-measured DBH and LiDAR tree heights, UAV nadir estimated tree heights, and UAV oblique estimated tree heights.

*Table 2-6. Species-specific allometric equations used in the study to calculate AGB*

| Species | Allometric Equation | $R^2$ | Country | Eq |
|---|---|---|---|---|
| **Alder** *(Alnus glutinosa)* | $AGB = D^{1.85749}.TH^{0.88675}.\exp(-2.5222)$ | 0.991 | Netherlands | (10) |
| **Douglas fir** *(Pseudotsuga menziesii)* | $AGB = D^{1.90053}.TH^{0.80726}.\exp(-2.43151)$ | 0.993 | Netherlands | (11) |
| **European Beech** *(Fagus sylvatica)* | $AGB = 0.049.D^{1.78189}.TH^{1.08345}$ | 0.999 | Netherlands | (12) |
| **European Larch** *(Larix decidua)* | $AGB = D^{1.86670}.TH^{1.08118}.\exp(-3.0488)$ | 0.996 | Netherlands | (13) |
| **European White Birch** *(Betula pendula)* | $AGB = D^{1.89060}.TH^{0.26595}.\exp(-1.07055)$ | 0.999 | Netherlands | (14) |

| | | | | |
|---|---|---|---|---|
| **Maple** <br> *(Acer pseudoplatanus)* | $AGB = D^{1.89756}.TH^{0.97716}.\exp(-2.94253)$ | 0.99 | Netherlands | (15) |
| **Norway spruce** <br> *(Picea abies)* | $AGB = 0.04143.D^{1.6704}.TH^{1.3337}$ | 0.995 | Netherlands | (16) |
| **Oak** <br> *(Quercus robur)* | $AGB = D^{2.00333}.TH^{0.85925}.\exp(-2.86353)$ | 0.995 | Netherlands | (17) |
| **Scot pine** <br> *(Pinus sylvestris)* | $AGB = D^{1.82075}.TH^{1.07427}.\exp(-2.8885)$ | 0.994 | Netherlands | (18) |

Where,

AGB is the above-ground biomass in kg/tree,

D is the diameter at breast height (DBH) in cm,

TH is the height of the tree in m.

### 2.7.5. AGB sensitivity analysis

Sensitivity analysis was carried out in a controlled manner with 30 trees selected at random to see how the tree height differences affected the AGB estimation. The RMSE identified during tree height accuracy assessment was used to inflate and deflate the tree heights extracted from UAV nadir CHM and UAV oblique CHM (Ojoatre, Zhang, Hussin, Kloosterman, & Ismail, 2019). AGB was calculated using the inflated and deflated tree height and was plotted using bar graphs to visualize the effect of tree height differences in each canopy density class (Frey & Patil, 2002). One-way ANOVA and Tucky HSD post hoc follow-up test were used to assess the significance of the difference between the reference AGB and AGB estimated from inflated and deflated UAV tree heights at a 95% confidence level ($\alpha = 0.05$).

# 3.  RESULTS

## 3.1.  Ground-truth data

The tree biometric data like DBH and species of 113 trees were recorded from 13 sample plots in the dense canopy block, and 171 trees were recorded from 10 sample plots in the medium dense canopy block. The number of trees per plot in different canopy density blocks is given in *Figure 3-1*. The distribution of species in different canopy density blocks is shown in *Figure 3-2*.
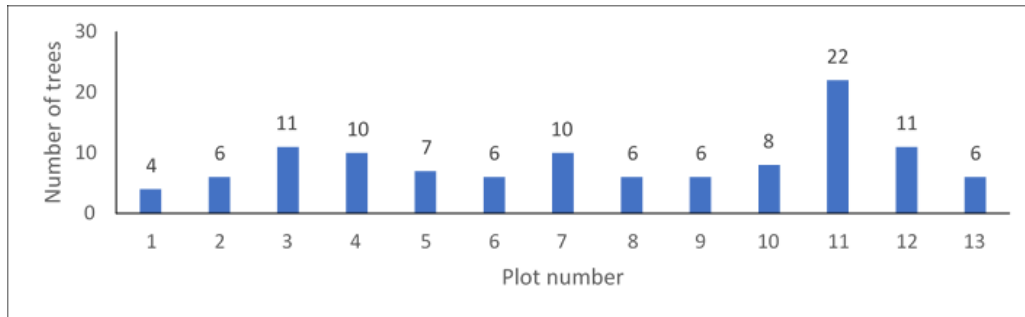


a)  Number of trees per plot in dense canopy block
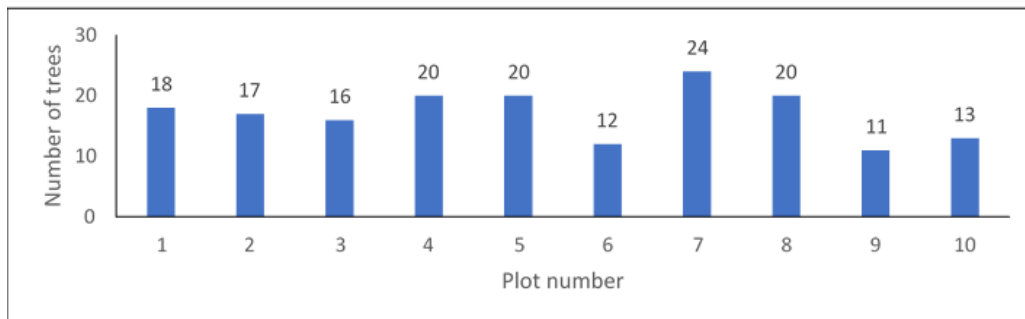


b)  Number of trees per plot in medium dense canopy block

*Figure 3-1. Number of trees per plot in dense and medium dense canopy blocks*
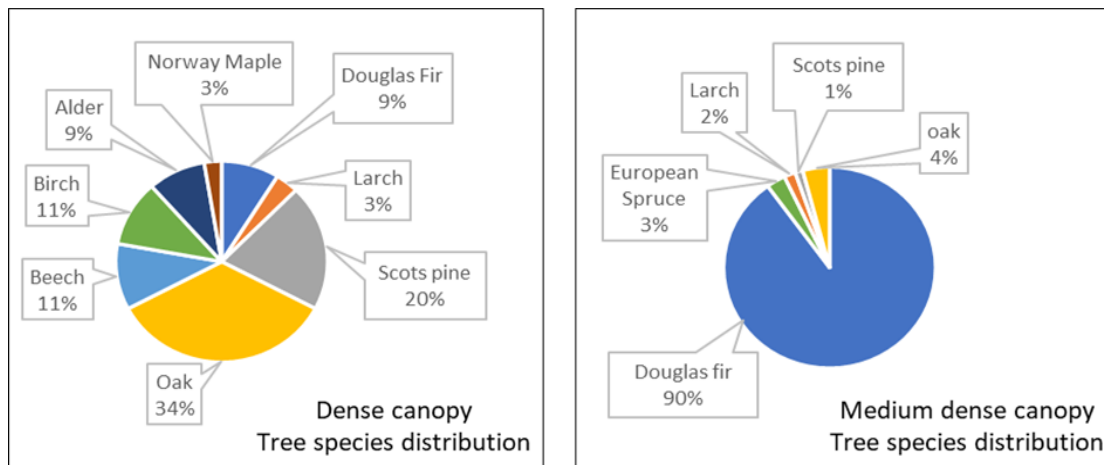


*Figure 3-2. Tree species distribution in dense and medium dense canopy blocks*

In the dense canopy block, the average number of trees per plot is 8, and the minimum and maximum number of trees found per plot are 4 and 22, respectively. In the medium dense canopy block, the average number of trees per plot is 17, and the minimum and maximum number of trees found per plot are 11 and 20, respectively. The dense canopy block predominantly had mature deciduous trees with interlocking tree crowns that overshadowed other understory trees. Only trees visible on orthophoto were sampled in the field during fieldwork. Therefore the total number of sampled trees in the dense canopy block is less with a comparatively lower average even though more sample plots were established. On the contrary, young coniferous trees planted at intervals characterize the medium dense canopy block. Almost all trees were distinctly visible on orthophoto and were measured in medium dense canopy block. Therefore, the average number of trees per plot is greater than the dense canopy block.

Among the trees sampled in the dense canopy block, deciduous trees like Oak, Beech, Birch, Alder, and Norway maple make up most of the sample, with 68%. On the other hand, in the medium dense canopy block, evergreen coniferous tree species like the Douglas fir, European Spruce, and Scots Pine make up most of the sample, with 94%.

The mean tree DBH of 113 trees that were measured in dense canopy block was 46.05cm. The maximum tree DBH measured was 101.90cm of a Beech tree, and the minimum tree DBH was 18.50cm of a Larch tree in the dense canopy block. In the medium dense canopy block, the mean DBH of the 171 trees measured was 33.74cm with a maximum and minimum DBH of 66.80cm and 13.00cm, respectively, of a Douglas Fir tree. The histogram of tree DBH measured from the dense and medium dense canopy blocks are given in *Figure 3-3*. The descriptive statistics of tree DBH measured from the dense and medium dense canopy blocks are given in *Table 3-1*. Detailed plot-wise descriptive statistics of field-measured tree DBH from different canopy density blocks are given in *Appendix 3*.
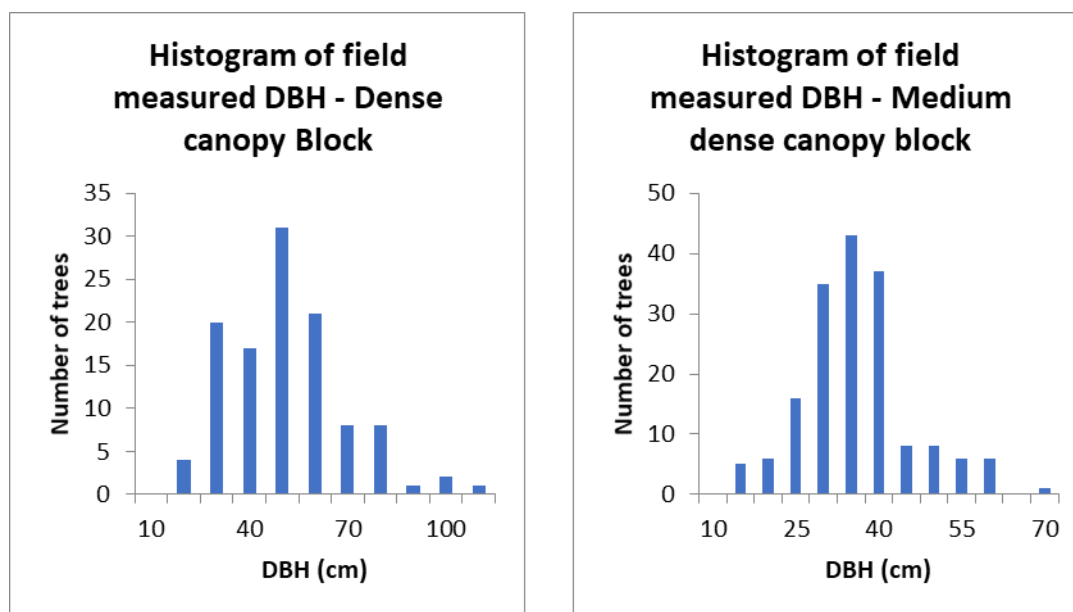


*Figure 3-3. Histogram of field measured tree DBH from dense and medium dense canopy blocks*

*Table 3-1. Descriptive statistics of field-measured tree DBH from dense and medium dense canopy blocks*

| DBH | Count | Mean | Std. Deviation | Minimum | Maximum |
|---|---|---|---|---|---|
| **Dense canopy block** | 113 | 46.06 | 17.39 | 18.50 | 101.90 |
| **Medium dense canopy block** | 171 | 33.74 | 9.75 | 13.00 | 66.80 |

## 3.2. Data Processing

The spatial resolution of the generated LiDAR DSM, DTM, and CHM$_{50cm}$ was 50cm. *Figure 3-4* shows the LiDAR DSM, DTM, and CHM$_{50cm}$ of the dense and medium dense canopy blocks. Since the LiDAR data was acquired during the leaf-off season and due to its penetration capabilities, the drainages in the forest floor are also captured in LiDAR DTM.

As the output of SfM processing in Pix4Dmapper, Orthophoto, DSM, and DTM were generated. The spatial resolution of orthophoto generated from the UAV nadir dataset and UAV oblique dataset was 4.5cm. The spatial resolution of the DSM and DTM generated from the UAV nadir dataset, and UAV oblique dataset was 4.5cm and 22cm. Orthophoto generated from the UAV nadir, and oblique datasets are given in *Appendix 4*. *Figures 3-5 and 3-6* show the DSM, DTM, and CHM$_{22cm}$ generated using UAV nadir and UAV oblique datasets for dense and medium dense canopy blocks. Not much difference is observed between UAV nadir and oblique orthophotos by visual interpretation in both the canopy density blocks *(Appendix 4)*. However, the minimum and maximum elevation of DTM and DSM differ between the UAV nadir and oblique datasets in both the dense and medium dense canopy blocks. In addition to that, the maximum values in LiDAR DTM and UAV DTM (nadir and oblique) in both the canopy density blocks have a large difference.



a) Dense canopy block



b) Medium dense canopy block
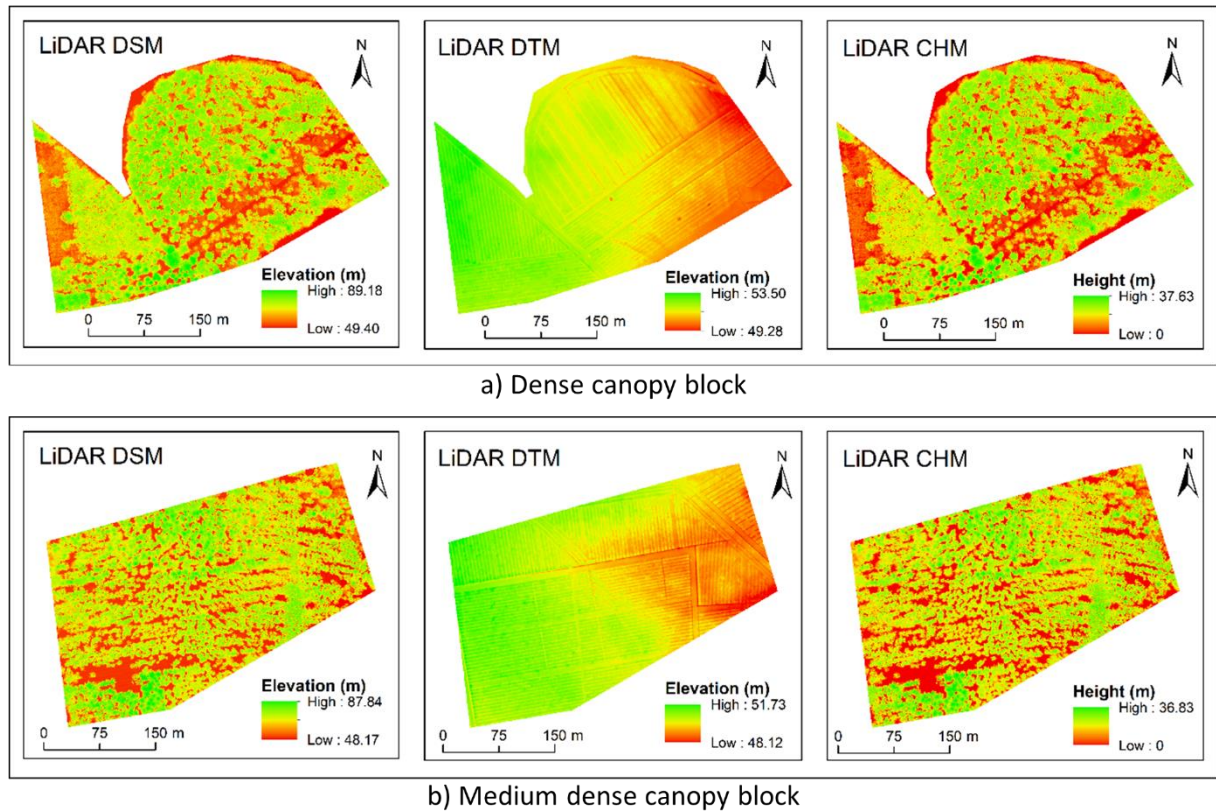
*Figure 3-4. LiDAR DSM, DTM and CHM of different canopy density blocks*
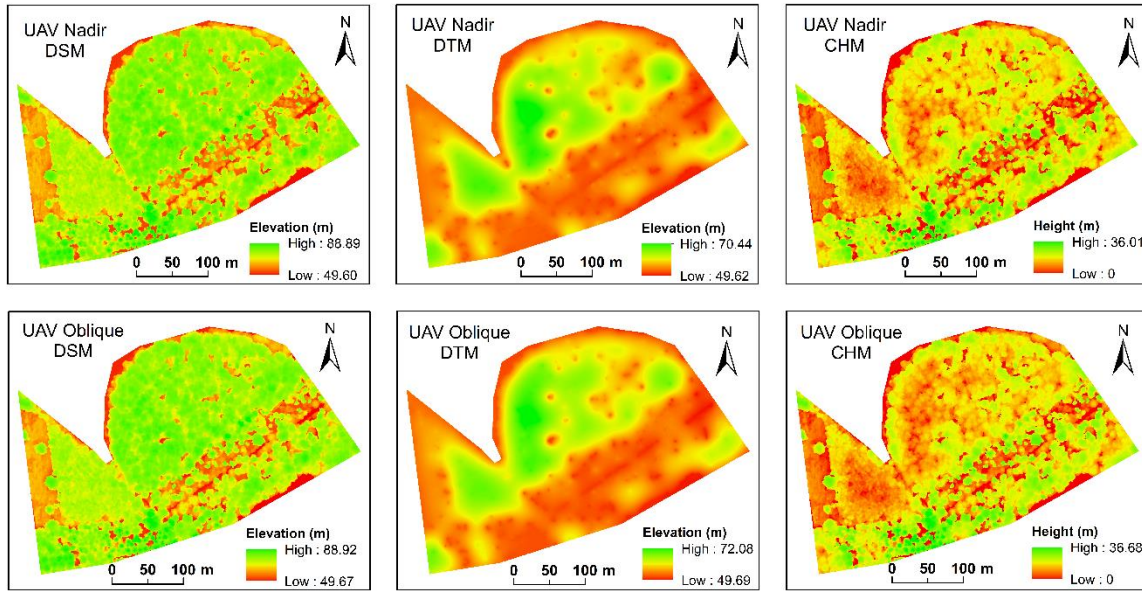
*Figure 3-5. UAV DSM, DTM and CHM of dense canopy block*
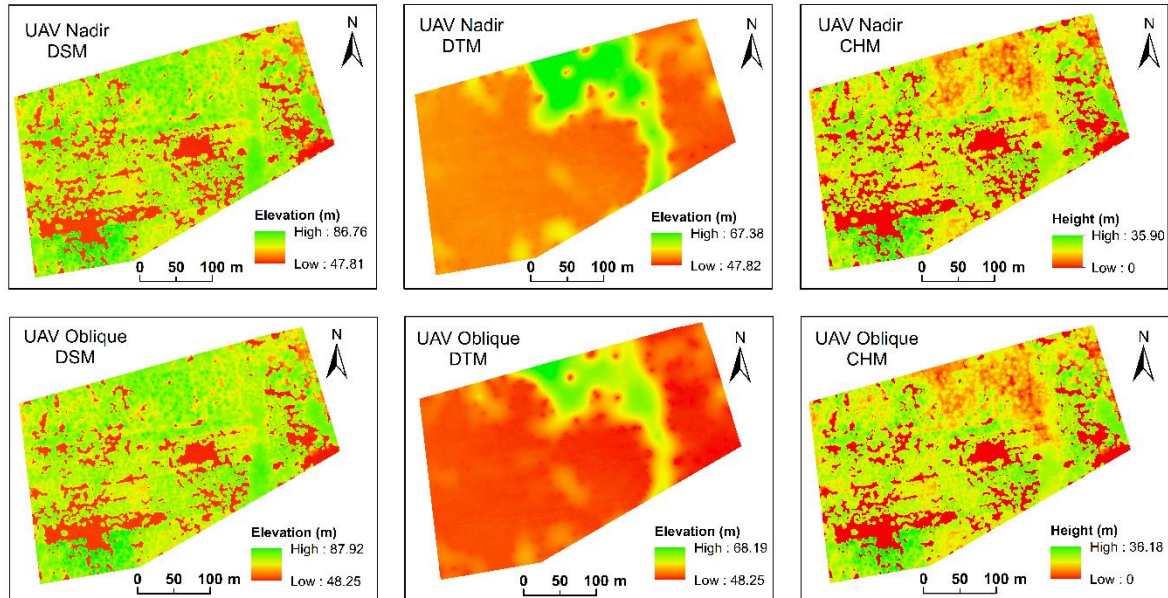


*Figure 3-6. UAV DSM, DTM and CHM of medium dense canopy block*

## 3.3.    DTM accuracy assessment

Research question one of the study is: What is the accuracy of DTM generated from UAV-Nadir images and UAV-Oblique images under dense and medium dense canopy compared to LiDAR DTM?

To answer this research question, elevation values of 100 random points from UAV DTMs were compared with the elevation values from LiDAR DTM in dense and medium dense canopy blocks. All the comparable DTMs were of 50cm resolution. Firstly, the accuracy of LiDAR DTM was validated using random elevation checkpoints measured by GNSS LEICA C15 in and around the study area. A total of 67 points were measured. The LiDAR DTM elevations and field measured elevations strongly correlated with an r-value of

0.95 and RMSE of 0.25m. The location of random checkpoints are given in *Figure 3-7*, and the scatter plot is shown in *Figure 3-8*
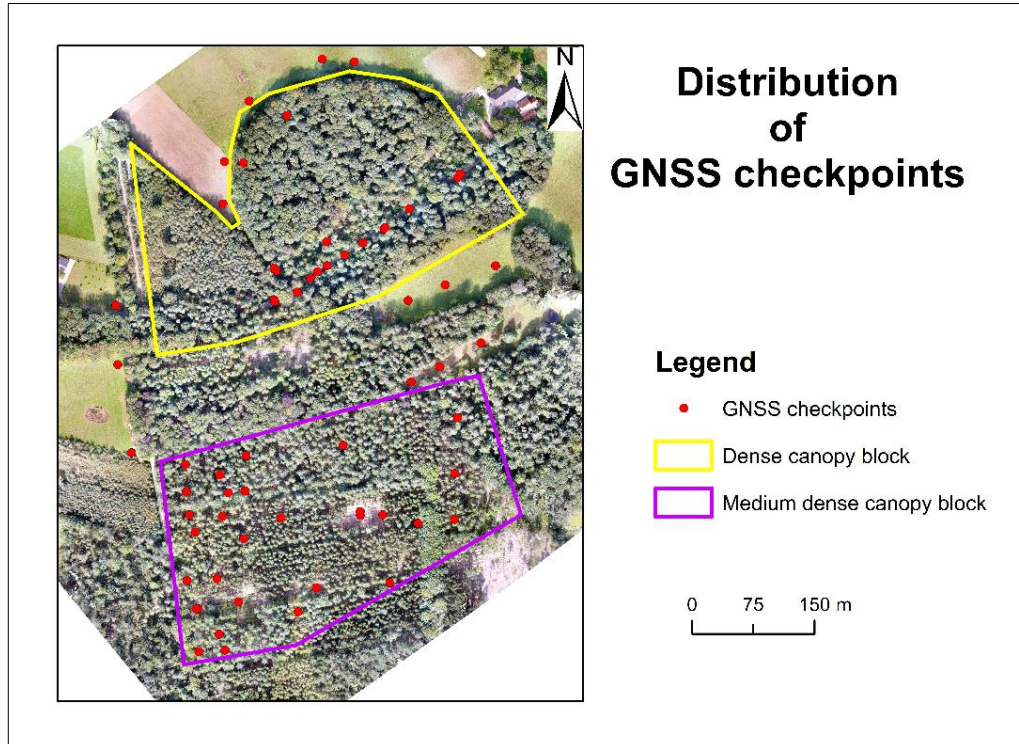


*Figure 3-7. Location of elevation checkpoints*
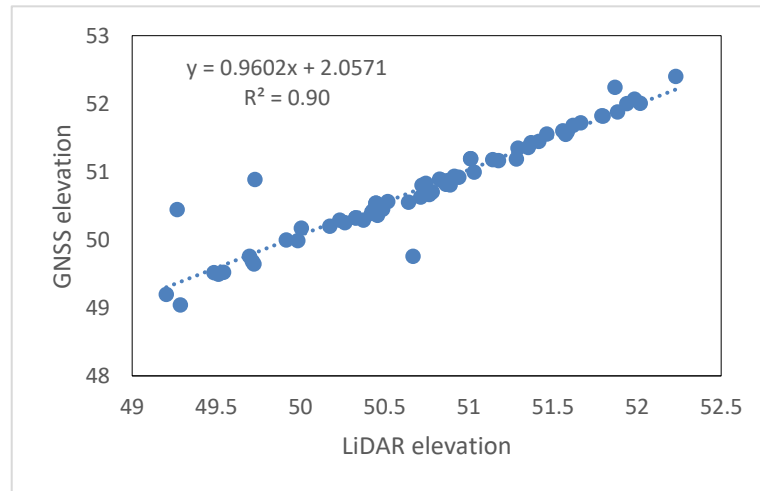


*Figure 3-8. Scatter plot of elevation from LiDAR DTM and GNSS checkpoints*

*Tables 3-2 and 3-3* provide the 100 random point elevation descriptive statistics in dense and medium dense canopy blocks. The mean elevation values of the generated 100 random points in the dense block from LiDAR, UAV nadir, and UAV oblique DTMs were 51.37m, 53.36m, and 53.95m, respectively. In the medium dense block, the mean elevation values of random points from LiDAR, UAV nadir, and UAV oblique DTMs were 50.08m, 50.32m, and 50.41m, respectively.

The mean elevation value from LiDAR DTM was lower than the mean elevations from UAV DTMs in the dense canopy block (*Table 3-2*), whereas in the medium dense canopy block difference in the elevation means

was very small (*Table 3-3*). However, there was a clear difference in the maximum elevation values between LiDAR DTMs and UAV DTMs in both the canopy density blocks. *Figures 3-9* show the distribution of random points in dense and medium dense canopy blocks. Histograms of 100 random points elevation in dense and medium dense canopy blocks from LiDAR, UAV nadir, and UAV oblique DTMs are given in *Appendix 5*.
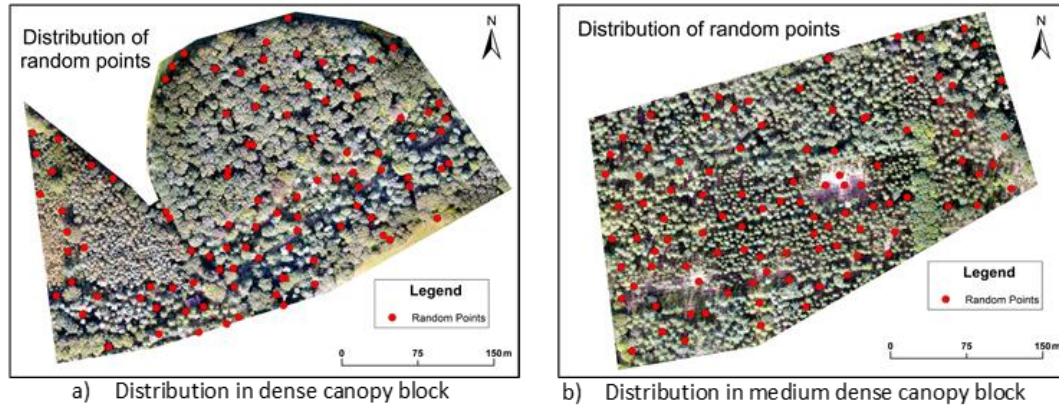


Figure 3-9. Distribution of generated random points in different canopy blocks

Table 3-2. Descriptive statistics of elevation of random points in dense canopy block

|  | Count | Mean | Std. Deviation | Minimum | Maximum |
|---|---|---|---|---|---|
| **LiDAR elevation** | 100 | 51.37 | 0.73 | 49.56 | 52.93 |
| **UAV Nadir elevation** | 100 | 53.36 | 1.89 | 50.41 | 59.73 |
| **UAV Oblique elevation** | 100 | 53.95 | 2.92 | 50.25 | 66.66 |

Table 3-3. Descriptive statistics of elevation of random points in medium dense canopy block

|  | Count | Mean | Std. Deviation | Minimum | Maximum |
|---|---|---|---|---|---|
| **LiDAR elevation** | 100 | 50.08 | 0.59 | 48.67 | 51.56 |
| **UAV Nadir elevation** | 100 | 50.32 | 0.64 | 48.52 | 53.00 |
| **UAV Oblique elevation** | 100 | 50.41 | 0.67 | 48.83 | 52.28 |

### 3.3.1. UAV nadir DTM and LiDAR DTM

From the simple linear relationship established between the elevations from UAV nadir DTM and LiDAR DTM, the $R^2$ values for dense and medium dense canopy blocks were 0.02 and 0.65, respectively. The RMSE values calculated for elevations in dense and medium dense canopy blocks were 2.77m (5.39%) and 0.45m (0.90%). In both canopy blocks, the UAV nadir DTM tends to overestimate the elevation with a bias of 1.99m in the dense canopy and 0.23m in the medium dense canopy. The scatter plots are given in *Figure 3-10*, and the regression statistics are given in *Table 3-4*.

Table 3-4. Regression statistics of elevation from UAV nadir and LiDAR DTM

|  | r | R Square | RMSE | RMSE% | Bias | Bias% |
|---|---|---|---|---|---|---|
| **Dense canopy** | 0.13 | 0.02 | 2.77 | 5.39 | 1.99 | 3.87 |
| **Medium dense canopy** | 0.80 | 0.65 | 0.45 | 0.90 | 0.23 | 0.46 |

a)  Dense canopy block    b)  Medium dense canopy block
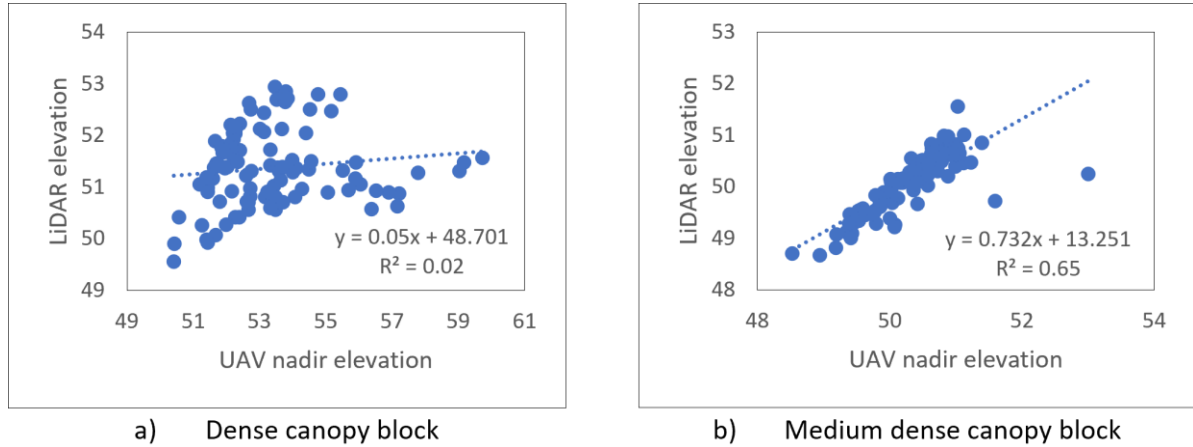
*Figure 3-10. Scatter plot of elevation from UAV nadir DTM and LiDAR DTM*

### 3.3.2.    UAV oblique DTM and LiDAR DTM

The $R^2$ values of the simple linear regression between the elevations from UAV oblique DTM and LiDAR DTM for dense and medium dense canopy blocks were 0.02 and 0.50, respectively. The RMSE values calculated for elevations in dense and medium dense canopy blocks were 3.87m (7.54%) and 0.59m (1.17%). In both the canopy density blocks, the UAV oblique DTM tends to overestimate the elevation. The bias was 2.58m in the dense canopy and 0.33m in the medium dense canopy block. The scatter plots are given in *Figure 3-11*, and the regression statistics are given in *Table 3-5*.



a)    Dense canopy block    b)    Medium dense canopy block
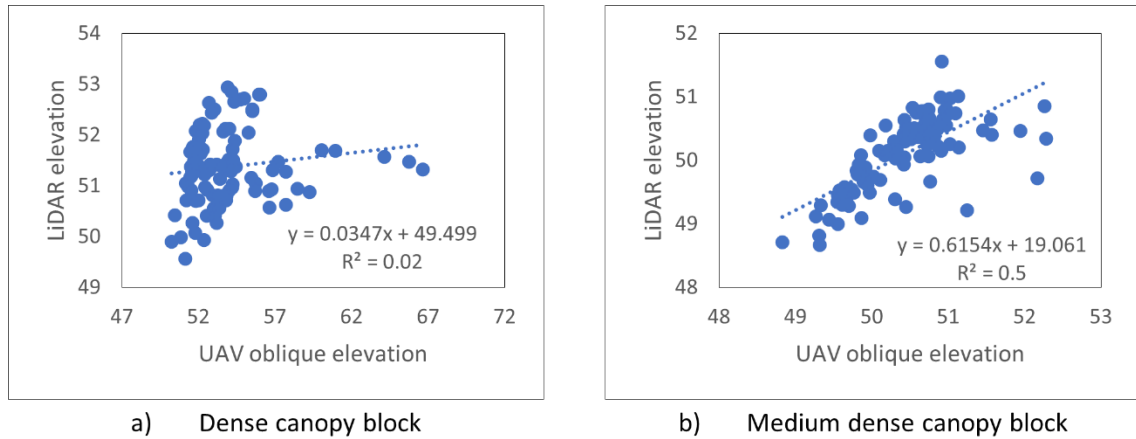
*Figure 3-11. Scatter plot of elevation from UAV oblique DTM and LiDAR DTM*

*Table 3-5. Regression statistics of elevation from UAV oblique and LiDAR DTM*

|  | r | R Square | RMSE | RMSE% | Bias | Bias% |
|---|---|---|---|---|---|---|
| **Dense canopy** | 0.14 | 0.02 | 3.87 | 7.54 | 2.58 | 5.02 |
| **Medium dense canopy** | 0.70 | 0.50 | 0.59 | 1.17 | 0.33 | 0.66 |

### 3.3.3.    DTM hypothesis testing

One-way ANOVA and Tucky HSD test at 95% confidence interval were used to answer research hypothesis one, which deals with testing if there is a significant difference between the UAV nadir, UAV oblique, and LiDAR DTMs.

In dense and medium dense canopy blocks, the results of One-way ANOVA showed a significant difference in the means of elevation ($p<0.05$). Tucky HSD post hoc follow-up test showed a significant difference

between the means of elevation from LiDAR DTM and UAV nadir DTM (p<0.05) and between LiDAR
DTM and UAV oblique DTM (p<0.05) in both dense and medium dense canopy blocks. However, there
was no significant difference between elevation means from UAV nadir and UAV oblique DTM (p>0.05)
in both dense and medium dense canopy blocks. *Appendix 6* provides the results of the One-way ANOVA
and Tukey HSD post hoc test.

## 3.4. Tree height

The mean values of tree heights extracted from LiDAR CHMs, and UAV CHMs are shown in bar graphs
given in *Figure 3-12*. A large difference is observed between the mean values of LiDAR tree height and UAV
tree height in the dense canopy block, whereas the difference is small in the medium dense canopy block
(*Figure 3-12*). The descriptive statistics of tree heights from LiDAR CHMs, UAV nadir CHMs, and UAV
oblique CHMs in different canopy density blocks are given in *Table 3-6, 3-7, and 3-8*. Histograms of tree
heights in dense and medium dense canopy blocks from different LiDAR, UAV nadir, and UAV oblique
CHMs are given in *Appendix 7 and 8*.



a)  Means of tree height in the dense canopy block



b)  Means of tree height in the medium dense canopy block

*Figure 3-12. Bar graphs of tree height means from LiDAR CHMs and UAV CHMs*

*Table 3-6. Descriptive statistics of tree height from LiDAR CHMs in different canopy density blocks*

| Canopy Density | LiDAR CHM | Count | Mean | Std. Deviation | Minimum | Maximum |
|---|---|---|---|---|---|---|
| Dense | $CHM_{50cm}$ | 113 | 24.85 | 3.24 | 15.40 | 34.59 |
| | $CHM_{1m}$ | 113 | 23.68 | 3.46 | 15.09 | 33.19 |
| Medium dense | $CHM_{50cm}$ | 171 | 22.96 | 3.91 | 11.81 | 36.51 |
| | $CHM_{1m}$ | 171 | 21.59 | 3.98 | 12.31 | 34.78 |

*Table 3-7. Descriptive statistics of tree height from UAV nadir CHMs in different canopy density blocks*

| Canopy Density | UAV Nadir CHM | Count | Mean | Std. Deviation | Minimum | Maximum |
|---|---|---|---|---|---|---|
| **Dense** | $CHM_{22cm}$ | 113 | 16.78 | 5.35 | 5.56 | 28.35 |
| | $CHM_{50cm}$ | 113 | 16.65 | 5.40 | 5.56 | 28.26 |
| | $CHM_{1m}$ | 113 | 16.54 | 5.38 | 4.82 | 27.86 |
| **Medium dense** | $CHM_{22cm}$ | 171 | 20.98 | 4.54 | 7.68 | 33.57 |
| | $CHM_{50cm}$ | 171 | 20.94 | 4.54 | 7.25 | 33.35 |
| | $CHM_{1m}$ | 171 | 20.75 | 4.57 | 6.21 | 32.83 |

*Table 3-8. Descriptive statistics of tree height from UAV oblique CHMs in different canopy density blocks*

| Canopy Density | UAV Oblique CHM | Count | Mean | Std. Deviation | Minimum | Maximum |
|---|---|---|---|---|---|---|
| **Dense** | $CHM_{22cm}$ | 113 | 16.16 | 5.71 | 4.29 | 28.42 |
| | $CHM_{50cm}$ | 113 | 16.05 | 5.72 | 4.29 | 28.42 |
| | $CHM_{1m}$ | 113 | 15.89 | 5.71 | 4.30 | 28.34 |
| **Medium dense** | $CHM_{22cm}$ | 171 | 21.18 | 4.87 | 7.27 | 34.85 |
| | $CHM_{50cm}$ | 171 | 21.13 | 4.87 | 7.10 | 34.84 |
| | $CHM_{1m}$ | 171 | 20.94 | 4.92 | 5.88 | 34.37 |

## 3.5. Tree height accuracy assessment

The second research question of this study is: How accurate are the tree heights derived from UAV-Nadir CHM and UAV-Oblique CHM under dense and medium dense canopy compared to LiDAR CHM?

To answer this research question, the accuracy assessment was performed by comparing the tree heights extracted from UAV nadir CHMs and UAV oblique CHMs of different resolutions with the tree heights extracted from LiDAR CHMs. The results are presented in the following sections.

### 3.5.1. UAV nadir tree height and LiDAR tree height

The different scenarios considered for tree height comparison in both the dense and medium dense canopy blocks are UAV $CHM_{22cm}$ vs LiDAR $CHM_{50cm}$, UAV $CHM_{50cm}$ vs LiDAR $CHM_{50cm}$, and UAV $CHM_{1m}$ vs LiDAR $CHM_{1m}$. The scatter plots are given in *Figure 3-13,* and the regression statistics are given in *Table 3-9.* Based on the r and $R^2$ values, a poor correlation is observed between the tree heights from UAV nadir CHMs and LiDAR CHMs in the dense canopy block. In contrast, in the medium dense canopy block, the correlation improved. However, between the fine resolutions of 22cm and 50cm, a very small difference is observed between the regression statistics and estimated errors in both canopy density blocks. In addition to that, the tree heights were underestimated by the UAV nadir CHMs in both the canopy density blocks, with a large bias observed in the dense canopy block.
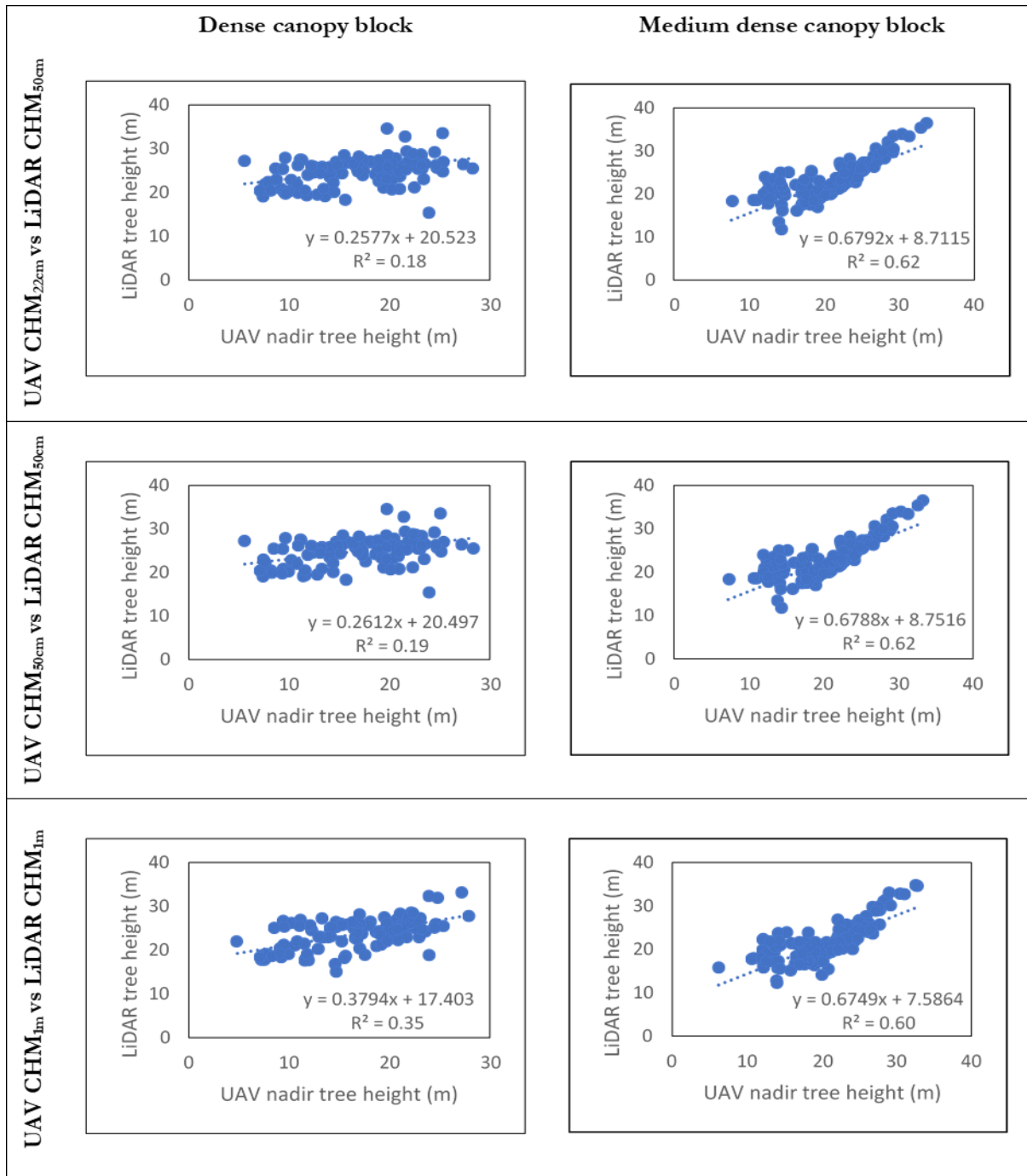
*Figure 3-13. Scatter plots of tree heights comparison between different UAV nadir CHMs and LiDAR CHMs*

*Table 3-9. Regression statistics of tree heights comparison between different UAV nadir CHMs and LiDAR CHMs*

| | | r | R² | RMSE | RMSE% | Bias | Bias% |
|---|---|---|---|---|---|---|---|
| Dense canopy | UAV CHM$_{22cm}$ vs LiDAR CHM$_{50cm}$ | 0.43 | 0.18 | 9.45 | 38.02 | -8.07 | -32.48 |
| | UAV CHM$_{50cm}$ vs LiDAR CHM$_{50cm}$ | 0.44 | 0.19 | 9.56 | 38.46 | -8.19 | -32.97 |
| | UAV CHM$_{1m}$ vs LiDAR CHM$_{1m}$ | 0.59 | 0.35 | 8.35 | 33.61 | -8.31 | -33.43 |
| Medium dense canopy | UAV CHM$_{22cm}$ vs LiDAR CHM$_{50cm}$ | 0.79 | 0.62 | 3.43 | 14.93 | -1.98 | -8.62 |
| | UAV CHM$_{50cm}$ vs LiDAR CHM$_{50cm}$ | 0.79 | 0.62 | 3.46 | 15.05 | -2.03 | -8.83 |
| | UAV CHM$_{1m}$ vs LiDAR CHM$_{1m}$ | 0.77 | 0.60 | 3.03 | 14.05 | -0.84 | -3.89 |

### 3.5.2. UAV oblique tree height and LiDAR tree height

A linear relationship was established, and tree heights from UAV oblique CHMs were compared with tree heights from LiDAR CHMs under three different scenarios, as mentioned in section 3.5.1. The scatter plots are given in *Figure 3-14*, and the regression statistics are given in *Table 3-10*. The r and R² values from *Table 3-10* prove that in the dense canopy block, the UAV oblique tree heights had a very poor relationship with the reference LiDAR tree heights for all three scenarios. In addition to that, the estimated error (RMSE and bias) was also higher for the trees in dense canopy block, with tree heights being underestimated. Whereas in the medium dense canopy block, improved correlation (r and R) was observed between the tree heights from UAV oblique CHMs and LiDAR CHMs. The RMSE and bias were also comparatively lower than the dense canopy block.
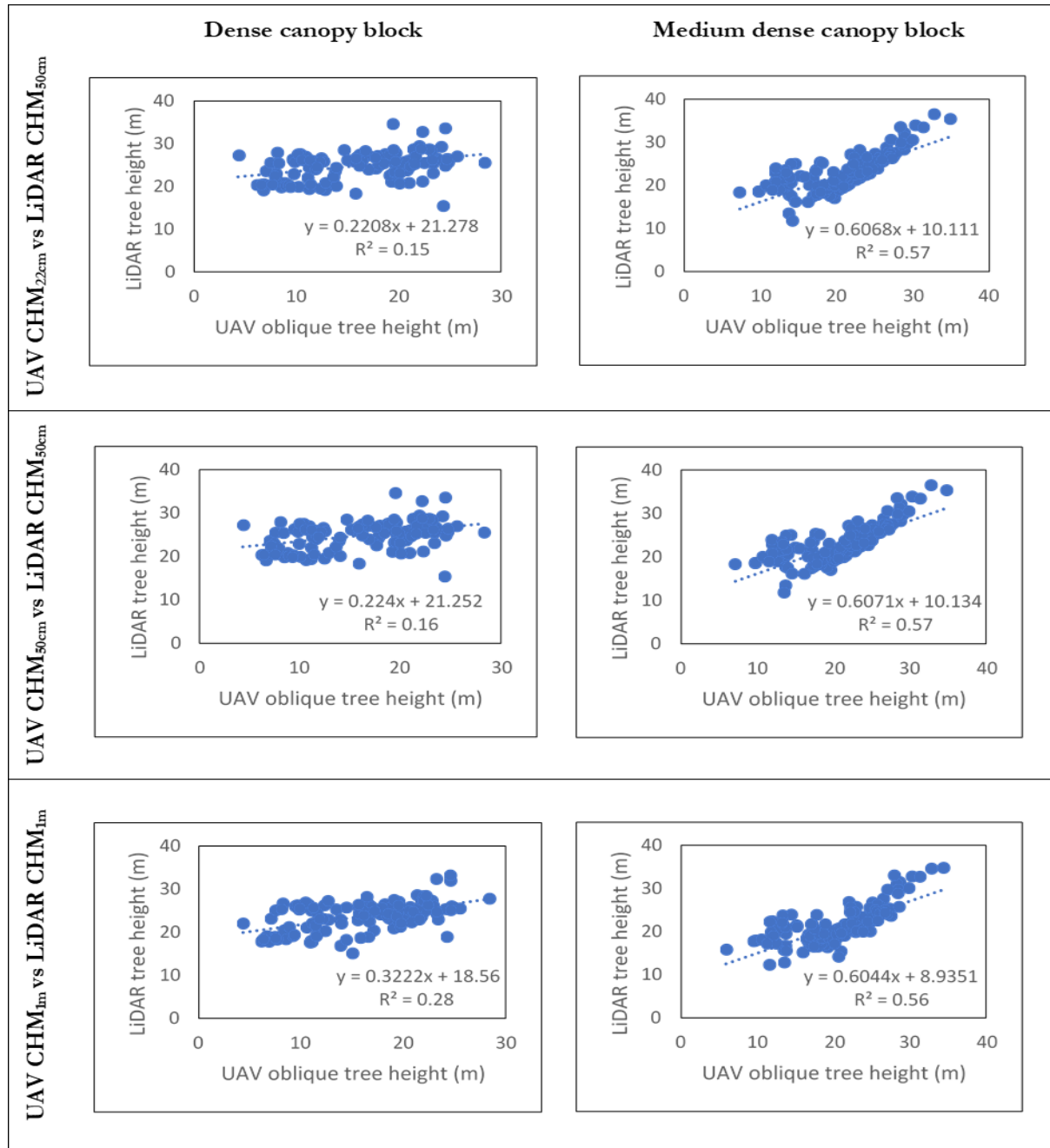


*Figure 3-14. Scatter plots of tree heights comparison between different UAV oblique CHMs and LiDAR CHMs*

*Table 3-10. Regression statistics of tree heights comparison between different UAV oblique CHMs and LiDAR CHMs*

|  |  | r | R² | RMSE | RMSE% | Bias | Bias% |
|---|---|---|---|---|---|---|---|
| **Dense canopy** | **UAV CHM$_{22cm}$ vs LiDAR CHM$_{50cm}$** | 0.39 | 0.15 | 10.20 | 41.03 | -8.07 | -34.98 |
|  | **UAV CHM$_{50cm}$ vs LiDAR CHM$_{50cm}$** | 0.40 | 0.16 | 10.28 | 41.38 | -8.80 | -35.41 |
|  | **UAV CHM$_{1m}$ vs LiDAR CHM$_{1m}$** | 0.53 | 0.28 | 9.17 | 36.90 | -8.96 | -36.06 |
| **Medium dense canopy** | **UAV CHM$_{22cm}$ vs LiDAR CHM$_{50cm}$** | 0.76 | 0.57 | 3.65 | 15.90 | -1.78 | -7.76 |
|  | **UAV CHM$_{50cm}$ vs LiDAR CHM$_{50cm}$** | 0.76 | 0.57 | 3.67 | 15.99 | -1.83 | -7.98 |
|  | **UAV CHM$_{1m}$ vs LiDAR CHM$_{1m}$** | 0.75 | 0.56 | 3.34 | 15.47 | -0.65 | -3.02 |

### 3.5.3. Tree height hypothesis testing

Research hypothesis two of this study deals with testing if there is a significant difference between the tree heights derived from UAV-Nadir, UAV-Oblique, and LiDAR CHMs. One-way ANOVA and Tucky HSD test at 95% confidence interval was used to test the hypothesis. The tests were conducted for three different scenarios, where they compared means of tree heights extracted from

1. UAV nadir CHM$_{22cm}$, UAV oblique CHM$_{22cm}$, and LiDAR CHM$_{50cm}$
2. UAV nadir CHM$_{50cm}$, UAV oblique CHM$_{50cm}$, and LiDAR CHM$_{50cm}$
3. UAV nadir CHM$_{1m}$, UAV oblique CHM$_{1m}$, and LiDAR CHM$_{1m}$

The results of the One-way ANOVA and Tucky HSD test are given in *Appendix 9, 10, and 11*, and the conclusions drawn from the results are summarised in *Table 3-11* for dense canopy block and *Table 3-12* for medium dense canopy block

*Table 3-11. Results of statistical testing comparing tree heights in the dense canopy block*

|  | Scenario 1 | Scenario 2 | Scenario 3 |
|---|---|---|---|
| **UAV Nadir TH vs LiDAR TH** | Different* | Different* | Different* |
| **UAV Oblique TH vs LiDAR TH** | Different* | Different* | Different* |
| **UAV Nadir TH vs UAV Oblique TH** | Not Different** | Not Different** | Not Different** |

*Significantly different where p<0.05
**Significantly not different where p>0.05

*Table 3-12. Results of statistical testing comparing tree heights in the medium dense canopy block*

|  | Scenario 1 | Scenario 2 | Scenario 3 |
|---|---|---|---|
| **UAV Nadir TH vs LiDAR TH** | Different* | Different* | Not Different** |
| **UAV Oblique TH vs LiDAR TH** | Different* | Different* | Not Different** |
| **UAV Nadir TH vs UAV Oblique TH** | Not Different** | Not Different** | Not Different** |

*Significantly different where p<0.05
**Significantly not different where p>0.05

The statistical test results summarized in *Table 3-11* show that in the dense canopy block, resampling the spatial resolution from finer 22cm to 50cm or from 50cm to coarser 1m resolution did not have any effect on tree heights extracted. Whereas in medium dense canopy block (*Table 3-12*), resampling from finer 50cm to coarser 1m resolution did affect the tree heights extracted. However, there was no significant difference between tree heights extracted from UAV nadir CHMs and UAV oblique CHMs in both dense and medium dense canopy blocks in all the scenarios.

## 3.6. DBH model development and validation

Research question three of this study is: How accurate is the DBH modeled using tree parameters extracted from UAV-Nadir images and UAV-Oblique images under dense and medium dense canopy compared to field-measured DBH?

To answer this research question, the best trees that were recognizable on orthophoto were selected from each canopy density block, and outliers were ignored. The trees that were partially seen on orthophoto and the trees with huge CPA but small DBH (due to field measurement errors) were considered outliers. A total of 100 trees in dense canopy block and 144 trees in medium dense canopy block were selected. They were divided into 60:40 for model building and validation.

### 3.6.1. UAV nadir model development

In dense canopy block, 60 trees (60% of the total trees considered) were used to model DBH. Among the different regression models and predictors used, the Quadratic model ($y = -0.0011x^2 + 0.4978x + 20.057$) with CD*TH as predictors performs better in the dense canopy (higher $R^2$ and lower RMSE). It explains about 54% of the variance in the DBH ($R^2 = 0.54$, RMSE = 11.36cm).

In the medium dense canopy block, 86 trees (60% of total trees) were used to develop the model. The quadratic model with CD*TH as predictors performed better by explaining about 80% of DBH variance ($R^2 = 0.8$ and RMSE = 3.77cm). Summary of different models used to predict the DBH using UAV nadir derived parameters in dense and medium dense canopy blocks are given in *Table 3-13* and *Appendix 12*. The scatter plots of the parameter (TH*CD) used and field-measured DBH in different canopy density blocks are given in *Figure 3-15*, and the regression statistics are given in *Table 3-14*.

*Table 3-13. DBH model development using UAV nadir derived parameters in different canopy density blocks*

|  | Predictor (X) | Model | Equation | R2 | RMSE |
|---|---|---|---|---|---|
| **Dense canopy** | CPA | Linear | $y = 0.3703x + 28.825$ | 0.52 | 11.68 |
|  | CD | Linear | $y = 9.1869x + 12.757$ | 0.53 | 11.56 |
|  | TH | Linear | $y = 1.7199x + 18.423$ | 0.32 | 13.88 |
|  | CD*TH | Linear | $y = 0.3418x + 24.33$ | 0.53 | 11.48 |
|  | CD*TH | Logarithmic | $y = 16.991\ln(x) - 20.847$ | 0.50 | 11.84 |
|  | CD*TH | **Quadratic** | **$y = -0.0011x^2 + 0.4978x + 20.057$** | **0.54** | **11.36** |
|  | CD*TH | Power | $y = 8.5864x^{0.4087}$ | 0.53 | 11.56 |
| **Medium dense canopy** | CPA | Linear | $y = 0.6402x + 21.139$ | 0.71 | 4.60 |
|  | CD | Linear | $y = 11.132x + 6.8908$ | 0.72 | 4.50 |
|  | TH | Linear | $y = 1.5619x - 0.2863$ | 0.47 | 6.16 |
|  | CD*TH | Linear | $y = 0.3522x + 14.911$ | 0.79 | 3.87 |
|  | CD*TH | Logarithmic | $y = 19.755\ln(x) - 43.382$ | 0.77 | 4.03 |
|  | CD*TH | **Quadratic** | **$y = -0.0013x^2 + 0.5241x + 9.9775$** | **0.80** | **3.77** |
|  | CD*TH | Power | $y = 3.4675x0.5749$ | 0.79 | 3.80 |

*Table 3-14. Regression statistics of models used to predict DBH (UAV nadir) in different canopy blocks*

| Canopy Density | r | R Square | RMSE | RMSE% | Bias | Bias% |
|---|---|---|---|---|---|---|
| **Dense canopy** | 0.73 | 0.54 | 11.36 | 23.92 | -0.16 | -0.34 |
| **Medium dense canopy** | 0.89 | 0.80 | 3.77 | 11.33 | -0.10 | -0.31 |
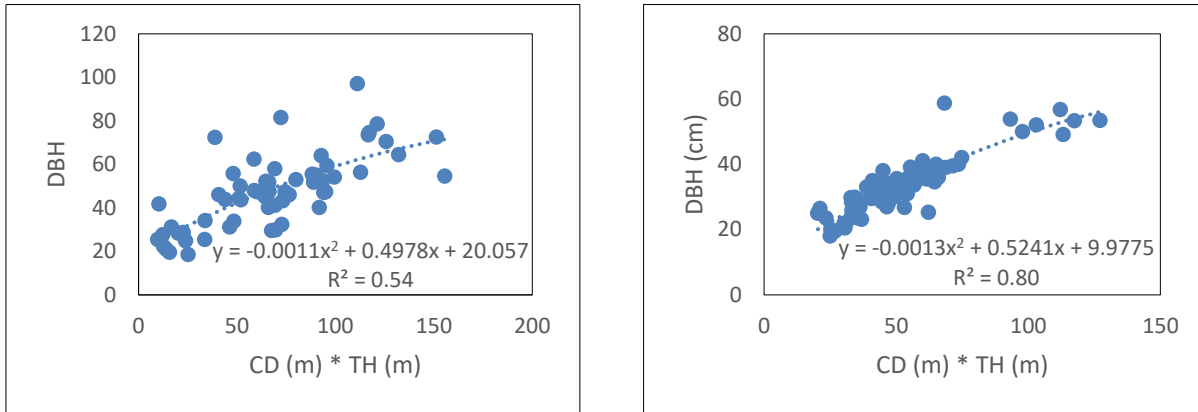
a) Scatter plot of CD*TH and field measured DBH in dense canopy block

b) Scatter plot of CD*TH and field measured DBH in medium dense canopy block

*Figure 3-15. Scatter plots of parameter estimated from UAV nadir dataset (CD\*TH) and field-measured DBH in different canopy blocks*

### 3.6.2. UAV oblique model development

The same trees considered earlier during UAV nadir-based model development were used for DBH model development using tree parameters derived from the UAV oblique dataset. In dense canopy block, the Quadratic model using CPA digitized from UAV oblique orthophoto as a lone predictor performed better in predicting the DBH. It explained about 52% of the variance in the DBH ($R^2 = 0.52$, RMSE = 11.57cm). In the medium dense canopy block, the quadratic model with CD*TH as predictors performed better in predicting the DBH. It explained about 77% of the variance in DBH ($R^2 = 0.77$ and RMSE = 4.08cm). *Table 3-15* summarizes the different models used to predict the DBH in dense and medium dense canopy blocks. The summary of other models tested are given in *Appendix 13*. The scatter plots of the parameter used and field measured DBH in different canopy density blocks are given in *Figure 3-16*, and the regression statistics are given in *Table 3-16*.

*Table 3-15. DBH model development using UAV oblique derived parameters in different canopy density blocks*

|  | Predictor (X) | Model | Equation | R2 | RMSE |
|---|---|---|---|---|---|
| **Dense canopy** | CPA | Linear | y = 0.3637x + 28.73 | 0.51 | 11.73 |
|  | CPA | Logarithmic | y = 15.761ln(x) - 10.842 | 0.50 | 11.87 |
|  | CPA | **Quadratic** | **y = -0.0011x² + 0.5066x + 25.62** | **0.52** | **11.57** |
|  | CPA | Power | y = 11.155x0.3734 | 0.52 | 11.69 |
|  | CD | Linear | y = 9.2313x + 12.106 | 0.52 | 11.59 |
|  | TH | Linear | y = 1.4854x + 23.131 | 0.27 | 14.31 |
|  | CD*TH | Linear | y = 0.3266x + 25.733 | 0.50 | 11.82 |
| **Medium dense canopy** | CPA | Linear | y = 0.632x + 20.685 | 0.67 | 4.86 |
|  | CD | Linear | y = 10.89x + 6.7556 | 0.68 | 4.81 |
|  | TH | Linear | y = 1.3959x + 2.8671 | 0.42 | 6.45 |
|  | CD*TH | Linear | y = 0.3484x + 14.399 | 0.77 | 4.09 |
|  | CD*TH | Logarithmic | y = 18.957ln(x) - 41.032 | 0.73 | 4.42 |
|  | CD*TH | **Quadratic** | **y = -0.0005x² + 0.4151x + 12.494** | **0.77** | **4.08** |
|  | CD*TH | Power | y = 3.6083x0.559 | 0.75 | 4.14 |

*Table 3-16. Regression statistics of models used to predict DBH (UAV oblique) in different canopy blocks*

| Canopy Density | r | R Square | RMSE | RMSE% | Bias | Bias% |
|---|---|---|---|---|---|---|
| Dense canopy | 0.72 | 0.52 | 11.57 | 24.37 | 0.13 | 0.29 |
| Medium dense canopy | 0.89 | 0.77 | 4.08 | 12.26 | 0.01 | 0.04 |
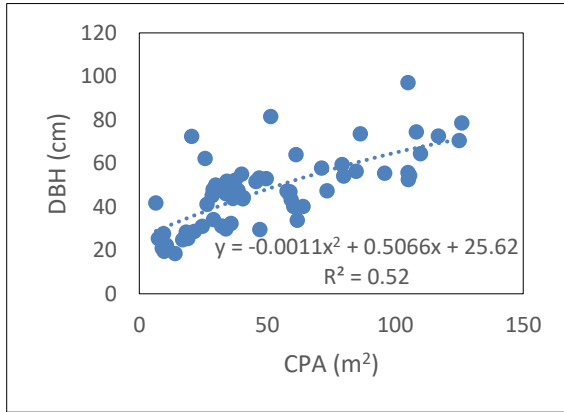


a) Scatter plot of CPA and field measured DBH in dense canopy block
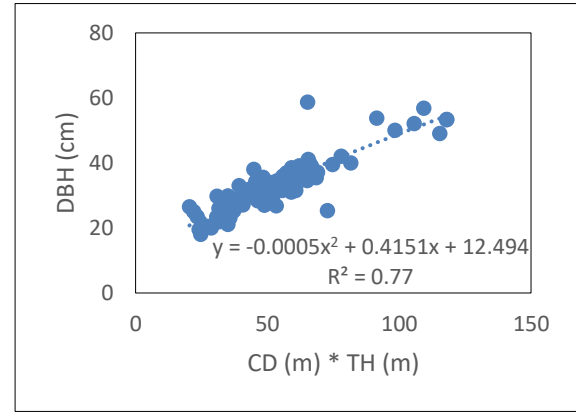
b) Scatter plot of CD*TH and field measured DBH in medium dense canopy block

*Figure 3-16. Scatter plots of parameters estimated from UAV oblique dataset and field measured DBH in different canopy blocks*

### 3.6.3. UAV nadir model validation

In dense and medium dense canopy blocks, a total of 40 and 58 trees (40% of the total trees considered) were used to validate the DBH model. The Quadratic model using CD*TH as preditors was used to predict tree DBH in the dense ($y = -0.0011x^2 + 0.4978x + 20.057$) and medium dense canopy blocks ($y = -0.0013x^2 + 0.5241x + 9.9775$). The accuracy of the predicted DBH was assessed by comparing it with field-measured DBH. The $R^2$ of the simple linear relationship established between the model predicted DBH and filed measured DBH in the dense and medium dense canopy blocks were 0.79 and 0.88, respectively. The RMSE values of the predicted DBH were 10.44cm (23.10%) and 3.78cm (10.65%), respectively, in the dense and medium dense canopy blocks. The models overestimated the DBH with a bias of 6.38cm in the dense canopy and underestimated with a bias of -0.45cm in the medium dense canopy. The scatter plots are given in *Figure 3-17*, and the regression statistics are given in *Table 3-17*.
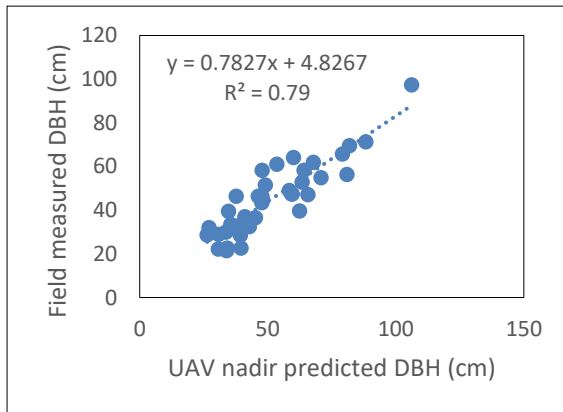


a) Scatter plot of predicted DBH and field measured DBH in dense canopy block
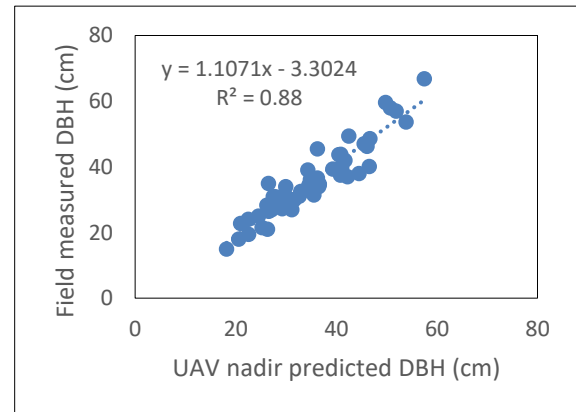
b) Scatter plot of predicted DBH and field measured DBH in medium dense canopy block

*Figure 3-17. Scatter plot of DBH predicted from UAV nadir validation model and field measured DBH in different canopy density blocks*

*Table 3-17. Regression statistics of UAV nadir validation models in different canopy density blocks*

|  | r | R Square | RMSE | RMSE% | Bias | Bias% |
|---|---|---|---|---|---|---|
| **Dense canopy** | 0.89 | 0.79 | 10.44 | 23.10 | 6.38 | 14.11 |
| **Medium dense canopy** | 0.94 | 0.88 | 3.78 | 10.65 | -0.45 | -1.27 |

### 3.6.4. UAV oblique model validation

The same trees used for UAV nadir-based model validation were used for UAV oblique-based DBH model validation. The Quadratic model with CPA and CD*TH as a predictor was used to predict the DBH in the dense ($y = -0.0011x^2 + 0.5066x + 25.62$) and medium dense canopy block ($y = -0.0005x^2 + 0.4151x + 12.494$), respectively. The $R^2$ of the simple linear relationship established between the model predicted DBH and filed measured DBH in the dense and medium dense canopy blocks were 0.72 and 0.87, respectively. The RMSE values of the predicted DBH were 8.57cm (18.99%) and 3.89cm (10.95%), respectively, in the dense and medium dense canopy. The models overestimate the DBH with a bias of 1.26cm in the dense canopy and underestimated with a bias of -0.18cm in the medium dense canopy. The scatter plots are given in *Figure 3-18*, and the regression statistics are given in *Table 3-18*.



a) Scatter plot of predicted DBH and field measured DBH in dense canopy block

b) Scatter plot of predicted DBH and field measured DBH in medium dense canopy block
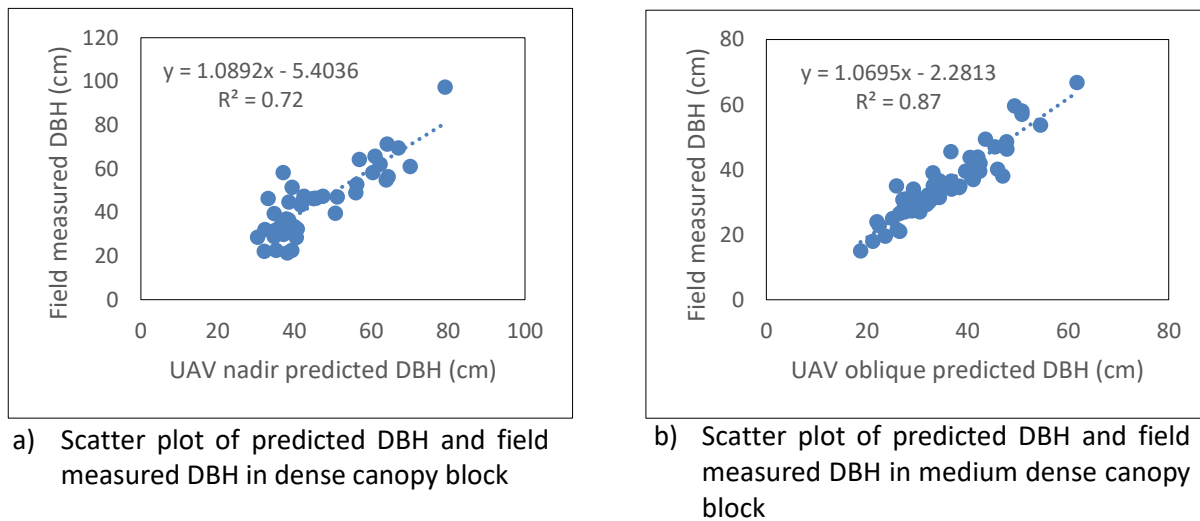
*Figure 3-18. Scatter plot of DBH predicted from UAV oblique validation model and field measured DBH in different canopy density blocks*

*Table 3-18. Regression statistics of UAV oblique validation models in different canopy density blocks*

|  | r | R Square | RMSE | RMSE% | Bias | Bias% |
|---|---|---|---|---|---|---|
| **Dense canopy** | 0.85 | 0.72 | 8.58 | 18.99 | 1.26 | 2.79 |
| **Medium dense canopy** | 0.93 | 0.87 | 3.89 | 10.95 | -0.18 | -0.49 |

### 3.6.5. DBH hypothesis testing

One-way ANOVA was used to answer the research hypothesis three dealing with testing if there is a significant difference between the DBH modeled from UAV-Nadir and UAV-Oblique derived tree parameters and field-measured DBH. In dense and medium dense canopy blocks, the One-way ANOVA test showed no significant difference between the means of field-measured DBH and DBH predicted using parameters estimated from the UAV nadir dataset and UAV oblique dataset ($p>0.05$). The One-way ANOVA test results for dense and medium dense canopy blocks are given in *Appendix 14*.

### 3.7. AGB estimation

The AGB was calculated for 113 trees in the dense canopy block and 171 trees in the medium dense canopy block using the allometric equations given in *Table 2-6*. The LiDAR-based AGB values were estimated using LiDAR tree height ($CHM_{50cm}$) and field measured DBH. The UAV nadir-based AGB and oblique-based AGB were estimated using tree heights from UAV nadir ($CHM_{50cm}$) and UAV oblique ($CHM_{50cm}$). The descriptive statistics of the AGB from different datasets in dense and medium dense canopy blocks are given in *Table 3-19*.

*Table 3-19. The descriptive statistics of the AGB (Mg/tree) from different datasets in dense and medium dense blocks*

| Canopy Density | AGB | Count | Mean | Std. Deviation | Minimum | Maximum | Sum |
|---|---|---|---|---|---|---|---|
| **Dense** | LiDAR based | 113 | 2.03 | 1.51 | 0.22 | 7.37 | 228.89 |
| | UAV nadir based | 113 | 1.50 | 1.25 | 0.14 | 6.97 | 169.36 |
| | UAV oblique based | 113 | 1.45 | 1.25 | 0.14 | 7.03 | 164.30 |
| **Medium dense** | LiDAR based | 171 | 1.01 | 0.74 | 0.11 | 4.39 | 173.54 |
| | UAV nadir based | 171 | 0.94 | 0.69 | 0.06 | 4.16 | 160.91 |
| | UAV oblique based | 171 | 0.95 | 0.69 | 0.06 | 4.16 | 162.02 |

In dense canopy block, the One-way ANOVA test showed that there was a significant difference between the means of AGB calculated using LiDAR-based, UAV nadir-based, and UAV oblique-based tree heights (p<0.05). Tucky HSD post hoc follow-up test revealed that there was a significant difference between LiDAR-based AGB and UAV nadir-based AGB (p<0.05) and between LiDAR-based and UAV oblique-based AGB (p<0.05). However, there was no significant difference between UAV nadir-based AGB and UAV oblique-based AGB.

One-way ANOVA test showed that there was no significant difference between the means of AGB calculated using LiDAR-based, UAV nadir-based, and UAV oblique-based tree heights in medium dense canopy block (p>0.05). The results of the statistical tests are given in *Appendix 15*.

### 3.8. Sensitivity analysis

Research question four of this study is: What is the effect of tree height estimation errors on AGB estimation under dense and medium dense canopy?

A sensitivity analysis was done in a controlled manner by selecting 30 trees in each canopy density block to answer this question. These trees were from all plots in each canopy density and included at least one tree from each species. The descriptive statistics of the selected trees from different blocks are given in *Table 3-20*.

*Table 3-20. Descriptive statistics of selected trees AGB (Mg/tree)*

| Canopy Density | AGB | Count | Mean | Std. Deviation | Minimum | Maximum |
|---|---|---|---|---|---|---|
| **Dense** | LiDAR based | 30 | 3.23 | 1.56 | 0.27 | 7.07 |
| | UAV nadir based | 30 | 2.33 | 1.11 | 0.15 | 5.36 |
| | UAV oblique based | 30 | 2.27 | 1.11 | 0.14 | 5.33 |
| **Medium dense** | LiDAR based | 30 | 1.18 | 0.86 | 0.11 | 3.34 |
| | UAV nadir based | 30 | 1.09 | 0.78 | 0.13 | 3.06 |
| | UAV oblique based | 30 | 1.10 | 0.79 | 0.12 | 3.23 |

To assess the effect of tree height estimation errors on the AGB estimates, the tree heights extracted from UAV nadir ($CHM_{50cm}$) and UAV oblique ($CHM_{50cm}$) were inflated and deflated according to the quantified error (RMSE). In the dense canopy block, the tree heights extracted from UAV nadir ($CHM_{50cm}$) were inflated and deflated by 9.56 m. The tree heights from the UAV oblique ($CHM_{50cm}$) were inflated and deflated by 10.28 m, then the corresponding AGB was calculated. Similarly, in the medium dense block, UAV nadir ($CHM_{50cm}$) tree heights were inflated and deflated by 3.46m, and the UAV oblique ($CHM_{50cm}$) tree heights were inflated and deflated by 3.67m.

*Table 3-21* provides the mean AGB values from different datasets. There is a very small difference between the means of the inflated and deflated AGB in both the UAV nadir based and UAB oblique based estimates in the medium dense canopy block. Whereas in the dense canopy block, the difference between the inflated and deflated AGB is higher in both the UAV nadir and UAV oblique-based estimates.

*Table 3-21. Mean AGB estimated using different datasets*

|  | Dense canopy | Medium dense canopy |
|---|---|---|
|  | AGB (Mg/tree) | AGB (Mg/tree) |
| **UAV nadir inflated** | 3.45 | 1.23 |
| **UAV nadir deflated** | 1.20 | 0.95 |
| **UAV oblique inflated** | 3.47 | 1.25 |
| **UAV oblique deflated** | 1.04 | 0.95 |

The variation in biomass of the 30 selected trees in dense and medium dense canopy block due to the errors in tree height are shown as bar graphs given in *Appendix 16*.

The fourth research hypothesis of this study is to test if the tree height estimation errors have a significant effect on AGB estimates. One-way ANOVA and Tucky HSD test were used to test this hypothesis. In the dense canopy, One-way ANOVA and Tucky HSD post hoc showed there was a significant difference between the mean values of AGB estimated using the actual UAV nadir tree height, inflated UAV nadir tree height, and deflated UAV nadir tree height ($p < 0.05$). Similar results were observed while comparing the mean values of AGB estimated from actual UAV oblique tree height, inflated UAV oblique tree height, and deflated UAV oblique tree height ($p < 0.05$) in dense canopy block. Thus proving that in dense canopy block, the errors in tree height estimation affect the AGB estimation.

However, in the medium dense canopy block, the One-way ANOVA test showed no significant difference between the mean values of AGB estimated using UAV nadir tree height, inflated and deflated UAV nadir tree height ($p > 0.05$), and also between actual UAV oblique tree height, inflated and deflated UAV oblique tree heights ($p > 0.05$). Thus, the errors in tree height estimation do not affect AGB estimation in the medium dense canopy block. The results of statistical tests are presented in *Appendix 17*.

# 4. DISCUSSION

## 4.1. Field measured DBH

The DBH measured during fieldwork for this study is right-skewed in both the dense canopy (skewness: 0.73) and medium dense canopy (skewness: 0.65). The skewness could be because during fieldwork trees with DBH less than 10cm were not measured as they do not contribute significantly to AGB estimation (Brown, 1997).

The average DBH (46.06cm) in the dense block is higher than the average DBH (33.74cm) in the medium dense block. The reason for the variation in average DBH could be the difference in species predominance, and ground truth data collection standards followed. The dense block was characterized by mature deciduous trees with interlocking tree crowns, and only huge trees that were visible on orthophoto were measured within the sample plot. Whereas young coniferous trees planted at intervals characterized the medium dense block, and almost all trees were sampled within the plot as they were visible on orthophoto. The selective measurement in the dense block could also be the reason for higher skewness in the dense block when compared to the medium dense block.

## 4.2. DTM accuracy

The first objective of this study was to assess the accuracy of DTM built from UAV nadir and UAV oblique data set, and the DTM from airborne LiDAR was used as a reference. Crespo-Peremarch, Torralba, Carbonell-Rivera, and Ruiz (2020), in their study, also assessed the accuracy of DTM generated from different data sources. They reported that the DTM generated from ALS data is the most accurate and closely resembles reality. Similar results were observed in this study when the LiDAR DTM was validated with 3D coordinates from GNSS (r = 0.95, R² = 0.9, RMSE = 0.25m). It is also important to note that the LiDAR data used in this study were acquired in the leaf-off season (February 2019), which also contributed to the improved accuracy of LiDAR DTM. Similar results were observed in the study by Simpson, Smith, and Wooster (2017), where they compared leaf-on and leaf-off LiDAR DTM with field measured elevation values (leaf-off DTM RMSE = 0.22m).

Crespo-Peremarch et al. (2020) stated that the canopy density influences the accuracy of DTM generated from the UAV SfM model. Under a dense canopy, the DTM is subjected to large errors. In their study under a dense canopy, the RSME of UAV DTM generated ranged between 1.5m to 7m. Similar results were observed in this study also where the RMSE (RMSE%) of UAV DTM generated from the nadir and oblique data sets in dense canopy block were 2.77m (5.39%) and 3.87m (7.54%). Crespo-Peremarch et al. (2020) and Wallace et al. (2016) stated that the accuracy of UAV DTM improves under sparse vegetation, and similar results are observed in this study. The RMSE of UAV nadir DTM and UAV oblique DTM in medium dense canopy block was lower than that in dense canopy block *(Table 3-4 and 3-5)*. In this study, the UAV nadir and UAV oblique DTM overestimated the elevation in both the dense and medium dense canopy. The bias was higher for dense canopy block when compared to medium dense canopy block *(Table 3-4 and 3-5)*.

The main reason for high RMSE and bias in the dense block is the limited ground surface visibility and the interpolation that caused overestimation. While generating the DTM, the gaps in the ground surface under a tree canopy are interpolated from the neighboring pixels (Kosmatin Fras, Kerin, Mesarič, Peterman, & Grigillo, 2016). The accuracy of the interpolated DTM is influenced by the number, distribution, and quality of pixels considered (Gosciewski, 2013). The dense canopy block in this study is characterized by interlocking tree crowns and dense understory vegetation, thus limiting the UAV from imaging the actual

ground. Consequently, a very small number of points that represented the ground is used for DTM interpolation. In addition to that, the understory vegetation in the dense canopy block influenced the elevation values of ground points. Therefore neighboring pixels considered for interpolation had higher elevation, leading to overestimating DTM elevation (Mlambo et al., 2017; Wallace et al., 2016).

*Table 4-1* shows the total number of ground points considered to interpolate DTM and ground points per square meter in dense and medium dense canopy blocks. The points per square meter in dense canopy block (Nadir: 9 points/m² and Oblique: 7 points/ m²) is lower than the medium dense canopy block (Nadir: 30 points/m² and Oblique: 27 points/ m²) in both the UAV nadir and UAV oblique 3D point cloud. *Figure 4-1* shows the distribution of ground points from UAV nadir and oblique SfM 3D point cloud considered for DTM interpolation. From *Figure 4-1*, it is clear that there are considerable huge gaps in the dense canopy block, whereas the gaps are comparatively small in the medium dense block, thereby producing higher RMSE and bias in dense canopy block and lower RMSE and bias in the medium dense block. Similar results were observed in the study by Obeng-Manu (2019), where the author compared the accuracy of UAV DTM under open, medium, and dense canopy conditions and concluded that the number of ground points in the dense canopy was lower and resulted in higher RMSE.

*Table 4-1. Ground points considered for DTM interpolation in different canopy density blocks*

|  |  | UAV nadir point cloud | UAV oblique point cloud |
|---|---|---|---|
| **Dense Canopy** | **Total Points** | 948297 | 708512 |
|  | **Points / m²** | 9 | 7 |
| **Medium dense canopy** | **Total Points** | 2904319 | 2659278 |
|  | **Points / m²** | 30 | 27 |

In this study, the accuracy of UAV oblique DTM was lower than the accuracy of UAV nadir DTM for both the dense and medium dense canopy blocks (*Table 3-4 and 3-5*). This can be attributed to the difference in the number of ground points considered for DTM interpolation from UAV nadir and oblique point cloud (*Table 4-1*). Even though the total number of 3D densified points in the oblique point cloud was higher than that of the nadir point cloud (*Appendix 2*), the number of ground points in the UAV oblique point cloud is less than the number of ground points in UAV nadir point cloud. The difference in ground point may be attributed to the classification algorithm used by Pix4Dmapper. Pix4Dmapper uses machine learning algorithms to classify points in the 3D point cloud to various classes. Features like the color (point and neighborhood color) and geometry (vertical height range, height below, height above, and covariance) are used to classify points (Becker, Rosinskaya, Häni, D'Angelo, & Strecha, 2018; "How to generate the point cloud classification – Support," 2021). In this case, the information about the forest structures from oblique images might have influenced the 3D point cloud classification, subsequently affecting the number of classified ground points.

The results of this study contradicted the results of the study by Meinen and Robinson (2020). Meinen and Robinson (2020) compared the accuracy of surface models built from UAV SfM incorporating oblique images and nadir images in combination and concluded that incorporating oblique images improved the accuracy of surface models. However, it is to be noted that the study of Meinen and Robinson (2020) was carried out in an agricultural terrain, and oblique images were acquired at both east and west-facing directions. Whereas this study was carried out in a forest with different canopy densities and, the oblique images were acquired in only an east-facing direction. Nevertheless, the statistical analysis proved no significant difference between mean elevation from UAV nadir and UAV oblique DTM in both the dense and medium dense canopy block.
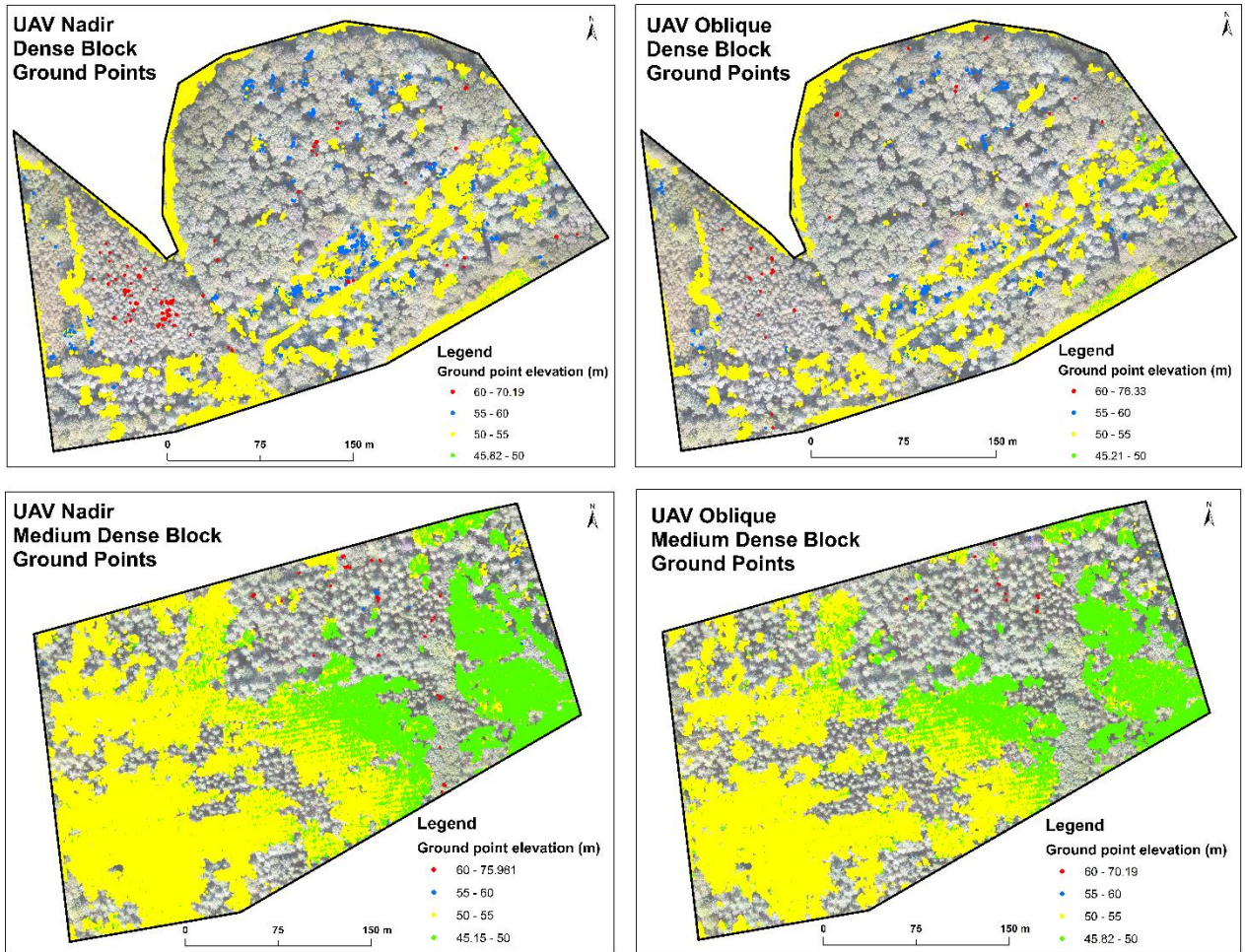
*Figure 4-1. Map showing ground points from UAV nadir and oblique 3D point cloud used for DTM generation*

## 4.3. Tree height accuracy

The second objective of this study is to assess the accuracy of tree heights from UAV nadir and oblique datasets. In dense canopy block, the tree heights derived from both the UAV nadir and UAV oblique CHMs of three different spatial resolutions showed a very poor correlation with LiDAR CHM and had high RMSE (*Table 3-9 and 3-10*). The accuracy of tree height in the medium dense canopy block from the UAV nadir and oblique CHMs were higher than the dense canopy block (*Table 3-9 and 3-10*). One of the main reasons for the high RMSE and poor correlation in the dense block is the poor quality of DTM generated (Iizuka et al., 2017). The accuracy of DTM plays a crucial role in the accuracy of tree height extracted from CHM (Fawcett et al., 2019). The errors from the DTM have propagated to the CHM, thus causing the higher RMSE in tree heights in the dense block. The error propagation is also evident through the tree height bias calculated (*Table 3-9, 3-10*). The tree heights in both the dense and medium dense blocks were underestimated, whereas the elevation from DTMs where overestimated.

This study's tree height accuracy is lower than the other studies that used UAV nadir data. (Birdal et al., 2017; Iizuka et al., 2017; Krause et al., 2019; Moe et al., 2020). It is important to note that Birdal et al. (2017) conducted the study in an open urban forest and compared the tree heights to field measurements. Krause et al. (2019) used a lower UAV flying height than the flying height used in this study, resulting in higher point cloud density and higher spatial resolution, and Moe et al. (2020) normalized the UAV DTM with

LiDAR DTM. The outlined difference in methods used and complexity of forest canopy could have caused the variations in the results produced.

In both dense and medium dense canopy blocks, it is observed that resampling the spatial layers to a coarser 1m resolution affects the accuracy of tree height extracted. In both the dense and medium dense canopy block, at 1m resolution, the RMSE of extracted tree heights was reduced (*Table 3-9, 3-10*). In addition to that, in the medium dense block, at 1m spatial resolution, the statistical analysis showed no significant difference between the tree heights extracted from UAV CHM (nadir and oblique) and LiDAR CHM. The reason for reduced RMSE could be the smoothing effect (extreme values smoothened) due to resampling.

There was no significant difference between the tree height extracted from the UAV nadir CHMs and UAV oblique CHMs in dense and medium dense canopy blocks. This is also because the DTMs generated from UAV nadir and oblique datasets did not differ significantly. No study was found that compared the UAV nadir derived tree heights and UAV oblique derived tree heights under different forest canopy densities. However, Lin et al. (2018) and Zhou and Zhang (2020) used UAV oblique images to estimate tree heights in their respective studies. Both the studies reported a good correlation ($R^2$ ranging between 0.8 to 0.9) between field-measured tree height and tree height extracted from UAV oblique CHM. Lin et al. (2018) carried out their study in a sparse coniferous stand, and oblique images were acquired at 70 degrees view angle (20 degrees tilt off-nadir). Lin et al. (2018) attributed the good correlation they achieved to the low canopy density of the study area. Zhou and Zhang (2020) used images acquired at nadir and five different oblique angles to study plantation forests and normalized the point cloud with the ALS point cloud. From the results of this study and the studies by Lin et al. (2018) and Zhou & Zhang (2020), it is clear that the accuracy of tree heights extracted from UAV oblique datasets depends on the structural complexity of the forest and the choice of the oblique view angle.

## 4.4. Tree DBH estimation

The third objective of this study is to assess the accuracy of DBH modeled using tree parameters like CPA, CD, and tree height derived from UAV nadir and oblique datasets. Iizuka et al. (2017) stated that the models using crown parameters like CPA and CD as predictors perform better than the models using tree height as a lone predictor. Similar results were observed in this study in both the dense and medium dense canopy blocks. The $R^2$ of the model using CPA or CD as a predictor was greater than the $R^2$ of the model using tree height as a lone predictor (*Table 3-13, 3-15 and Appendix 12, 13*).

Jucker et al. (2017), in their study, used tree height and CD as a compound variable (TH*CD) to predict DBH and found that the TH*CD model performed better than the model that used tree height or CD as a lone predictor. One of the reasons for the poor performance of the tree height-DBH model could be the difficulty in estimating tree height from the UAV dataset due to the uncertainties in the interpolated surface models (Iizuka et al., 2017). Another reason could be that the tree height is influenced by neighborhood competition. The trees tend to grow faster to compete for sunlight at an early stage, whereas the DBH grows throughout its life span, resulting in trees of similar heights having different DBH. Therefore using tree height as a lone predictor becomes a problem in DBH modeling (Iizuka et al., 2017; Jucker et al., 2017; King, 2005). Jucker et al. (2017) stated that while modeling DBH using the compound product TH*CD, CD played an essential role in differentiating trees having the same height but different DBH, thereby improving the model accuracy.

In the medium dense block, for both the UAV nadir and UAV oblique datasets, the model with TH*CD performed better (*Table 3-13 and 3-15*). In the dense block of this study, TH*CD proved to be better predictors of DBH for the UAV nadir dataset (*Table 3-13*). Whereas for the UAV oblique dataset in the

dense block, CPA performed better in predicting DBH (*Table 3-15*). The reason could be the large error associated with tree heights extracted from UAV oblique CHM (RMSE = 10.28m). In addition to that, the crown diameter was calculated using *Eq (9)*, assuming the crowns to be a circle. However, as mentioned earlier, the dense block had trees with interlocking crowns, which may have affected the tree crown's lateral expansion and made the crown shapes elongated. Therefore generalizing them to be circles and calculating the crown diameter may have added to the error. Also, few deciduous trees like common ash and oak with interlocking tree crowns were challenging to delineate from orthophoto. Those trees affected the DBH modeling accuracy in the dense canopy block (*Figure 3-15a, 3-16a*). Nevertheless, the statistical analysis of this study proves that there is no significant difference between the DBH estimated using UAV-derived parameters and field-measured DBH in both the dense and medium dense canopy (*Appendix 14*).

Another important thing to note is that for some isolated coniferous trees, the crown edges were observed better in UAV oblique orthophoto. Whereas for deciduous trees, not much notable difference was observed. *Figure 4-2* shows the difference in crown between UAV nadir orthophoto and UAV oblique orthophoto. However, statistical tests show no significant difference between the CPA from nadir orthophoto and oblique orthophoto in both the canopy densities (*Appendix 18*).
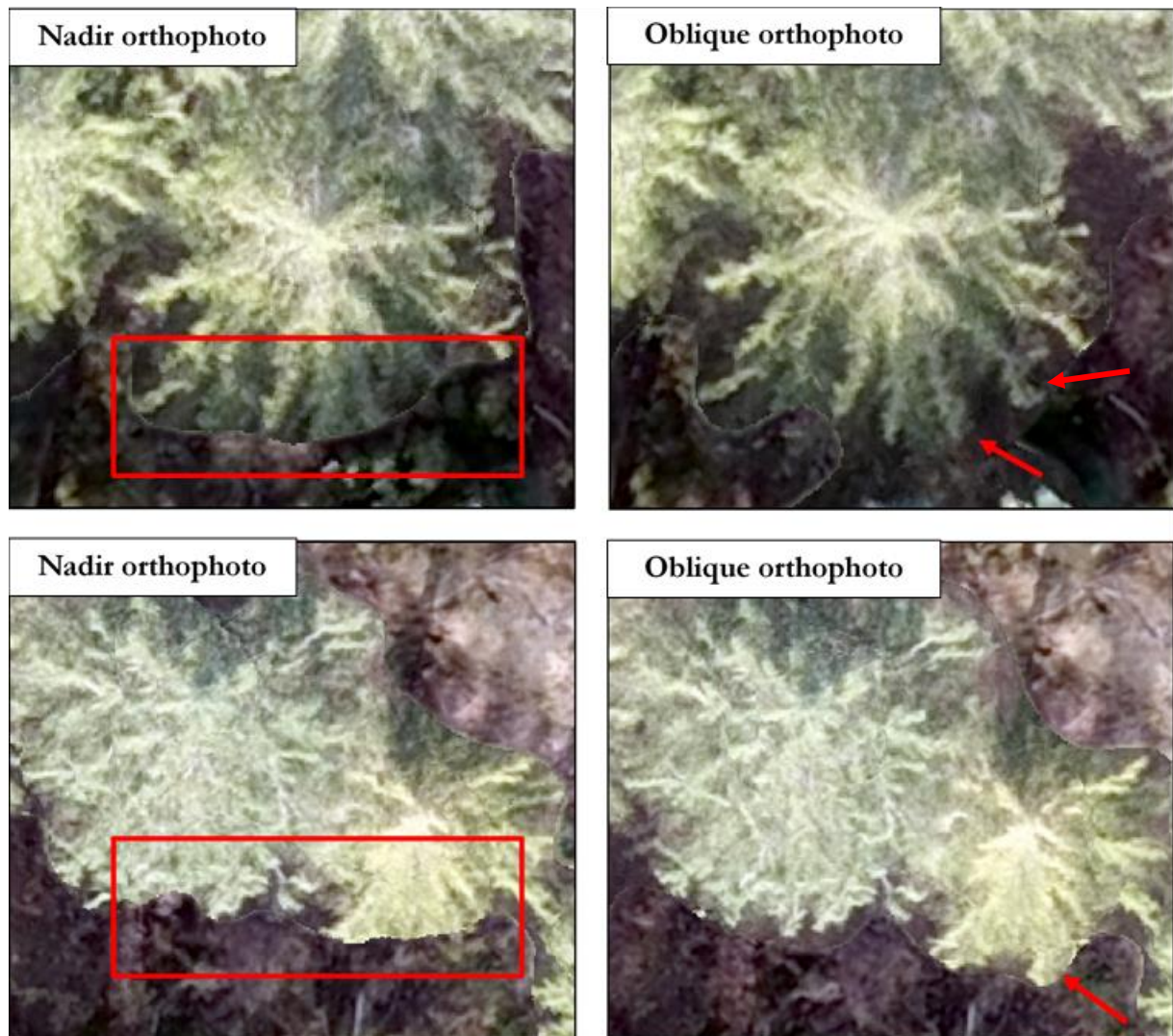


*Figure 4-2. Difference in crown between UAV nadir and oblique orthophoto*

## 4.5. Effect of tree height error on AGB

The fourth objective of this was to verify whether the errors in the tree height estimated from UAV nadir and UAV oblique CHM affect the AGB estimation under different canopy densities. The sensitivity analysis was carried out by inflating and deflating the tree heights based on the estimated tree height errors. In the dense block, the statistical analysis showed that there was a significant difference in the means of AGB estimated using inflated and deflated tree heights. Thus proving that the errors in UAV nadir and oblique tree heights affected the AGB estimated in the dense block. This can be attributed to poor DTM accuracy (Nadir DTM RMSE= 2.77m and Oblique DTM RMSE = 3.87m). The error in interpolated DTM has indeed propagated to the tree height estimated. Since tree height was one of the input parameters of the allometric equation used for AGB estimation, the error in the tree height subsequently affected the AGB estimation. From the graphs in *Appendix 16*, it can be observed that the variation in AGB is higher for big trees with high DBH, and the difference is smaller for trees with small DBH.

Whereas in the medium dense block, the statistical analysis showed that there was no significant difference between the means of the AGB estimated using inflated and deflated tree heights. It can be attributed to the improved accuracy of the interpolated DTM in the medium dense block (Nadir DTM RMSE= 0.45m and Oblique DTM RMSE = 0.59m). The accuracy of both the UAV nadir and oblique DTM in the medium dene block was higher than the dense block, and so was the accuracy of the tree height. Though there was error propagation in the medium dense block, it did not significantly affect the accuracy of AGB estimation.

## 4.6. Limitations

One of the study's major limitations is the species mix in the study area. The canopy density blocks identified in this study area did not have a good mix of deciduous and coniferous tree species. The dense block was predominantly deciduous, and the medium dense block was predominantly coniferous. Therefore, this study could not investigate the species-specific impact of incorporating oblique images in the SfM model under different canopy densities.

In addition to that, the oblique images were acquired at 75 degrees east-facing angle only due to time constraints. Acquiring the oblique images in both the east and west-facing direction might improve the accuracy of the point cloud. Also, other oblique angles were not tested in this study.

In this study, the CPA was manually digitized. Even though manual digitization is considered to be the most accurate method, there are chances of judgemental errors due to human bias. Especially in the dense block with interlocking tree crowns, identifying a particular field sampled tree, and its exact crown was challenging.

The crown diameter was calculated using the formula in equation 9, assuming it to be a circle. However, in most cases in the dense block, crowns were elongated. The accuracy of the crown diameter was not assessed in this study.

# 5.  CONCLUSION AND RECOMMENDATIONS

## 5.1.  Conclusion

This study assessed the effect of UAV oblique imaging on the tree parameter accuracy in the dense and medium dense canopy. The accuracy of tree parameters extracted from the UAV oblique dataset built by incorporating oblique images and nadir images in SfM did not vary significantly when compared with the accuracy of tree parameters extracted from UAV nadir only datasets. The answers to the research questions of this study are presented below.

1)  **What is the accuracy of DTM generated from UAV-Nadir images and UAV-Oblique images under dense and medium dense canopy compared to LiDAR DTM?**
    - The RMSE of UAV nadir DTM and oblique DTM in the dense canopy block is 2.77m and 3.87m
    - The RMSE of UAV nadir DTM and oblique DTM in the medium dense canopy block is 0.45m and 0.59m
    - The result of the statistical analysis proved there was no significant difference between elevation means from UAV nadir and UAV oblique DTM ($p>0.05$) in both dense and medium dense canopy blocks

2)  **How accurate are the tree heights derived from UAV-Nadir CHM and UAV-Oblique CHM under dense and medium dense canopy compared to LiDAR CHM?**
    - The RMSE of tree height from UAV nadir $CHM_{22cm}$ and oblique $CHM_{22cm}$ in the dense canopy block is 9.45m and 10.20m
    - The RMSE of tree height from UAV nadir $CHM_{22cm}$ and oblique $CHM_{22cm}$ in the medium dense canopy block is 3.43m and 3.65m
    - The result of the statistical analysis proved there was no significant difference between tree heights extracted from UAV nadir CHM and oblique CHM ($p>0.05$) in both dense and medium dense canopy blocks

3)  **How accurate is the DBH modeled using tree parameters extracted from UAV-Nadir images and UAV-Oblique images under dense and medium dense canopy compared to field-measured DBH?**
    - The RMSE of DBH models from UAV nadir derived tree parameters, and UAV oblique derived tree parameters in the dense canopy block is 8.39cm and 8.74cm
    - The RMSE of DBH models from UAV nadir derived tree parameters, and UAV oblique derived tree parameters in the medium dense canopy block is 3.78cm and 3.89cm
    - The result of the statistical analysis proved there was no significant difference between DBH modeled from UAV nadir derived tree parameters, and UAV oblique derived tree parameters ($p>0.05$) in both dense and medium dense canopy blocks

4)  **What is the effect of tree height estimation errors on AGB estimation under dense and medium dense canopy?**
    - The statistical analysis proved that the tree height estimation errors affected the AGB estimated in the dense canopy block. Whereas in the medium dense block, the tree height estimation errors did not affect the AGB estimated.

## 5.2. Recommendation

From the results of this study, few points to be considered for future research are

- Incorporating oblique images acquired at both east and west-facing directions in the SfM workflow
- Since in this study, the crowns of isolated trees were observed better in UAV oblique orthophoto, there is a potential in testing the method of incorporating oblique imaging in the SfM model in an open-canopy forest
- For this study, the crown segmentation was done by manual digitization. However, several studies have used segmentation methods like multiresolution segmentation, region growing, inverse watershed segmentation, etc. These segmentation methods can also be tested for CPA delineation from UAV nadir and oblique datasets.

# LIST OF REFERENCES

Amhar, F., Jansa, J., & Ries, C. (1998). The generation of true orthophotos using a 3D building model in conjunction with a conventional DTM. *The International Archives of the Photogrammetry, Remote Sensing and Spatial Information Sciences*, *32*(4), 16–22. Retrieved from https://www.researchgate.net/publication/228789530_The_generation_of_true_orthophotos_using _a_3D_building_model_in_conjunction_with_a_conventional_DTM

Automatic point cloud classification for construction | Pix4D. (2017). Retrieved from https://www.pix4d.com/blog/construction-surveys-point-cloud-classification

Avitabile, V., Baccini, A., Friedl, M. A., & Schmullius, C. (2012). Capabilities and limitations of Landsat and land cover data for aboveground woody biomass estimation of Uganda. *Remote Sensing of Environment*, *117*, 366–380. https://doi.org/10.1016/j.rse.2011.10.012

Banu, T. P., Borlea, G. F., & Banu, C. (2016). The Use of Drones in Forestry. *Journal of Environmental Science and Engineering B*, *5*(11), 557–562. https://doi.org/10.17265/2162-5263/2016.11.007

Barazzetti, L., Brumana, R., Oreni, D., Previtali, M., & Roncoroni, F. (2014). True-orthophoto generation from UAV images: Implementation of a combined photogrammetric and computer vision approach. *ISPRS Annals of the Photogrammetry, Remote Sensing and Spatial Information Sciences*, *2*(5), 57–63. https://doi.org/10.5194/isprsannals-II-5-57-2014

Barber, J., Bush, R., & Berglund, D. (2011). *The Region 1 Existing Vegetation Classification System and its Relationship to Region 1 Inventory Data and Map Products*. Retrieved from https://www.fs.usda.gov/Internet/FSE_DOCUMENTS/stelprdb5342838.pdf

Bazezew, M. N., Hussin, Y. A., & Kloosterman, E. H. (2018). Integrating Airborne LiDAR and Terrestrial Laser Scanner forest parameters for accurate above-ground biomass/carbon estimation in Ayer Hitam tropical forest, Malaysia. *International Journal of Applied Earth Observation and Geoinformation*, *73*, 638–652. https://doi.org/10.1016/j.jag.2018.07.026

Becker, C., Rosinskaya, E., Häni, N., D'Angelo, E., & Strecha, C. (2018). Classification of Aerial Photogrammetric 3D Point Clouds. *Photogrammetric Engineering and Remote Sensing*, *84*(5), 287–295. https://doi.org/10.14358/PERS.84.5.287

Berhe, H. (2018). *Towards A UAV Based Standalone System For Estimating And Mapping Aboveground Biomass/ Carbon Stock In Berkelah Tropical Rain Forest, Malaysia* (Masters' thesis). Retrieved from https://library.itc.utwente.nl/login/2018/msc/nrm/berhe.pdf

Berie, H. T., & Burud, I. (2018). Application of unmanned aerial vehicles in earth resources monitoring: Focus on evaluating potentials for forest monitoring in Ethiopia. *European Journal of Remote Sensing*, *51*(1), 326–335. https://doi.org/10.1080/22797254.2018.1432993

Birdal, A. C., Avdan, U., & Türk, T. (2017). Estimating tree heights with images from an unmanned aerial vehicle. *Geomatics, Natural Hazards and Risk*, *8*(2), 1144–1156. https://doi.org/10.1080/19475705.2017.1300608

Bombelli, A., Avitabile, V., Balzter, H., Luca Belelli Marchesini, M. B., Brady, M., Hall, R., … Wulder, M. (2009). *Assessment of the status of the development of the standards for the terrestrial essential climate variables: biomass* (Vol. 10). Retrieved from https://www.researchgate.net/publication/237196758_BIOMASS_Assessment_of_the_status_of_t he_development_of_the_standards_for_the_Terrestrial_Essential_Climate_Variables

Brohman, R., & Bryant, L. (2005). *Existing Vegetation Classification and Mapping Technical Guide Version 1.0*. Retrieved from https://www.fs.fed.us/emc/rig/documents/integrated_inventory/ FS_ExistingVEG_classif_mapping_TG_05.pdf

Brown, S. (1997). *Estimating Biomass and Biomass Change of Tropical Forests: a Primer*. Retrieved from http://www.fao.org/3/W4095E/w4095e04.htm#1.1 previous estimates of forest biomass

Chave, J., Réjou-Méchain, M., Búrquez, A., Chidumayo, E., Colgan, M. S., Delitti, W. B. C., … Vieilledent, G. (2014). Improved allometric models to estimate the aboveground biomass of tropical trees. *Global Change Biology*, *20*(10), 3177–3190. https://doi.org/10.1111/gcb.12629

Crespo-Peremarch, P., Torralba, J., Carbonell-Rivera, J. P., & Ruiz, L. A. (2020). Comparing the generation of DTM in a forest ecosystem using TLS, ALS and UAV-DAP, and different software tools. *The International Archives of the Photogrammetry, Remote Sensing and Spatial Information Sciences*, *43*, 575–582. https://doi.org/10.5194/isprs-archives-XLIII-B3-2020-575-2020

Dalponte, M., Frizzera, L., Ørka, H. O., Gobakken, T., Næsset, E., & Gianelle, D. (2018). Predicting stem diameters and aboveground biomass of individual trees using remote sensing data. *Ecological*

*Indicators*, *85*, 367–376. https://doi.org/10.1016/j.ecolind.2017.10.066

Dayamit, O. M., Pedro, M. F., Ernesto, R. R., & Fernando, B. L. (2015). Digital elevation model from non-metric camera in UAS compared with LIDAR technology. *The International Archives of the Photogrammetry, Remote Sensing and Spatial Information Sciences*, *40*(1), 411–414. https://doi.org/10.5194/isprsarchives-XL-1-W4-411-2015

Eric, A., & Mart-Jan, S. (2019). *National Forestry Accounting Plan.* Retrieved from https://english.rvo.nl/sites/default/files/2019/12/National Forestry Accounting Plan.pdf

FAO. (2003). Forests Without Trees? A Note on Problematic Forest Definitions and Change Assessments. Retrieved from http://www.fao.org/3/XII/0173-B1.htm

FAO. (2012). Roles of forests in climate change. Retrieved from http://www.fao.org/forestry/climatechange/53459/en/

FAO, & UNEP. (2020). *The State of the World's Forests 2020. Forests, biodiversity and people.* https://doi.org/10.4060/ca8642en

Fawcett, D., Azlan, B., Hill, T. C., Kho, L. K., Bennie, J., & Anderson, K. (2019). Unmanned aerial vehicle (UAV) derived structure-from-motion photogrammetry point clouds for oil palm (Elaeis guineensis) canopy segmentation and height estimation. *International Journal of Remote Sensing*, *40*(19), 7538–7560. https://doi.org/10.1080/01431161.2019.1591651

Fernandes, M. R., Aguiar, F. C., Martins, M. J., Rico, N., Ferreira, M. T., & Correia, A. C. (2020). Carbon stock estimations in a mediterranean riparian forest: A case study combining field data and UAV imagery. *Forests*, *11*(4), 376. https://doi.org/10.3390/F11040376

Frey, H. C., & Patil, S. R. (2002). Identification and review of sensitivity analysis methods. *Risk Analysis*, *22*(3), 553–578. https://doi.org/10.1111/0272-4332.00039

Frost, J. (2021). Using Post Hoc Tests with ANOVA. Retrieved from https://statisticsbyjim.com/anova/post-hoc-tests-anova/

Gaden, K. (2020). *Assessing Potential Of UAV Multispectral Imagery For Estimation Of AGB And Carbon Stock In Conifer Forest Over UAV RGB Imagery* (Masters' thesis). Retrieved from http://essay.utwente.nl/85200/1/gaden.pdf

Gatziolis, D., Lienard, J. F., Vogs, A., & Strigul, N. S. (2015). 3D Tree Dimensionality Assessment Using Photogrammetry and Small Unmanned Aerial Vehicles. *PloS ONE*, *10*(9), e0137765. https://doi.org/10.1371/journal.pone.0137765

González-Jaramillo, V., Fries, A., Zeilinger, J., Homeier, J., Paladines-Benitez, J., & Bendix, J. (2018). Estimation of above ground biomass in a tropical mountain forest in southern Ecuador using airborne LiDAR data. *Remote Sensing*, *10*(5), 660. https://doi.org/10.3390/rs10050660

Gosciewski, D. (2013). The effect of the distribution of measurement points around the node on the accuracy of interpolation of the digital terrain model. *Journal of Geographical Systems*, *15*(4), 513–535. https://doi.org/10.1007/s10109-012-0176-x

Halperin, J., LeMay, V., Chidumayo, E., Verchot, L., & Marshall, P. (2016). Model-based estimation of above-ground biomass in the miombo ecoregion of Zambia. *Forest Ecosystems*, *3*(1), 1–17. https://doi.org/10.1186/s40663-016-0077-4

Harvey, B. (2012). *Survey Computations.* Retrieved from https://www.sage.unsw.edu.au/sites/sage/files/u112/BRH_Survey_Comps textbook.pdf

Harwell, M. (2018). A strategy for using bias and RMSE as outcomes in Monte Carlo studies in statistics. *Journal of Modern Applied Statistical Methods*, *17*(2), 2938. https://doi.org/10.22237/jmasm/1551907966

Holopainen, M., Vastaranta, M., & Hyyppä, J. (2014). Outlook for the next generation's precision forestry in Finland. *Forests*, *5*(7), 1682–1694. https://doi.org/10.3390/f5071682

How to generate the point cloud classification – Support. (2021). Retrieved from https://support.pix4d.com/hc/en-us/articles/115004864586-How-to-generate-the-point-cloud-classification

Iglhaut, J., Cabo, C., Puliti, S., Piermattei, L., O'Connor, J., & Rosette, J. (2019). Structure from Motion Photogrammetry in Forestry: a Review. *Current Forestry Reports*, *5*(3), 155–168. https://doi.org/10.1007/s40725-019-00094-3

Iizuka, K., Yonehara, T., Itoh, M., & Kosugi, Y. (2017). Estimating Tree Height and Diameter at Breast Height (DBH) from Digital Surface Models and Orthophotos Obtained with an Unmanned Aerial System for a Japanese Cypress (Chamaecyparis obtusa) Forest. *Remote Sensing*, *10*(1), 13. https://doi.org/10.3390/rs10010013

IPCC. (2006). *Guidelines for National Greenhouse Gas Inventories - Volume 4 - Agriculture, Forestry and Other Land*

*Use*. Retrieved from https://www.ipcc-nggip.iges.or.jp/public/2006gl/vol4.html

IPCC. (2007). *Climate Change 2007: Impacts, Adaptation and Vulnerability, Contribution of Working Group II to the Fourth Assessment Report of the Intergovernmental Panel on Climate Change*. Retrieved from https://www.ipcc.ch/report/ar4/wg2/

IPCC. (2014a). *Climate Change 2014 Mitigation of Climate Change Working Group III Contribution to the Fifth Assessment Report of the Intergovernmental Panel on Climate Change*. Retrieved from www.cambridge.org / 9781107654815

IPCC. (2014b). Greenhouse gas inventory methodologies. Retrieved from https://reddcompass.org/mgd-content-v1/dita-webhelp/en/d0e1258.html

IUCN. (2017). *Forests and Climate Change*. Retrieved from https://www.iucn.org/resources/issues-briefs/forests-and-climate-change

Jayathunga, S., Owari, T., & Tsuyuki, S. (2018). Evaluating the Performance of Photogrammetric Products Using Fixed-Wing UAV Imagery over a Mixed Conifer–Broadleaf Forest: Comparison with Airborne Laser Scanning. *Remote Sensing, 10*(2), 187. https://doi.org/10.3390/rs10020187

Jucker, T., Caspersen, J., Chave, J., Antin, C., Barbier, N., Bongers, F., … Coomes, D. A. (2017). Allometric equations for integrating remote sensing imagery into forest monitoring programmes. *Global Change Biology, 23*(1), 177–190. https://doi.org/10.1111/gcb.13388

Kachamba, D. J., Ørka, H. O., Næsset, E., Eid, T., & Gobakken, T. (2017). Influence of plot size on efficiency of biomass estimates in inventories of dry tropical forests assisted by photogrammetric data from an unmanned aircraft system. *Remote Sensing, 9*(6), 610. https://doi.org/10.3390/rs9060610

Kachamba, D., Ørka, H., Gobakken, T., Eid, T., & Mwase, W. (2016). Biomass Estimation Using 3D Data from Unmanned Aerial Vehicle Imagery in a Tropical Woodland. *Remote Sensing, 8*(11), 968. https://doi.org/10.3390/rs8110968

Kahyani, S., Hosseini, S. M., & Basiri, R. (2011). The Basic of Analytical of Simple Linear Regression in Forestry Studies (Case Study: Relationship Between Basal Area and Tree Coverage of Quercus brantii Lindl. In Absardeh, Chahar Mahale and Bakhtiari). *World Applied Sciences Journal, 14*(10), 1599–1606. Retrieved from https://www.semanticscholar.org/paper/The-Basic-of-Analytical-of-Simple-Linear-Regression-Kahyani-Basiri/ac905ed60de706da7d198276036a75bcfe3c4bb6

Kattenborn, T., Hernández, J., Lopatin, J., Kattenborn, G., & Fassnacht, F. E. (2018). Pilot Study On The Retrieval Of DBH And Diameter Distribution Of Deciduous Forest Stands Using Cast Shadows In Uav-Based Orthomosaics. *ISPRS Annals of the Photogrammetry, Remote Sensing and Spatial Information Sciences, 4*(1), 93–99. https://doi.org/10.5194/isprs-annals-IV-1-93-2018

Ke, Y., & Quackenbush, L. . (2011). A review of methods for automatic individual tree-crown detection and delineation from passive remote sensing. *International Journal of Remote Sensing, 32*(17), 4725–4747. https://doi.org/10.1080/01431161.2010.494184

Kebede, B., & Soromessa, T. (2018). Allometric equations for aboveground biomass estimation of Olea europaea L. subsp. cuspidata in Mana Angetu Forest. *Ecosystem Health and Sustainability, 4*(1), 1–12. https://doi.org/10.1080/20964129.2018.1433951

Kershaw, J., Ducey, M., Beers, T., & Husch, B. (2017). *Forest Mensuration* (5th ed.). Retrieved from https://lccn.loc.gov/2016036142

King, D. A. (2005). Linking tree form, allocation and growth with an allometrically explicit model. *Ecological Modelling, 185*(1), 77–91. https://doi.org/10.1016/j.ecolmodel.2004.11.017

Köhl, M., Magnussen, S., & Marchetti, M. (2006). *Sampling Methods, Remote Sensing and GIS Multiresource Forest Inventory* (1st ed.). https://doi.org/https://doi.org/10.1007/978-3-540-32572-7

Kosmatin Fras, M., Kerin, A., Mesarič, M., Peterman, V., & Grigillo, D. (2016). Assessment of the quality of digital terrain model produced from unmanned aerial system imagery. *The International Archives of the Photogrammetry, Remote Sensing and Spatial Information Sciences, 41*, 893–899. https://doi.org/10.5194/isprsarchives-XLI-B1-893-2016

Krause, S., Sanders, T. G. M., Mund, J. P., & Greve, K. (2019). UAV-based photogrammetric tree height measurement for intensive forest monitoring. *Remote Sensing, 11*(7), 1–19. https://doi.org/10.3390/rs11070758

Kumar, L., & Mutanga, O. (2017). Remote sensing of above-ground biomass. *Remote Sensing, 9*(9), 1–8. https://doi.org/10.3390/rs9090935

Lim, Y. S., La, P. H., Park, J. S., Lee, M. H., Pyeon, M. W., & Kim, J. I. (2015). Calculation of tree height and canopy crown from drone images using segmentation. *Journal of the Korean Society of Surveying, Geodesy, Photogrammetry and Cartography, 33*(6), 605–613. https://doi.org/10.7848/ksgpc.2015.33.6.605

Lin, J., Wang, M., Ma, M., & Lin, Y. (2018). Aboveground Tree Biomass Estimation of Sparse Subalpine Coniferous Forest with UAV Oblique Photography. *Remote Sensing*, *10*(11), 1849. https://doi.org/10.3390/rs10111849

Liu, Y., Zheng, X., Ai, G., Zhang, Y., & Zuo, Y. (2018). Generating a High-Precision True Digital Orthophoto Map Based on UAV Images. *ISPRS International Journal of Geo-Information*, *7*(9), 333. https://doi.org/10.3390/ijgi7090333

Lof, M., Schenau, S., De, R., Roy, J., Graveland, R. C., & Hein, L. (2017). *The SEEA EEA carbon account for the Netherlands*. Retrieved from https://library.wur.nl/WebQuery/wurpubs/fulltext/426532

Lu, D. (2005). Aboveground biomass estimation using Landsat TM data in the Brazilian Amazon. *International Journal of Remote Sensing*, *26*(12), 2509–2525. https://doi.org/10.1080/01431160500142145

Lu, Dengsheng. (2006). The potential and challenge of remote sensing-based biomass estimation. *International Journal of Remote Sensing*, *27*(7), 1297–1328. https://doi.org/10.1080/01431160500486732

Lu, J., Wang, H., Qin, S., Cao, L., Pu, R., Li, G., & Sun, J. (2020). Estimation of aboveground biomass of Robinia pseudoacacia forest in the Yellow River Delta based on UAV and Backpack LiDAR point clouds. *International Journal of Applied Earth Observation and Geoinformation*, *86*, 102014. https://doi.org/10.1016/j.jag.2019.102014

Maniatis, D., & Mollicone, D. (2010). Options for sampling and stratification for national forest inventories to implement REDD+ under the UNFCCC. *Carbon Balance and Management*, *5*(1), 9. https://doi.org/10.1186/1750-0680-5-9

Means, J. E., Acker, S. A., Harding, D. J., Blair, J. B., Lefsky, M. A., Cohen, W. B., … McKee, W. A. (1999). Use of large-footprint scanning airborne Lidar to estimate forest stand characteristics in the western cascades of Oregon. *Remote Sensing of Environment*, *67*(3), 298–308. https://doi.org/10.1016/S0034-4257(98)00091-1

Meinen, B. U., & Robinson, D. T. (2020). Mapping erosion and deposition in an agricultural landscape: Optimization of UAV image acquisition schemes for SfM-MVS. *Remote Sensing of Environment*, *239*, 111666. https://doi.org/10.1016/j.rse.2020.111666

Micheletti, N., Chandler, J. H., & Lane, S. N. (2015). Structure from Motion (SfM) Photogrammetry. In *Geomorphological Techniques*. Retrieved from https://www.geomorphology.org.uk/sites/default/files/geom_tech_chapters/2.2.2_sfm.pdf

Mitchell, A. L., Rosenqvist, A., & Mora, B. (2017). Current remote sensing approaches to monitoring forest degradation in support of countries measurement, reporting and verification (MRV) systems for REDD+. *Carbon Balance and Management*, *12*(1), 9. https://doi.org/10.1186/s13021-017-0078-9

Mlambo, R., Woodhouse, I., Gerard, F., & Anderson, K. (2017). Structure from Motion (SfM) Photogrammetry with Drone Data: A Low Cost Method for Monitoring Greenhouse Gas Emissions from Forests in Developing Countries. *Forests*, *8*(3), 68. https://doi.org/10.3390/f8030068

Moe, K. T., Owari, T., Furuya, N., & Hiroshima, T. (2020). Comparing individual tree height information derived from field surveys, LiDAR and UAV-DAP for high-value timber species in Northern Japan. *Forests*, *11*(2), 1–16. https://doi.org/10.3390/f11020223

Moe, K. T., Owari, T., Furuya, N., Hiroshima, T., & Morimoto, J. (2020). Application of uav photogrammetry with lidar data to facilitate the estimation of tree locations and dbh values for high-value timber species in Northern Japanese mixed-wood forests. *Remote Sensing*, *12*(17), 1–19. https://doi.org/10.3390/rs12172865

Mohan, M., Silva, C. A., Klauberg, C., Jat, P., Catts, G., Cardil, A., … Dia, M. (2017). Individual tree detection from unmanned aerial vehicle (UAV) derived canopy height model in an open canopy mixed conifer forest. *Forests*, *8*(9), 340. https://doi.org/10.3390/f8090340

Mohren, G., Hasenauer, H., Köhl, M., & Nabuurs, G.-J. (2012). Forest inventories for carbon change assessments. *Current Opinion in Environmental Sustainability*, *4*(6), 686–695. https://doi.org/10.1016/j.cosust.2012.10.002

Nesbit, P., & Hugenholtz, C. (2019). Enhancing UAV–SfM 3D Model Accuracy in High-Relief Landscapes by Incorporating Oblique Images. *Remote Sensing*, *11*(3), 239. https://doi.org/10.3390/rs11030239

Obeng-Manu, C. (2019). *Assessing the accuracy of UAV-DTM generated under different forest canopy density and its effect on estimation of aboveground carbon in Asubima forest, Ghana* (Masters' thesis). Retrieved from http://essay.utwente.nl/83733/1/obeng-manu.pdf

Ojoatre, S., Zhang, C., Hussin, Y. A., Kloosterman, H. E., & Ismail, M. H. (2019). Assessing the Uncertainty of Tree Height and Aboveground Biomass from Terrestrial Laser Scanner and

Hypsometer Using Airborne LiDAR Data in Tropical Rainforests. *IEEE Journal of Selected Topics in Applied Earth Observations and Remote Sensing*, *12*(10), 4149–4159. https://doi.org/10.1109/JSTARS.2019.2944779

Ota, T., Ogawa, M., Shimizu, K., Kajisa, T., Mizoue, N., Yoshida, S., … Ket, N. (2015). Aboveground Biomass Estimation Using Structure from Motion Approach with Aerial Photographs in a Seasonal Tropical Forest. *Forests*, *6*(12), 3882–3898. https://doi.org/10.3390/f6113882

Pandey, P. C., Srivastava, P. K., Chetri, T., Choudhary, B. K., & Kumar, P. (2019). Forest biomass estimation using remote sensing and field inventory: a case study of Tripura, India. *Environmental Monitoring and Assessment*, *191*(9), 1–15. https://doi.org/10.1007/s10661-019-7730-7

Paudel, P., & Mandal, R. (2019). Comparing Growing Stock using Circular, Square and Rectangular Plots Shape in Inventory (A study from Community Forests in Chitwan District, Nepal). *Canadian Journal of Soil Science*, *4*(1), 448–454. https://doi.org/10.32474/OAJESS.2019.04.000177

Pepe, M., Fregonese, L., & Scaioni, M. (2018). Planning airborne photogrammetry and remote-sensing missions with modern platforms and sensors. *European Journal of Remote Sensing*, *51*(1), 412–435. https://doi.org/10.1080/22797254.2018.1444945

Photo stitching vs orthomosaic generation – Pix4D. (2021). Retrieved from https://support.pix4d.com/hc/en-us/articles/202558869-Photo-stitching-vs-orthomosaic-generation

Pizaña, J. M. G., Hernández, J. M. N., & Romero, N. C. (2016). Remote Sensing-Based Biomass Estimation. In M. Marghany (Ed.), *Environmental Applications of Remote Sensing* (pp. 3–40). https://doi.org/10.5772/61813

Popescu, S. C. (2007). Estimating biomass of individual pine trees using airborne lidar. *Biomass and Bioenergy*, *31*(9), 646–655. https://doi.org/10.1016/j.biombioe.2007.06.022

Pouliot, D. A., King, D. J., Bell, F. W., & Pitt, D. G. (2002). Automated tree crown detection and delineation in high-resolution digital camera imagery of coniferous forest regeneration. *Remote Sensing of Environment*, *82*(2–3), 322–334. https://doi.org/10.1016/S0034-4257(02)00050-0

Priedītis, G., Šmits, I., Arhipova, I., Daǎis, S., & Dubrovskis, D. (2012). Tree Diameter Models from Field and Remote s ensing data. *International Journal Of Mathematical Models And Methods In Applied Sciences*, *6*(6), 707–714. Retrieved from https://naun.org/main/NAUN/ijmmas/16-373.pdf

Processing steps – Support. (2021). Retrieved from https://support.pix4d.com/hc/en-us/articles/115002472186-Processing-steps

Quality description | AHN. (2019). Retrieved from Actueel Hoogtebestand Netherlands website: https://www.ahn.nl/kwaliteitsbeschrijving

Reder, S., Waßermann, L., & Mund, J.-P. (2019). UAV-based Tree Height Estimation in Dense Tropical Rainforest Areas in Ecuador and Brazil. *Journal for Geographic Information System*, *7*(2), 47–59. https://doi.org/10.1553/giscience2019_02_s47

Roy, P. S., & Ravan, S. A. (1996). Biomass estimation using satellite remote sensing data - An investigation on possible approaches for natural forest. *Journal of Biosciences*, *21*(4), 535–561. https://doi.org/10.1007/BF02703218

Ruiz, L. A., Hermosilla, T., Mauro, F., & Godino, M. (2014). Analysis of the influence of plot size and LiDAR density on forest structure attribute estimates. *Forests*, *5*(5), 936–951. https://doi.org/10.3390/f5050936

Sadadi, O. (2016). *Accuracy Of Measuring Tree Height Using Airborne Lidar And Terrestrial Laser Scanner And Its Effect On Estimating Forest Biomass And Carbon Stock In Ayer Hitam Tropical Rain Forest Reserve, Malaysia* (Masters' thesis). Retrieved from http://essay.utwente.nl/83906/1/ojoatre.pdf

Scheme of classification: Forest Survey of India. (2018). Retrieved from https://fsi.nic.in/scheme-of-classification

Shi, L., & Liu, S. (2017). Methods of Estimating Forest Biomass: A Review. In *Biomass Volume Estimation and Valorization for Energy* (pp. 23–46). https://doi.org/10.5772/65733

Shimano, K. (1997). Analysis of the relationship between DBH and crown projection area using a new model. *Journal of Forest Research*, *2*(4), 237–242. https://doi.org/10.1007/BF02348322

Simpson, J. E., Smith, T. E. L., & Wooster, M. J. (2017). Assessment of errors caused by forest vegetation structure in airborne LiDAR-derived DTMs. *Remote Sensing*, *9*(11), 1101. https://doi.org/10.3390/rs9111101

Sinha, S., Jeganathan, C., Sharma, L. K., & Nathawat, M. S. (2015). A review of radar remote sensing for biomass estimation. *International Journal of Environmental Science and Technology*, *12*(5), 1779–1792. https://doi.org/10.1007/s13762-015-0750-0

Sousa, A. M. O., Gonçalves, A. C., Mesquita, P., & Marques da Silva, J. R. (2015). Biomass estimation with high resolution satellite images: A case study of Quercus rotundifolia. *ISPRS Journal of Photogrammetry and Remote Sensing*, *101*, 69–79. https://doi.org/10.1016/j.isprsjprs.2014.12.004

Stereńczak, K., Zasada, M., & Brach, M. (2013). The accuracy assessment of DTM generated from LIDAR data for forest area - A case study for Scots Pine stands in Poland. *Baltic Forestry*, *19*(2), 252–262. Retrieved from https://www.researchgate.net/publication/261070391_The_Accuracy_Assessment_of_DTM_Generated_from_LIDAR_Data_for_Forest_Area_-_a_Case_Study_for_Scots_Pine_Stands_in_Poland

Stoll, A. (2017). Post Hoc Tests: Tukey Honestly Significant Difference Test. In M. Allen (Ed.), *The SAGE Encyclopedia of Communication Research Methods* (pp. 1306–1307). https://doi.org/10.4135/9781483381411

Thapa Magar, A. (2014). *Estimation and mapping of forest biomass and carbon using point-clouds derived from airborne LiDAR and from 3D photogrammetric matching of aerial images* (Master's Thesis). Retrieved from https://webapps.itc.utwente.nl/librarywww/papers_2014/msc/gem/thapamagar.pdf

Thenkabail, P. S., Enclona, E. A., Ashton, M. S., Legg, C., & De Dieu, M. J. (2004). Hyperion, IKONOS, ALI, and ETM+ sensors in the study of African rainforests. *Remote Sensing of Environment*, *90*(1), 23–43. https://doi.org/10.1016/j.rse.2003.11.018

Tichý, L. (2016). Field test of canopy cover estimation by hemispherical photographs taken with a smartphone. *Journal of Vegetation Science*, *27*(2), 427–435. https://doi.org/10.1111/jvs.12350

Timothy, D., Onisimo, M., Cletah, S., Adelabu, S., & Tsitsi, B. (2016). Remote sensing of aboveground forest biomass: A review. *Tropical Ecology*, *57*(2), 125–132. Retrieved from https://www.researchgate.net/publication/287224448

UNFCCC. (2021). About the Secretariat | UNFCCC. Retrieved from https://unfccc.int/about-us/about-the-secretariat

Vandendriesche, D. (2013). *A Compendium of NFS Regional Vegetation Classification Algorithms*. Retrieved from https://www.fs.fed.us/fmsc/ftp/fvs/docs/gtr/NFS_Reg_Veg_Class.pdf

Vashum, K. T., & Jayakumar, S. (2012). Methods to Estimate Above-Ground Biomass and Carbon Stock in Natural Forests - A Review. *Journal of Ecosystem & Ecography*, *2*(4), 1–7. https://doi.org/10.4172/2157-7625.1000116

Vastaranta, M., Yu, X., Luoma, V., Karjalainen, M., Saarinen, N., Wulder, M. A., … Hyyppä, J. (2018). Aboveground forest biomass derived using multiple dates of WorldView-2 stereo-imagery: quantifying the improvement in estimation accuracy. *International Journal of Remote Sensing*, *39*(23), 8766–8783. https://doi.org/10.1080/01431161.2018.1492176

Verma, N. K., Lamb, D. W., Reid, N., & Wilson, B. (2014). An allometric model for estimating DBH of isolated and clustered Eucalyptus trees from measurements of crown projection area. *Forest Ecology and Management*, *326*, 125–132. https://doi.org/10.1016/j.foreco.2014.04.003

Voortgang AHN 2019. (2019). Retrieved from Actueel Hoogtebestand Netherlands website: https://www.ahn.nl/voortgang-ahn-2019

Wagner, F. H., Ferreira, M. P., Sanchez, A., Hirye, M. C. M., Zortea, M., Gloor, E., … Aragão, L. E. O. C. (2018). Individual tree crown delineation in a highly diverse tropical forest using very high resolution satellite images. *ISPRS Journal of Photogrammetry and Remote Sensing*, *145*, 362–377. https://doi.org/10.1016/j.isprsjprs.2018.09.013

Wahyuni, S., Jaya, I. N. S., & Puspaningsih, N. (2016). Model for estimating above ground biomass of reclamation forest using unmanned aerial vehicles. *Indonesian Journal of Electrical Engineering and Computer Science*, *4*(3), 586–593. https://doi.org/10.11591/ijeecs.v4.i3.pp586-593

Wakawa, L. . (2016). Biomass Estimation in Forest Ecosystems -A Review. *Journal of Research in Forestry, Wildlife and Environment*, *8*(2), 126–144. Retrieved from https://www.researchgate.net/publication/313402463_Biomass_Estimation_in_Forest_Ecosystems_-A_Review

Wallace, L., Lucieer, A., Malenovskỳ, Z., Turner, D., & Vopěnka, P. (2016). Assessment of forest structure using two UAV techniques: A comparison of airborne laser scanning and structure from motion (SfM) point clouds. *Forests*, *7*(3), 62. https://doi.org/10.3390/f7030062

Wang, Y., Lehtomäki, M., Liang, X., Pyörälä, J., Kukko, A., Jaakkola, A., … Hyyppä, J. (2019). Is field-measured tree height as reliable as believed – A comparison study of tree height estimates from field measurement, airborne laser scanning and terrestrial laser scanning in a boreal forest. *ISPRS Journal of Photogrammetry and Remote Sensing*, *147*, 132–145. https://doi.org/10.1016/j.isprsjprs.2018.11.008

Wenzel, K., Rothermel, M., Fritsch, D., & Haala, N. (2013). Image Acquisition And Model Selection For

Multi-View Stereo. *The International Archives of the Photogrammetry, Remote Sensing and Spatial Information Sciences*, *40*(5W), 251–258. https://doi.org/10.5194/isprsarchives-xl-5-w1-251-2013

Westoby, M. J., Brasington, J., Glasser, N. F., Hambrey, M. J., & Reynolds, J. M. (2012). "Structure-from-Motion" photogrammetry: A low-cost, effective tool for geoscience applications. *Geomorphology*, *179*, 300–314. https://doi.org/10.1016/j.geomorph.2012.08.021

Wilson, A. D. (2000). *New Methods, Algorithms, and Software for Rapid Mapping of Tree Positions in Coordinate Forest Plots*. Retrieved from https://www.srs.fs.fed.us/pubs/rp/rp_srs019.pdf

Yin, D., & Wang, L. (2016). How to assess the accuracy of the individual tree-based forest inventory derived from remotely sensed data: a review. *International Journal of Remote Sensing*, *37*(19), 4521–4553. https://doi.org/10.1080/01431161.2016.1214302

Yin, G., Zhang, Y., Sun, Y., Wang, T., Zeng, Z., & Piao, S. (2015). MODIS based estimation of forest aboveground biomass in China. *PLoS ONE*, *10*(6), e0130143. https://doi.org/10.1371/journal.pone.0130143

Zhou, X., & Zhang, X. (2020). Individual tree parameters estimation for plantation forests based on UAV oblique photography. *IEEE Access*, *8*, 96184–96198. https://doi.org/10.1109/ACCESS.2020.2994911

Zianis, D., Muukkonen, P., Mäkipää, R., & Mencuccini, M. (2005). Biomass and Stem Volume Equations for Tree Species in Europe. In *Silva Fennica Monographs* (Vol. 4). Retrieved from https://www.silvafennica.fi/pdf/smf004.pdf

# APPENDICES

Appendix 1. Data entry sheet used during field data collection

| The data entry sheet for tree parameters in Haagse Bos | | | | | | |
|---|---|---|---|---|---|---|
| **Observer name:** | | | **Date:** | | **Plot No:** | |
| **Central point** | **Logitude (X):** | | | | **Latitude (Y):** | |
| **Canopy Density** | **Center** | **North** | **South** | **East** | **West** | **Average** |
| | | | | | | |
| **General comment:** | | | | | | |

| Tree No | Species | DBH (m) | Height (m) | Crown diameter (m) | | Tree position | | Comment |
|---|---|---|---|---|---|---|---|---|
| | | | | **N-S** | **W-E** | **Distance from centre point (m)** | **Compass bearing (degrees)** | |
| | | | | | | | | |
| | | | | | | | | |
| | | | | | | | | |
| | | | | | | | | |
| | | | | | | | | |
| | | | | | | | | |
| | | | | | | | | |
| | | | | | | | | |
| | | | | | | | | |
| | | | | | | | | |
| | | | | | | | | |
| | | | | | | | | |
| | | | | | | | | |
| | | | | | | | | |
| | | | | | | | | |
| | | | | | | | | |
| | | | | | | | | |

Appendix 2: Summary of quality report of UAV image processing in Pix4Dmapper

| | UAV Nadir | UAV Oblique |
|---|---|---|
| **Quality:** | | |
| Dataset | 1470 out of 1470 images calibrated (100%) | 2181 out of 2181 images calibrated (100%) |
| Number of GCP | 9 | 9 |
| Georeferencing RMSE | 0.01m | 0.02m |
| **Bundle block adjustment** | | |
| Mean Reprojection Error [pixels] | 0.25 | 0.28 |
| **Geolocation** | | |
| GCP RMSE (m) | x=0.016, y=0.015, z=0.005 | x= 0.021, y=0.018, z=0.025 |
| Check point RMSE (m) | x=0.051, y=0.043, z=0.055 | x=0.036, y=0.032, z=0.093 |
| **Coordinate system** | | |
| Image coordinate system | WGS 84 | WGS 84 |
| GCP coordinate system | Amersfoort / RD New | Amersfoort / RD New |
| Output coordinate system | Amersfoort / RD New | Amersfoort / RD New |
| **Point Cloud Densification** | | |
| Number of 3D Densified Points | 78684624 | 97180064 |
| Average Density (per m$^3$) | 49.72 | 50.78 |

Appendix 3: Plot-wise descriptive statistics of field-measured tree DBH in different canopy density blocks

| Dense canopy Block (cm) | | | | |
|---|---|---|---|---|
| Plot No | Mean | Minimum | Maximum | Std Deviation |
| 1 | 49.78 | 34.80 | 56.30 | 10.12 |
| 2 | 46.45 | 40.20 | 57.90 | 6.17 |
| 3 | 45.16 | 18.50 | 78.60 | 21.12 |
| 4 | 43.73 | 19.20 | 55.00 | 10.75 |
| 5 | 52.81 | 29.80 | 72.50 | 18.87 |
| 6 | 66.70 | 47.10 | 97.10 | 20.57 |
| 7 | 51.87 | 36.50 | 71.00 | 10.44 |
| 8 | 66.82 | 47.40 | 97.40 | 17.75 |
| 9 | 54.82 | 40.20 | 70.50 | 12.36 |
| 10 | 45.55 | 31.20 | 61.00 | 10.60 |
| 11 | 27.72 | 19.60 | 41.80 | 5.29 |
| 12 | 44.01 | 31.10 | 72.40 | 11.12 |
| 13 | 52.67 | 23.60 | 101.90 | 26.86 |

| Medium dense canopy Block (cm) | | | | |
|---|---|---|---|---|
| Plot No | Mean | Minimum | Maximum | Std Deviation |
| 1 | 32.31 | 22 | 45.5 | 5.53 |
| 2 | 33.32 | 13.5 | 58 | 11.34 |
| 3 | 36.48 | 25.00 | 56.80 | 9.02 |
| 4 | 27.89 | 15.00 | 37.10 | 5.93 |
| 5 | 32.47 | 20.00 | 42.00 | 6.17 |
| 6 | 44.03 | 34.30 | 59.60 | 9.33 |
| 7 | 29.24 | 18.00 | 37.00 | 5.18 |
| 8 | 31.25 | 13.00 | 46.20 | 9.00 |
| 9 | 35.64 | 25.30 | 42.10 | 5.51 |
| 10 | 44.92 | 13.50 | 66.80 | 16.16 |

Appendix 4: UAV-Nadir and UAV-Oblique orthophoto of dense and medium dense canopy blocks
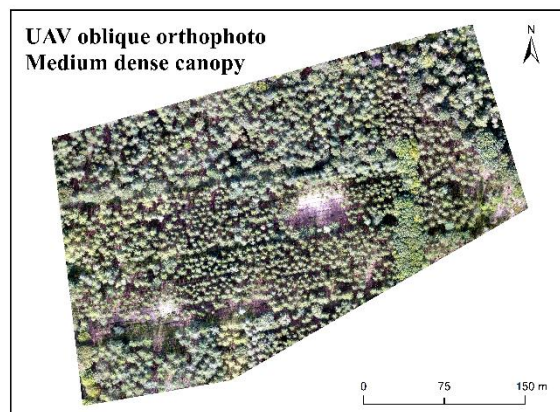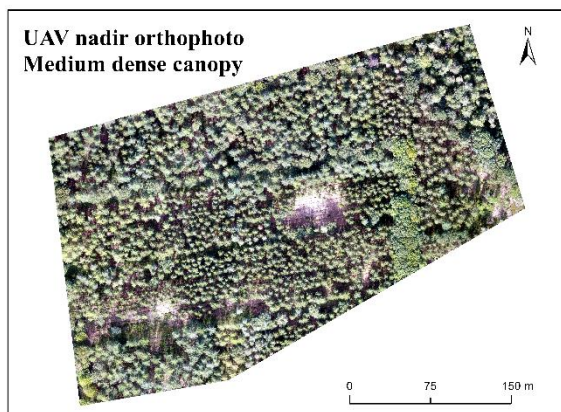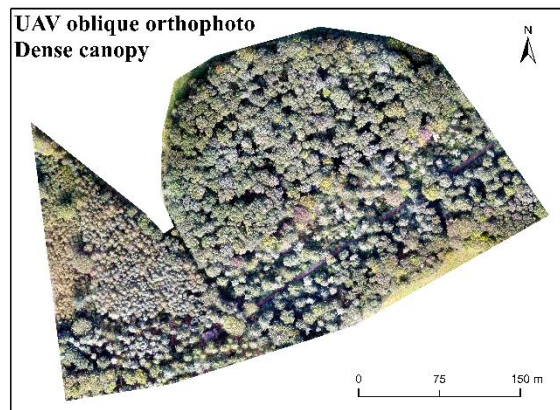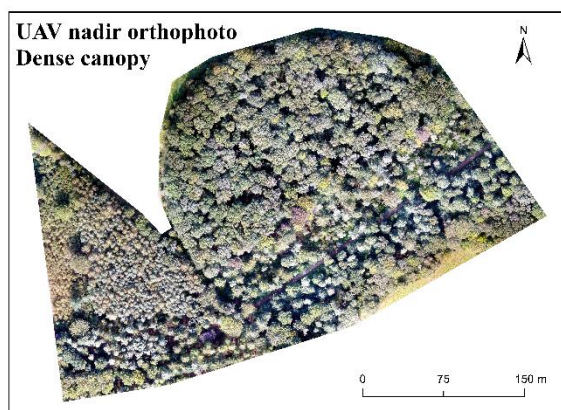
Appendix 5: Histogram of random point elevation from LiDAR, UAV nadir and UAV oblique DTMs in different canopy density block
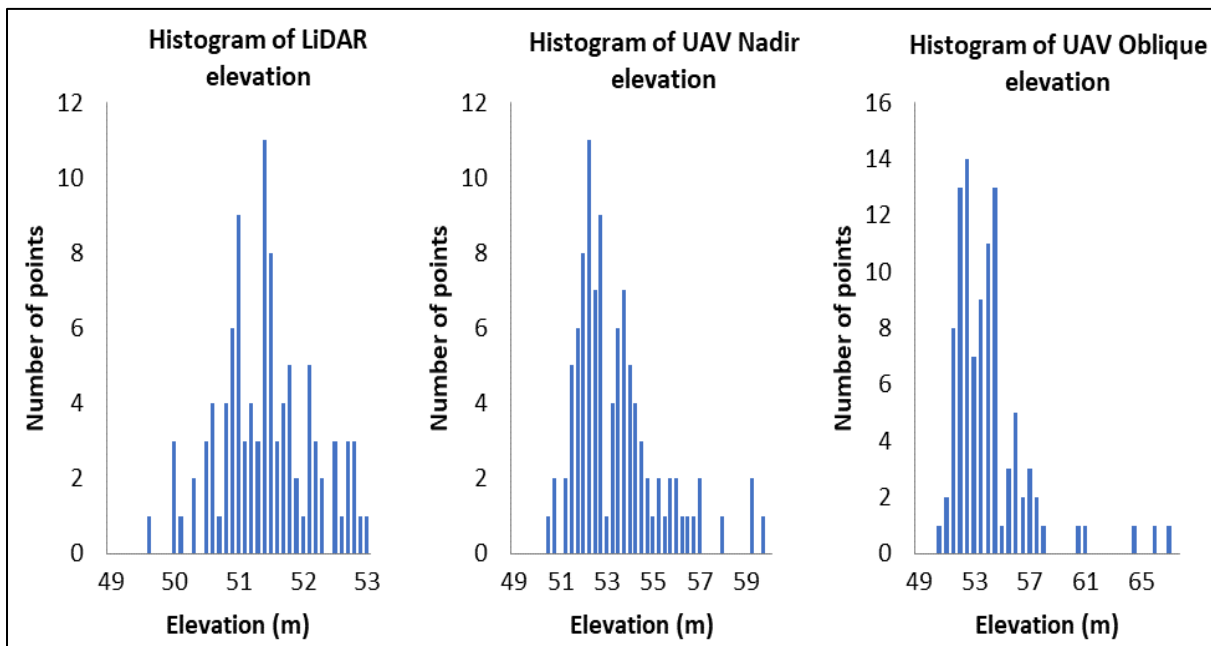


a) Histogram of random point elevation in dense canopy block from LiDAR, UAV nadir and UAV oblique DTMs
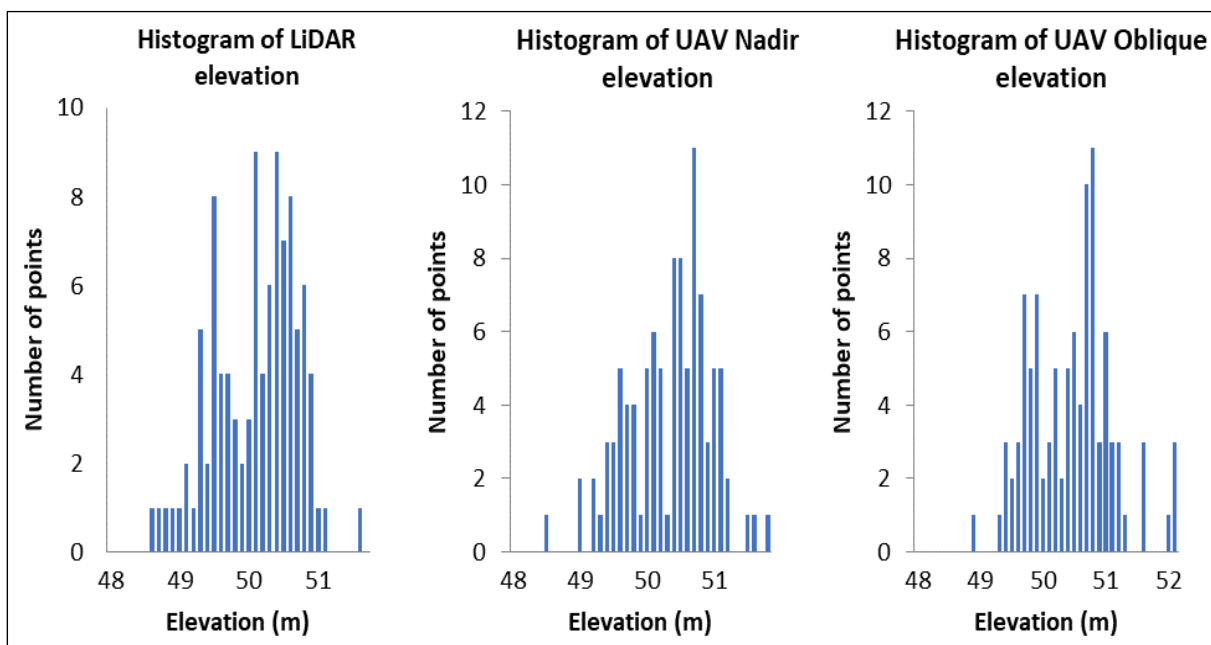


b) Histogram of random point elevation in medium dense cnopy block from LiDAR, UAV nadir and UAV oblique DTMs

Appendix 6: One-way ANOVA and Tucky HSD results of comparison between the means of elevation from LiDAR DTM and UAV nadir DTM and UAV oblique DTM in different canopy density blocks

*One-way ANOVA test result of elevation (dense canopy block)*

| SUMMARY | | | | |
|---|---|---|---|---|
| *Groups* | *Count* | *Sum* | *Average* | *Variance* |
| **LiDAR elevation (m)** | 100 | 5137.07 | 51.37 | 0.54 |
| **UAV nadir elevation (m)** | 100 | 5336.07 | 53.36 | 3.57 |
| **UAV oblique elevation (m)** | 100 | 5394.74 | 53.95 | 8.51 |
| ANOVA | | | | |
| *Source of Variation* | *SS* | *df* | *MS* | *F* | *P-value* | *F crit* |
| **Between Groups** | 364.79 | 2 | 182.39 | 43.37 | 0.00 | 3.03 |
| **Within Groups** | 1248.94 | 297 | 4.21 | | | |
| **Total** | 1613.72 | 299 | | | | |

*Tucky HSD post hoc test of elevation (dense canopy block)*

| **Multiple Comparisons** | | **Mean Difference** | **Std. Error** | **Sig.** | **95% Confidence Interval** | |
|---|---|---|---|---|---|---|
| | | | | | **Lower Bound** | **Upper Bound** |
| LiDAR elevation (m) | UAV nadir elevation (m) | -1.99* | 0.29 | 0.00 | -2.67 | -1.31 |
| | UAV oblique elevation (m) | -2.58* | 0.29 | 0.00 | -3.26 | -1.89 |
| UAV nadir elevation (m) | LiDAR elevation (m) | 1.99* | 0.29 | 0.00 | 1.31 | 2.67 |
| | UAV oblique elevation (m) | -0.59 | 0.29 | 0.11 | -1.27 | 0.10 |
| UAV oblique elevation (m) | LiDAR elevation (m) | 2.58* | 0.29 | 0.00 | 1.89 | 3.26 |
| | UAV nadir elevation (m) | 0.59 | 0.29 | 0.11 | -0.10 | 1.27 |

* The mean difference is significant at the 0.05 level.

*One-way ANOVA test result of elevation (medium dense canopy block)*

| SUMMARY | | | | |
|---|---|---|---|---|
| *Groups* | *Count* | *Sum* | *Average* | *Variance* |
| **LiDAR elevation (m)** | 100 | 5008.41 | 50.08 | 0.34 |
| **UAV nadir elevation (m)** | 100 | 5031.66 | 50.32 | 0.41 |
| **UAV oblique elevation (m)** | 100 | 5041.40 | 50.41 | 0.45 |
| ANOVA | | | | |
| *Source of Variation* | *SS* | *df* | *MS* | *F* | *P-value* | *F crit* |
| **Between Groups** | 5.75 | 2 | 2.87 | 7.15 | 0.00 | 3.03 |
| **Within Groups** | 119.37 | 297 | 0.40 | | | |
| **Total** | 125.12 | 299 | | | | |

*Tucky HSD post hoc test of elevation (medium dense canopy block)*

| Multiple Comparisons | | Mean Difference | Std. Error | Sig. | 95% Confidence Interval | |
|---|---|---|---|---|---|---|
| | | | | | Lower Bound | Upper Bound |
| **LiDAR elevation (m)** | UAV nadir elevation (m) | -0.23* | 0.09 | 0.03 | -0.44 | -0.02 |
| | UAV oblique elevation (m) | -0.33* | 0.09 | 0.00 | -0.54 | -0.12 |
| **UAV nadir elevation (m)** | LiDAR elevation (m) | 0.23* | 0.09 | 0.03 | 0.02 | 0.44 |
| | UAV oblique elevation (m) | -0.10 | 0.09 | 0.52 | -0.31 | 0.11 |
| **UAV oblique elevation (m)** | LiDAR elevation (m) | -0.33* | 0.09 | 0.00 | 0.12 | 0.54 |
| | UAV nadir elevation (m) | 0.10 | 0.09 | 0.52 | -0.11 | 0.31 |

* The mean difference is significant at the 0.05 level.

Appendix 7: Histogram of tree heights in dense canopy block from different LiDAR, UAV nadir, and UAV oblique CHMs
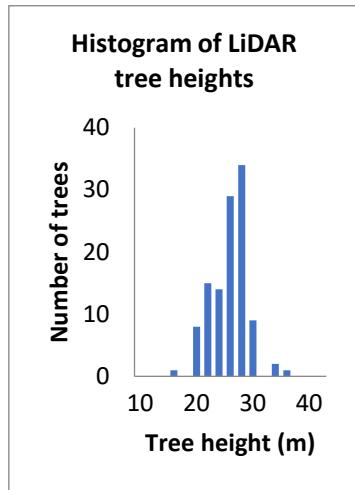


a) Histogram of tree heights from LiDAR CHM$_{50cm}$
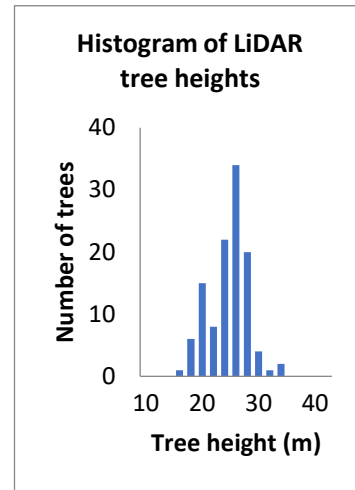
b) Histogram of tree heights from LiDAR CHM$_{1m}$
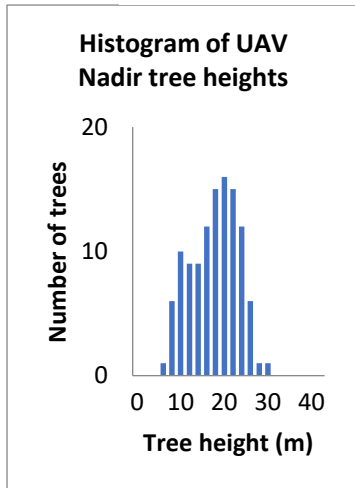
c) Histogram of tree heights from UAV nadir CHM$_{22cm}$
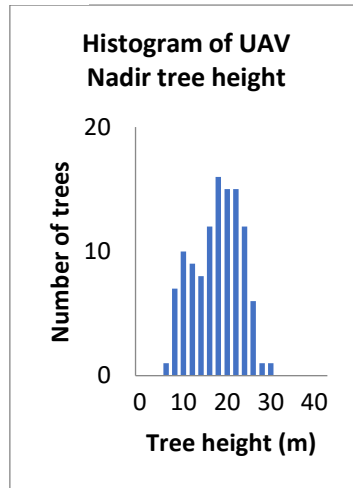
d) Histogram of tree heights from UAV nadir CHM$_{50cm}$
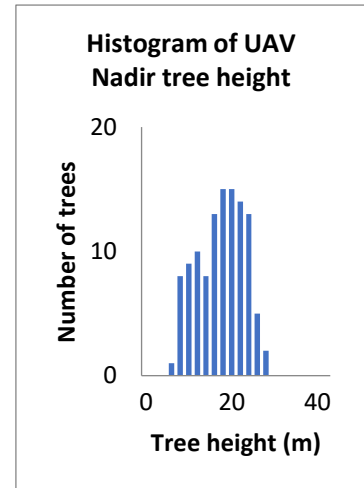
e) Histogram of tree heights from UAV nadir CHM$_{1m}$
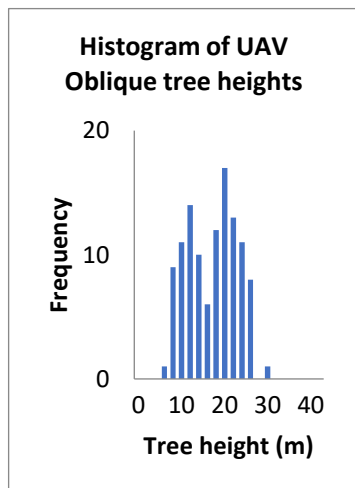
f) Histogram of tree heights from UAV oblique CHM$_{22cm}$
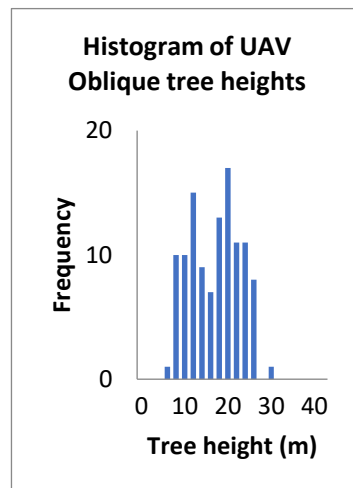
g) Histogram of tree heights from UAV oblique CHM$_{50cm}$
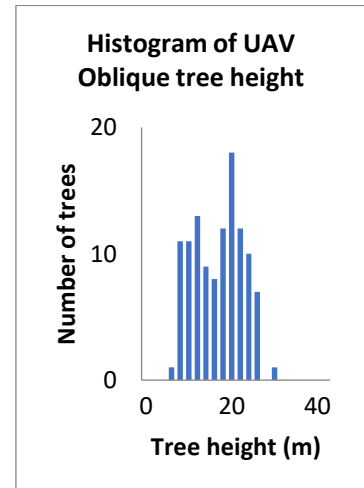
h) Histogram of tree heights from UAV oblique CHM$_{1m}$

Appendix 8: Histogram of tree heights in medium dense canopy block from different LiDAR, UAV nadir, and UAV oblique CHMs



a) Histogram of tree heights from LiDAR CHM$_{50cm}$
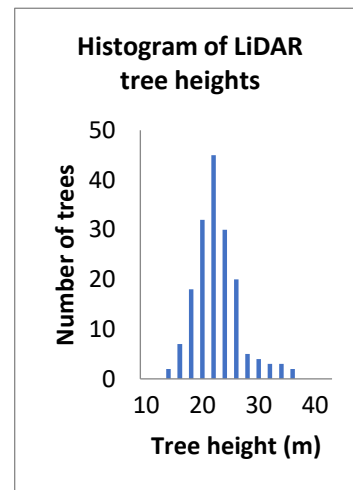
b) Histogram of tree heights from LiDAR CHM$_{1m}$
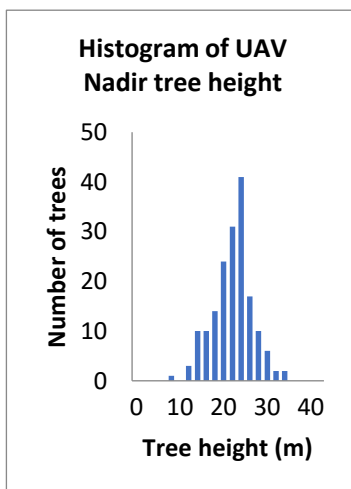
c) Histogram of tree heights from UAV nadir CHM$_{22cm}$
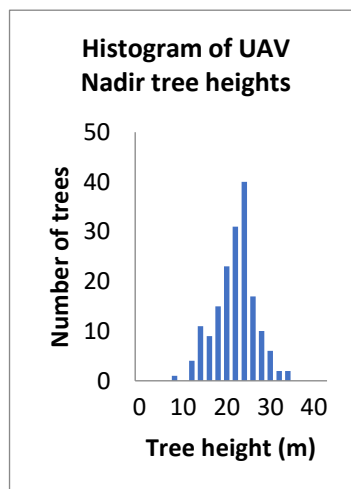
d) Histogram of tree heights from UAV nadir CHM$_{50cm}$
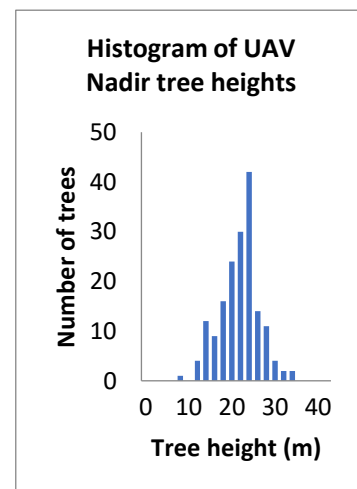
e) Histogram of tree heights from UAV nadir CHM$_{1m}$
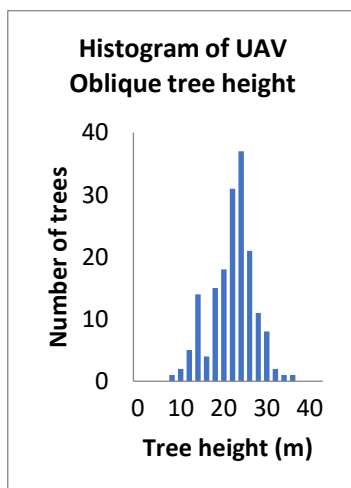
f) Histogram of tree heights from UAV oblique CHM$_{22cm}$

g) Histogram of tree heights from UAV oblique CHM$_{50cm}$
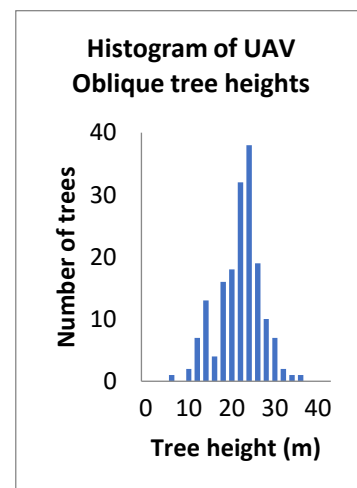
h) Histogram of tree heights from UAV oblique CHM$_{1m}$

Appendix 9: One-way ANOVA and Tucky HSD results of comparison between the means of tree heights from UAV nadir $CHM_{22cm}$, UAV oblique $CHM_{22cm}$, and LiDAR $CHM_{50cm}$ in different canopy density blocks

*One-way ANOVA test result of tree heights (dense canopy block)*

**SUMMARY**

| Groups | Count | Sum | Average | Variance | |
|---|---|---|---|---|---|
| **LiDAR TH (m)** | 113 | 2807.58 | 24.85 | 10.48 | |
| **UAV nadir TH (m)** | 113 | 1895.78 | 16.78 | 28.62 | |
| **UAV oblique TH (m)** | 113 | 1825.57 | 16.16 | 32.59 | |

**ANOVA**

| Source of Variation | SS | df | MS | F | P-value | F crit |
|---|---|---|---|---|---|---|
| **Between Groups** | 5311.64 | 2 | 2655.82 | 111.14 | 0.00 | 3.02 |
| **Within Groups** | 8029.03 | 336 | 23.90 | | | |
| **Total** | 13340.67 | 338 | | | | |

*Tucky HSD post hoc test of tree heights (dense canopy block)*

| Multiple Comparisons | | Mean Difference | Std. Error | Sig. | 95% Confidence Interval | |
|---|---|---|---|---|---|---|
| | | | | | Lower Bound | Upper Bound |
| **LiDAR TH (m)** | UAV nadir TH (m) | 8.07* | 0.65 | 0.00 | 6.54 | 9.60 |
| | UAV oblique TH (m) | 8.69* | 0.65 | 0.00 | 7.16 | 10.22 |
| **UAV nadir TH (m)** | LiDAR TH (m) | -8.07* | 0.65 | 0.00 | -9.60 | -6.54 |
| | UAV oblique TH (m) | 0.62 | 0.65 | 0.61 | -0.91 | 2.15 |
| **UAV oblique TH (m)** | LiDAR TH (m) | -8.69* | 0.65 | 0.00 | -10.22 | -7.16 |
| | UAV nadir TH (m) | -0.62 | 0.65 | 0.61 | -2.15 | 0.91 |

* The mean difference is significant at the 0.05 level.

*One-way ANOVA test result of tree heights (medium dense canopy block)*

**SUMMARY**

| Groups | Count | Sum | Average | Variance | |
|---|---|---|---|---|---|
| **LiDAR TH (m)** | 171 | 3926.55 | 22.96 | 15.27 | |
| **UAV nadir TH (m)** | 171 | 3587.92 | 20.98 | 20.60 | |
| **UAV oblique TH (m)** | 171 | 3621.75 | 21.18 | 23.68 | |

**ANOVA**

| Source of Variation | SS | df | MS | F | P-value | F crit |
|---|---|---|---|---|---|---|
| **Between Groups** | 406.86 | 2 | 203.43 | 10.25 | 0.00 | 3.01 |
| **Within Groups** | 10123.87 | 510 | 19.85 | | | |
| **Total** | 10530.73 | 512 | | | | |

*Tucky HSD post hoc test of tree heights (medium dense canopy block)*

| Multiple Comparisons | | Mean Difference | Std. Error | Sig. | 95% Confidence Interval | |
|---|---|---|---|---|---|---|
| | | | | | Lower Bound | Upper Bound |
| **LiDAR TH (m)** | UAV nadir TH (m) | 1.98* | 0.48 | 0.00 | 0.85 | 3.11 |
| | UAV oblique TH (m) | 1.78* | 0.48 | 0.00 | 0.65 | 2.92 |
| **UAV nadir TH (m)** | LiDAR TH (m) | -1.98* | 0.48 | 0.00 | -3.11 | -0.85 |
| | UAV oblique TH (m) | -0.20 | 0.48 | 0.91 | -1.33 | 0.93 |
| **UAV oblique TH (m)** | LiDAR TH (m) | -1.78* | 0.48 | 0.00 | -2.92 | -0.65 |
| | UAV nadir TH (m) | 0.20 | 0.48 | 0.91 | -0.93 | 1.33 |

* The mean difference is significant at the 0.05 level.

*Tucky HSD post hoc test of tree heights (medium dense canopy block)*

Appendix 10: One-way ANOVA and Tucky HSD results of comparison between the means of tree heights from UAV nadir $CHM_{50cm}$, UAV oblique $CHM_{50cm}$, and LiDAR $CHM_{50cm}$ in different canopy density blocks

*One-way ANOVA test result of tree heights (dense canopy block)*

**SUMMARY**

| Groups | Count | Sum | Average | Variance | | |
|---|---|---|---|---|---|---|
| **LiDAR TH (m)** | 113 | 2807.58 | 24.85 | 10.48 | | |
| **UAV nadir TH (m)** | 113 | 1881.87 | 16.65 | 29.20 | | |
| **UAV oblique TH (m)** | 113 | 1813.36 | 16.05 | 32.73 | | |

**ANOVA**

| Source of Variation | SS | df | MS | F | P-value | F crit |
|---|---|---|---|---|---|---|
| **Between Groups** | 5457.52 | 2 | 2728.76 | 113.06 | 0.00 | 3.02 |
| **Within Groups** | 8109.39 | 336 | 24.14 | | | |
| **Total** | 13566.92 | 338 | | | | |

*Tucky HSD post hoc test of tree heights (dense canopy block)*

| Multiple Comparisons | | Mean Difference | Std. Error | Sig. | 95% Confidence Interval | |
|---|---|---|---|---|---|---|
| | | | | | Lower Bound | Upper Bound |
| **LiDAR TH (m)** | UAV nadir TH (m) | 8.19* | 0.65 | 0.00 | 6.65 | 9.73 |
| | UAV oblique TH (m) | 8.80* | 0.65 | 0.00 | 7.26 | 10.34 |
| **UAV nadir TH (m)** | LiDAR TH (m) | -8.19* | 0.65 | 0.00 | -9.73 | -6.65 |
| | UAV oblique TH (m) | 0.61 | 0.65 | 0.62 | -0.93 | 2.14 |
| **UAV oblique TH (m)** | LiDAR TH (m) | -8.80* | 0.65 | 0.00 | -10.34 | -7.26 |
| | UAV nadir TH (m) | -0.61 | 0.65 | 0.62 | -2.14 | 0.93 |

* The mean difference is significant at the 0.05 level.

*One-way ANOVA test result of tree heights (medium dense canopy block)*

**SUMMARY**

| Groups | Count | Sum | Average | Variance | | |
|---|---|---|---|---|---|---|
| **LiDAR TH (m)** | 171 | 3926.55 | 22.96 | 15.27 | | |
| **UAV nadir TH (m)** | 171 | 3579.94 | 20.94 | 20.65 | | |
| **UAV oblique TH (m)** | 171 | 3613.06 | 21.13 | 23.76 | | |

**ANOVA**

| Source of Variation | SS | df | MS | F | P-value | F crit |
|---|---|---|---|---|---|---|
| **Between Groups** | 427.89 | 2 | 213.95 | 10.76 | 0.00 | 3.01 |
| **Within Groups** | 10143.73 | 510 | 19.89 | | | |
| **Total** | 10571.62 | 512 | | | | |

*Tucky HSD post hoc test of tree heights (medium dense canopy block)*

| Multiple Comparisons | | Mean Difference | Std. Error | Sig. | 95% Confidence Interval | |
|---|---|---|---|---|---|---|
| | | | | | Lower Bound | Upper Bound |
| **LiDAR TH (m)** | UAV nadir TH (m) | 2.03* | 0.48 | 0.00 | 0.89 | 3.16 |
| | UAV oblique TH (m) | 1.83* | 0.48 | 0.00 | 0.70 | 2.97 |
| **UAV nadir TH (m)** | LiDAR TH (m) | -2.03* | 0.48 | 0.00 | -3.16 | -0.89 |
| | UAV oblique TH (m) | -0.19 | 0.48 | 0.92 | -1.33 | 0.94 |
| **UAV oblique TH (m)** | LiDAR TH (m) | -1.83* | 0.48 | 0.00 | -2.97 | -0.70 |
| | UAV nadir TH (m) | 0.19 | 0.48 | 0.92 | -0.94 | 1.33 |

* The mean difference is significant at the 0.05 level.

Appendix 11: One-way ANOVA and Tucky HSD results of comparison between the means of tree heights from UAV nadir CHM$_{1m}$, UAV oblique CHM$_{1m}$, and LiDAR CHM$_{1m}$ in different canopy density blocks

*One-way ANOVA test result of tree heights (dense canopy block)*

**SUMMARY**

| Groups | Count | Sum | Average | Variance | |
|---|---|---|---|---|---|
| **LiDAR TH (m)** | 113 | 2675.59 | 23.68 | 11.97 | |
| **UAV nadir TH (m)** | 113 | 1869.07 | 16.54 | 28.93 | |
| **UAV oblique TH (m)** | 113 | 1795.15 | 15.89 | 32.59 | |

**ANOVA**

| Source of Variation | SS | df | MS | F | P-value | F crit |
|---|---|---|---|---|---|---|
| **Between Groups** | 4221.60 | 2 | 2110.80 | 86.16 | 0.00 | 3.02 |
| **Within Groups** | 8231.10 | 336 | 24.50 | | | |
| **Total** | 12452.70 | 338 | | | | |

*Tucky HSD post hoc test of tree heights (dense canopy block)*

| Multiple Comparisons | | Mean Difference | Std. Error | Sig. | 95% Confidence Interval | |
|---|---|---|---|---|---|---|
| | | | | | Lower Bound | Upper Bound |
| **LiDAR TH (m)** | UAV nadir TH (m) | 7.14* | 0.66 | 0.00 | 5.59 | 8.69 |
| | UAV oblique TH (m) | 7.79* | 0.66 | 0.00 | 6.24 | 9.34 |
| **UAV nadir TH (m)** | LiDAR TH (m) | -7.14* | 0.66 | 0.00 | -8.69 | -5.59 |
| | UAV oblique TH (m) | 0.65 | 0.66 | 0.58 | -0.90 | 2.20 |
| **UAV oblique TH (m)** | LiDAR TH (m) | -7.79* | 0.66 | 0.00 | -9.34 | -6.24 |
| | UAV nadir TH (m) | -0.65 | 0.66 | 0.58 | -2.20 | 0.90 |

* The mean difference is significant at the 0.05 level.

*One-way ANOVA test result of tree heights (medium dense canopy block)*

**SUMMARY**

| Groups | Count | Sum | Average | Variance | |
|---|---|---|---|---|---|
| **LiDAR TH (m)** | 171 | 3691.86 | 21.59 | 15.84 | |
| **UAV nadir TH (m)** | 171 | 3548.21 | 20.75 | 20.85 | |
| **UAV oblique TH (m)** | 171 | 3580.31 | 20.94 | 24.20 | |

**ANOVA**

| Source of Variation | SS | df | MS | F | P-value | F crit |
|---|---|---|---|---|---|---|
| **Between Groups** | 66.49 | 2 | 33.24 | 1.64 | 0.20 | 3.01 |
| **Within Groups** | 10353.03 | 510 | 20.30 | | | |
| **Total** | 10419.52 | 512 | | | | |

Appendix 12: Summary of different models used for DBH predictions in dense and medium dense canopy blocks. (UAV Nadir based parameters)

*DBH model development using parameters from UAV nadir datasets (dense canopy block)*

| Predictor (X) | Model | Equation | R2 | RMSE |
|---|---|---|---|---|
| **CPA** | Linear | $y = 0.3703x + 28.825$ | 0.52 | 11.68 |
| | Logarithmic | $y = 15.144\ln(x) - 8.0131$ | 0.50 | 11.89 |
| | Quadratic | $y = -0.0009x^2 + 0.4805x + 26.519$ | 0.52 | 11.64 |
| | Power | $y = 11.878x^{0.36}$ | 0.52 | 11.68 |
| **CD** | Linear | $y = 9.1869x + 12.757$ | 0.53 | 11.56 |
| | Logarithmic | $y = 30.288\ln(x) + 9.3229$ | 0.50 | 22.12 |
| | Quadratic | $y = 0.2605x^2 + 7.1826x + 16.155$ | 0.53 | 11.55 |
| | Power | $y = 17.935x^{0.7199}$ | 0.52 | 11.68 |
| **TH** | Linear | $y = 1.7199x + 18.423$ | 0.32 | 13.88 |
| | Logarithmic | $y = 25.021\ln(x) - 21.621$ | 0.33 | 13.75 |
| | Quadratic | $y = -0.0921x^2 + 4.6542x - 2.0861$ | 0.34 | 14.23 |
| | Power | $y = 8.2228x^{0.6108}$ | 0.33 | 13.92 |
| **CD*TH** | Linear | $y = 0.3418x + 24.33$ | 0.53 | 11.48 |
| | Logarithmic | $y = 16.991\ln(x) - 20.847$ | 0.50 | 11.84 |
| | **Quadratic** | **$y = -0.0011x^2 + 0.4978x + 20.057$** | **0.54** | **11.36** |
| | Power | $y = 8.5864x^{0.4087}$ | 0.53 | 11.56 |

*DBH model development using parameters from UAV nadir datasets (medium dense canopy block)*

| Predictor (X) | Model | Equation | R2 | RMSE |
|---|---|---|---|---|
| **CPA** | Linear | $y = 0.6402x + 21.139$ | 0.71 | 4.60 |
| | Logarithmic | $y = 13.771\ln(x) - 5.3202$ | 0.70 | 4.68 |
| | Quadratic | $y = -0.0049x^2 + 0.9183x + 18.238$ | 0.71 | 4.53 |
| | Power | $y = 10.585x^{0.3978}$ | 0.72 | 4.53 |
| **CD** | Linear | $y = 11.132x + 6.8908$ | 0.72 | 4.50 |
| | Logarithmic | $y = 27.541\ln(x) + 10.444$ | 0.70 | 4.68 |
| | Quadratic | $y = 0.3187x^2 + 9.4058x + 9.0598$ | 0.72 | 4.50 |
| | Power | $y = 16.689x^{0.7955}$ | 0.72 | 4.53 |
| **TH** | Linear | $y = 1.5619x - 0.2863$ | 0.47 | 6.16 |
| | Logarithmic | $y = 30.364\ln(x) - 59.388$ | 0.42 | 6.44 |
| | Quadratic | $y = 0.0588x^2 - 0.9822x + 26.428$ | 0.50 | 6.00 |
| | Power | $y = 2.0986x^{0.8955}$ | 0.47 | 6.25 |
| **CD*TH** | Linear | $y = 0.3522x + 14.911$ | 0.79 | 3.87 |
| | Logarithmic | $y = 19.755\ln(x) - 43.382$ | 0.77 | 4.03 |
| | **Quadratic** | **$y = -0.0013x^2 + 0.5241x + 9.9775$** | **0.80** | **3.77** |
| | Power | $y = 3.4675x^{0.5749}$ | 0.79 | 3.80 |

Appendix 13: Summary of different models used for DBH predictions in dense and medium dense canopy blocks. (UAV Oblique based parameters)

*DBH model development using parameters from UAV oblique datasets (dense canopy block)*

| Predictor (X) | Model | Equation | R2 | RMSE |
|---|---|---|---|---|
| **CPA** | Linear | $y = 0.3637x + 28.73$ | 0.51 | 11.73 |
| | Logarithmic | $y = 15.761\ln(x) - 10.842$ | 0.50 | 11.87 |
| | **Quadratic** | **$y = -0.0011x^2 + 0.5066x + 25.62$** | **0.52** | **11.57** |
| | Power | $y = 11.155x^{0.3734}$ | 0.52 | 11.69 |
| **CD** | Linear | $y = 9.2313x + 12.106$ | 0.52 | 11.59 |
| | Logarithmic | $y = 31.522\ln(x) + 7.2004$ | 0.50 | 11.87 |
| | Quadratic | $y = 0.1568x^2 + 7.9982x + 14.257$ | 0.52 | 11.58 |
| | Power | $y = 17.105x^{0.7469}$ | 0.52 | 11.70 |
| **TH** | Linear | $y = 1.4854x + 23.131$ | 0.27 | 14.31 |
| | Logarithmic | $y = 20.02\ln(x) - 6.8414$ | 0.27 | 14.30 |
| | Quadratic | $y = -0.0663x^2 + 3.5054x + 10.144$ | 0.29 | 14.18 |
| | Power | $y = 11.89x^{0.4857}$ | 0.28 | 14.42 |
| **CD*TH** | Linear | $y = 0.3266x + 25.733$ | 0.50 | 11.82 |
| | Logarithmic | $y = 16.062\ln(x) - 16.626$ | 0.47 | 12.17 |
| | Quadratic | $y = -0.0006x^2 + 0.4112x + 23.532$ | 0.51 | 11.79 |
| | Power | $y = 9.5632x^{0.3848}$ | 0.50 | 11.96 |

*DBH model development using parameters from UAV oblique datasets (medium dense canopy block)*

| Predictor (X) | Model | Equation | R2 | RMSE |
|---|---|---|---|---|
| **CPA** | Linear | $y = 0.632x + 20.685$ | 0.67 | 4.86 |
| | Logarithmic | $y = 13.36\ln(x) - 4.9173$ | 0.65 | 4.99 |
| | Quadratic | $y = -0.0034x2 + 0.8203x + 18.681$ | 0.67 | 4.83 |
| | Power | $y = 10.513x0.3924$ | 0.67 | 4.84 |
| **CD** | Linear | $y = 10.89x + 6.7556$ | 0.68 | 4.81 |
| | Logarithmic | $y = 26.721\ln(x) + 10.377$ | 0.65 | 4.99 |
| | Quadratic | $y = 0.5781x2 + 7.777x + 10.671$ | 0.68 | 4.80 |
| | Power | $y = 16.473x0.7847$ | 0.67 | 4.85 |
| **TH** | Linear | $y = 1.3959x + 2.8671$ | 0.42 | 6.45 |
| | Logarithmic | $y = 26.07\ln(x) - 46.583$ | 0.36 | 6.76 |
| | Quadratic | $y = 0.0697x2 - 1.5824x + 33.61$ | 0.47 | 6.20 |
| | Power | $y = 3.0135x0.774$ | 0.38 | 6.59 |
| **CD*TH** | Linear | $y = 0.3484x + 14.399$ | 0.77 | 4.09 |
| | Logarithmic | $y = 18.957\ln(x) - 41.032$ | 0.73 | 4.42 |
| | **Quadratic** | **$y = -0.0005x2 + 0.4151x + 12.494$** | **0.77** | **4.08** |
| | Power | $y = 3.6083x0.559$ | 0.75 | 4.14 |

Appendix 14: One-way ANOVA results of comparison between the means of DBH modeled using UAV nadir based tree parameters, UAV based tree parameter, and field measured DBH

*One-way ANOVA test result of DBH (dense canopy block)*

**SUMMARY**

| Groups | Count | Sum | Average | Variance | |
|---|---|---|---|---|---|
| **Field DBH (cm)** | 40 | 1807.30 | 45.18 | 260.96 | |
| **UAV nadir DBH (cm)** | 40 | 2062.32 | 51.56 | 337.68 | |
| **UAV oblique DBH (cm)** | 40 | 1857.74 | 46.44 | 158.79 | |

**ANOVA**

| *Source of Variation* | *SS* | *df* | *MS* | *F* | *P-value* | *F crit* |
|---|---|---|---|---|---|---|
| **Between Groups** | 911.90 | 2 | 455.95 | 1.81 | 0.17 | 3.07 |
| **Within Groups** | 29539.89 | 117 | 252.48 | | | |
| **Total** | 30451.79 | 119 | | | | |

*One-way ANOVA test result of DBH (medium dense canopy block)*

**SUMMARY**

| Groups | Count | Sum | Average | Variance | |
|---|---|---|---|---|---|
| **Field DBH (cm)** | 58 | 2059.60 | 35.51 | 110.54 | |
| **UAV nadir DBH (cm)** | 58 | 2033.38 | 35.06 | 79.22 | |
| **UAV oblique DBH (cm)** | 58 | 2049.44 | 35.34 | 83.55 | |

**ANOVA**

| *Source of Variation* | *SS* | *df* | *MS* | *F* | *P-value* | *F crit* |
|---|---|---|---|---|---|---|
| **Between Groups** | 6.03 | 2 | 3.01 | 0.03 | 0.97 | 3.05 |
| **Within Groups** | 15578.71 | 171 | 91.10 | | | |
| **Total** | 15584.73 | 173 | | | | |

Appendix 15: One-way ANOVA and Tucky HSD results comparing the means of AGB calculated using LiDAR-based, UAV nadir-based, and UAV oblique-based tree heights in different canopy density blocks

*One-way ANOVA test result of AGB (dense canopy block)*

**SUMMARY**

| Groups | Count | Sum | Average | Variance |
|---|---|---|---|---|
| **LiDAR AGB (Mg/tree)** | 113 | 228.89 | 2.03 | 2.29 |
| **UAV nadir AGB (Mg/tree)** | 113 | 169.36 | 1.50 | 1.56 |
| **UAV oblique AGB (Mg/tree)** | 113 | 164.30 | 1.45 | 1.56 |

**ANOVA**

| Source of Variation | SS | df | MS | F | P-value | F crit |
|---|---|---|---|---|---|---|
| **Between Groups** | 22.83 | 2 | 11.42 | 6.33 | 0.00 | 3.02 |
| **Within Groups** | 605.70 | 336 | 1.80 | | | |
| **Total** | 628.53 | 338 | | | | |

*Tucky HSD post hoc test of AGB (dense canopy block)*

| Multiple Comparisons | | Mean Difference | Std. Error | Sig. | 95% Confidence Interval | |
|---|---|---|---|---|---|---|
| | | | | | Lower Bound | Upper Bound |
| **LiDAR AGB (Mg/tree)** | UAV nadir AGB (Mg/tree) | 0.53* | 0.18 | 0.01 | 0.11 | 0.95 |
| | UAV oblique AGB (Mg/tree) | 0.57* | 0.18 | 0.00 | 0.15 | 0.99 |
| **UAV nadir AGB (Mg/tree)** | LiDAR AGB (Mg/tree) | -0.53* | 0.18 | 0.01 | -0.95 | -0.11 |
| | UAV AGB (Mg/tree) | 0.04 | 0.18 | 0.97 | -0.38 | 0.47 |
| **UAV oblique AGB (Mg/tree)** | LiDAR AGB (Mg/tree) | -0.57* | 0.18 | 0.00 | -0.99 | -0.15 |
| | UAV nadir AGB (Mg/tree) | -0.04 | 0.18 | 0.97 | -0.47 | 0.38 |

* The mean difference is significant at the 0.05 level.

*One-way ANOVA test result of AGB (medium dense canopy block)*

**SUMMARY**

| Groups | Count | Sum | Average | Variance |
|---|---|---|---|---|
| **LiDAR based (Mg/tree)** | 171 | 173.54 | 1.01 | 0.55 |
| **UAV nadir based (Mg/tree)** | 171 | 160.91 | 0.94 | 0.47 |
| **UAV oblique based (Mg/tree)** | 171 | 162.02 | 0.95 | 0.48 |

**ANOVA**

| Source of Variation | SS | df | MS | F | P-value | F crit |
|---|---|---|---|---|---|---|
| **Between Groups** | 0.57 | 2 | 0.29 | 0.57 | 0.56 | 3.01 |
| **Within Groups** | 253.87 | 510 | 0.50 | | | |
| **Total** | 254.45 | 512 | | | | |

Appendix 16: The variation in biomass of the 30 selected trees in dense and medium dense canopy block due to the errors in tree height is shown

*In the Graphs, the trees are arranged in increasing order of DBH
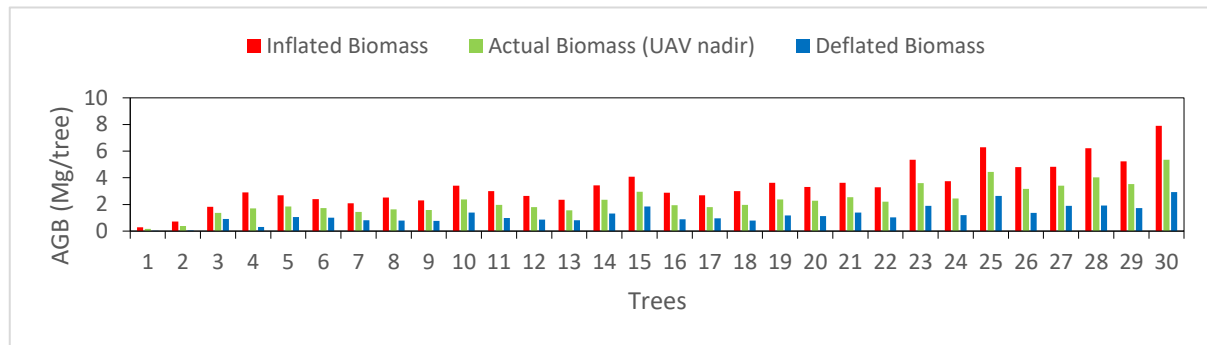


a) Comparison of AGB estimated from inflated, deflated and actual UAV nadir tree heights
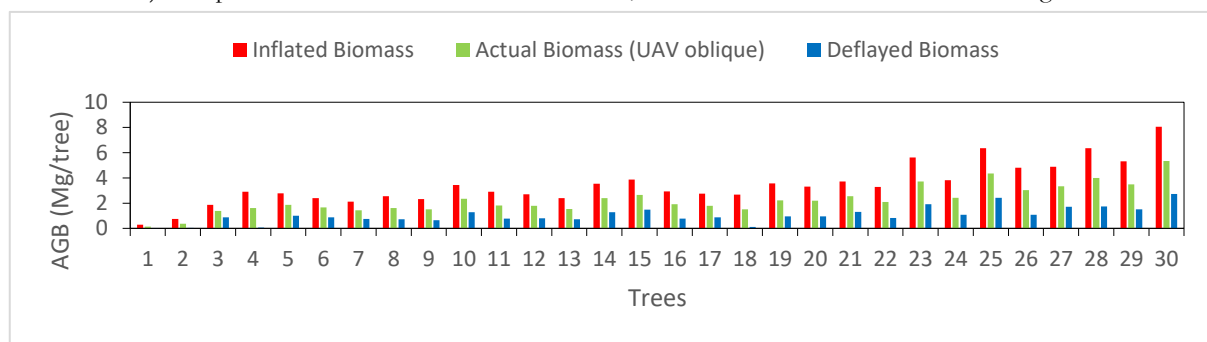


b) Comparison of AGB estimated from inflated, deflated and actual UAV oblique tree heights

**Comparison of variation in AGB due to errors in tree height estimation (dense canopy block)**
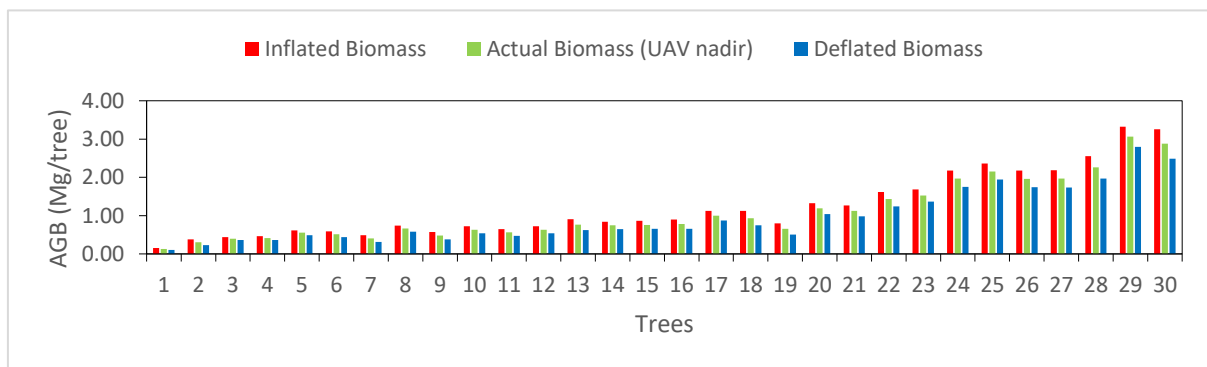


a) Comparison of AGB estimated from inflated, deflated and actual UAV nadir tree heights
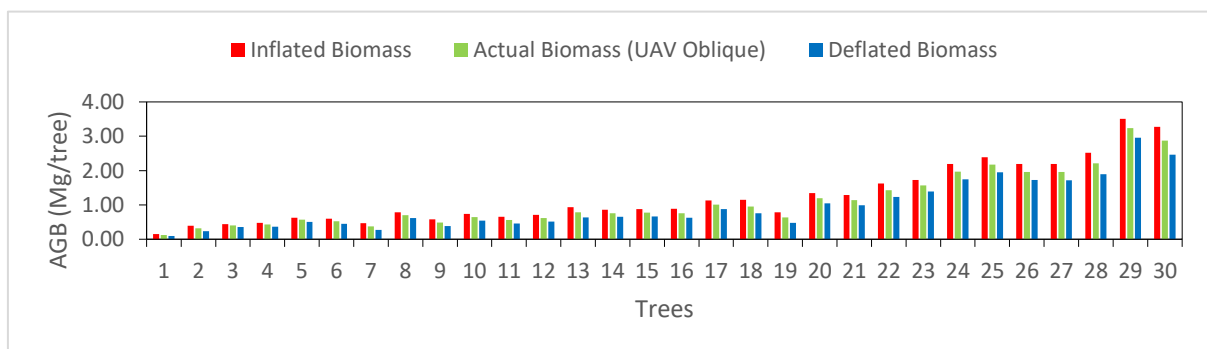


b) Comparison of AGB estimated from inflated, deflated and actual UAV oblique tree heights

**Comparison of variation in AGB due to errors in tree height estimation (medium dense canopy**

Appendix 17: One-way ANOVA and Tucky HSD results comparing the means of selected 30 trees AGB calculated using inflated and deflated UAV nadir-based, and UAV oblique-based tree heights in different canopy density blocks

*One-way ANOVA test result of UAV Nadir AGB (dense canopy block)*

| SUMMARY | | | | | | |
|---|---|---|---|---|---|---|
| *Groups* | *Count* | *Sum* | *Average* | *Variance* | | |
| **LiDAR reference based AGB (Mg/tree)** | 30 | 96.79 | 3.23 | 2.44 | | |
| **Inflated UAV nadir AGB (Mg/tree)** | 30 | 103.44 | 3.45 | 2.62 | | |
| **Deflated UAV nadir AGB (Mg/tree)** | 30 | 35.85 | 1.20 | 0.42 | | |
| **UAV nadir AGB (Mg/tree)** | 30 | 69.89 | 2.33 | 1.23 | | |
| ANOVA | | | | | | |
| *Source of Variation* | *SS* | *df* | *MS* | *F* | *P-value* | *F crit* |
| **Between Groups** | 94.44 | 3 | 31.48 | 18.75 | 0.00 | 2.68 |
| **Within Groups** | 194.73 | 116 | 1.68 | | | |
| **Total** | 289.17 | 119 | | | | |

*Tucky HSD post hoc test of UAV Nadir AGB (dense canopy block)*

| **Multiple Comparisons** | | **Mean Difference** | **Std. Error** | **Sig.** | **95% Confidence Interval** | |
|---|---|---|---|---|---|---|
| | | | | | **Lower Bound** | **Upper Bound** |
| **LiDAR reference based AGB (Mg/tree)** | Inflated UAV nadir AGB (Mg/tree) | -0.22 | 0.33 | 0.91 | -1.09 | 0.65 |
| | Deflated UAV nadir AGB (Mg/tree) | 2.03* | 0.33 | 0.00 | 1.16 | 2.90 |
| | UAV nadir AGB (Mg/tree) | 0.90* | 0.33 | 0.04 | 0.02 | 1.77 |
| **Inflated UAV nadir AGB (Mg/tree)** | LiDAR reference based AGB (Mg/tree) | 0.22 | 0.33 | 0.91 | -0.65 | 1.09 |
| | Deflated UAV nadir AGB (Mg/tree) | 2.25* | 0.33 | 0.00 | 1.38 | 3.12 |
| | UAV nadir AGB (Mg/tree) | 1.12* | 0.33 | 0.01 | 0.25 | 1.99 |
| **Deflated UAV nadir AGB (Mg/tree)** | LiDAR reference based AGB (Mg/tree) | -2.03* | 0.33 | 0.00 | -2.90 | -1.16 |
| | Inflated UAV nadir AGB (Mg/tree) | -2.25* | 0.33 | 0.00 | -3.12 | -1.38 |
| | UAV nadir AGB (Mg/tree) | -1.13* | 0.33 | 0.01 | -2.01 | -0.26 |

| UAV nadir AGB (Mg/tree) | LiDAR reference based AGB (Mg/tree) | -0.90* | 0.33 | 0.04 | -1.77 | -0.02 |
| | Inflated UAV nadir AGB (Mg/tree) | -1.12* | 0.33 | 0.01 | -1.99 | -0.25 |
| | Deflated UAV nadir AGB (Mg/tree) | 1.13* | 0.33 | 0.01 | 0.26 | 2.01 |

* The mean difference is significant at the 0.05 level.

*One-way ANOVA test result of UAV Oblique AGB (dense canopy block)*

**SUMMARY**

| Groups | Count | Sum | Average | Variance |
|---|---|---|---|---|
| **LiDAR reference based AGB (Mg/tree)** | 30 | 96.79 | 3.23 | 2.44 |
| **Inflated UAV oblique AGB (Mg/tree)** | 30 | 104.24 | 3.47 | 2.74 |
| **Deflated UAV oblique AGB (Mg/tree)** | 30 | 31.26 | 1.04 | 0.40 |
| **UAV oblique AGB (Mg/tree)** | 30 | 68.13 | 2.27 | 1.24 |

**ANOVA**

| Source of Variation | SS | df | MS | F | P-value | F crit |
|---|---|---|---|---|---|---|
| **Between Groups** | 109.69 | 3 | 36.56 | 21.44 | 0.00 | 2.68 |
| **Within Groups** | 197.85 | 116 | 1.71 | | | |
| **Total** | 307.54 | 119 | | | | |

*Tucky HSD post hoc test of UAV oblique AGB (dense canopy block)*

| Multiple Comparisons | | Mean Difference | Std. Error | Sig. | 95% Confidence Interval | |
|---|---|---|---|---|---|---|
| | | | | | Lower Bound | Upper Bound |
| **LiDAR reference based AGB (Mg/tree)** | Inflated UAV nadir AGB (Mg/tree) | -0.25 | 0.34 | 0.88 | -1.13 | 0.63 |
| | Deflated UAV nadir AGB (Mg/tree) | 2.18* | 0.34 | 0.00 | 1.31 | 3.06 |
| | UAV nadir AGB (Mg/tree) | 0.96* | 0.34 | 0.03 | 0.08 | 1.83 |
| **Inflated UAV nadir AGB (Mg/tree)** | LiDAR reference based AGB (Mg/tree) | 0.25 | 0.34 | 0.88 | -0.63 | 1.13 |
| | Deflated UAV nadir AGB (Mg/tree) | 2.43* | 0.34 | 0.00 | 1.55 | 3.31 |
| | UAV nadir AGB (Mg/tree) | 1.20* | 0.34 | 0.00 | 0.32 | 2.08 |

| | | | | | | |
|---|---|---|---|---|---|---|
| **Deflated UAV nadir AGB (Mg/tree)** | LiDAR reference based AGB (Mg/tree) | -2.18* | 0.34 | 0.00 | -3.06 | -1.31 |
| | Inflated UAV nadir AGB (Mg/tree) | -2.43* | 0.34 | 0.00 | -3.31 | -1.55 |
| | UAV nadir AGB (Mg/tree) | -1.23* | 0.34 | 0.00 | -2.11 | -0.35 |
| **UAV nadir AGB (Mg/tree)** | LiDAR reference based AGB (Mg/tree) | -0.96* | 0.34 | 0.03 | -1.83 | -0.08 |
| | Inflated UAV nadir AGB (Mg/tree) | -1.20* | 0.34 | 0.00 | -2.08 | -0.32 |
| | Deflated UAV nadir AGB (Mg/tree) | 1.23* | 0.34 | 0.00 | 0.35 | 2.11 |

* The mean difference is significant at the 0.05 level.

*One-way ANOVA test result of UAV Nadir AGB (medium dense canopy block)*

| **SUMMARY** | | | | | | |
|---|---|---|---|---|---|---|
| *Groups* | *Count* | *Sum* | *Average* | *Variance* | | |
| **LiDAR reference based AGB (Mg/tree)** | 30 | 35.41 | 1.18 | 0.74 | | |
| **Inflated UAV nadir AGB (Mg/tree)** | 30 | 37.01 | 1.23 | 0.73 | | |
| **Deflated UAV nadir AGB (Mg/tree)** | 30 | 28.58 | 0.95 | 0.50 | | |
| **UAV nadir AGB (Mg/tree)** | 30 | 32.85 | 1.09 | 0.61 | | |
| **ANOVA** | | | | | | |
| *Source of Variation* | *SS* | *df* | *MS* | *F* | *P-value* | *F crit* |
| **Between Groups** | 1.35 | 3 | 0.45 | 0.70 | 0.55 | 2.68 |
| **Within Groups** | 74.76 | 116 | 0.64 | | | |
| **Total** | 76.12 | 119 | | | | |

*One-way ANOVA test result of UAV Oblique AGB (medium dense canopy block)*

| SUMMARY | | | | | |
|---|---|---|---|---|---|
| *Groups* | *Count* | *Sum* | *Average* | *Variance* | |
| **LiDAR reference-based AGB (Mg/tree)** | 30 | 35.41 | 1.18 | 0.74 | |
| **Inflated UAV oblique AGB (Mg/tree)** | 30 | 37.53 | 1.25 | 0.76 | |
| **Deflated UAV oblique AGB (Mg/tree)** | 30 | 28.59 | 0.95 | 0.51 | |
| **UAV oblique AGB (Mg/tree)** | 30 | 33.11 | 1.10 | 0.63 | |

| ANOVA | | | | | | |
|---|---|---|---|---|---|---|
| *Source of Variation* | *SS* | *df* | *MS* | *F* | *P-value* | *F crit* |
| **Between Groups** | 1.47 | 3 | 0.49 | 0.74 | 0.53 | 2.68 |
| **Within Groups** | 76.58 | 116 | 0.66 | | | |
| **Total** | 78.05 | 119 | | | | |

Appendix 18: F-test for Variance and t-Test (equal variance) comparing means of CPA from UAV nadir and oblique orthophoto in different canopy densities

*F-Test Two-Sample for Variance*

| | Medium dense canopy | | Dense canopy | |
|---|---|---|---|---|
| | *Nadir CPA* | *Oblique CPA* | *Nadir CPA* | *Oblique CPA* |
| **Mean** | 20.30 | 21.43 | 49.12 | 50.52 |
| **Variance** | 152.74 | 158.27 | 1088.71 | 1159.18 |
| **Observations** | 144 | 144 | 100 | 100 |
| **df** | 143 | 143 | 99 | 99 |
| **F** | 0.97 | | 0.94 | |
| **P(F<=f) one-tail** | 0.42 | | 0.38 | |
| **F Critical one-tail** | 0.76 | | 0.72 | |

t-Test (equal variance)

| | Medium dense canopy | | Dense canopy | |
|---|---|---|---|---|
| | *Nadir CPA* | *Oblique CPA* | *Nadir CPA* | *Oblique CPA* |
| **Mean** | 20.30 | 21.43 | 49.12 | 50.52 |
| **Variance** | 152.74 | 158.27 | 1088.71 | 1159.18 |
| **Observations** | 144 | 144 | 100 | 100 |
| **Pooled Variance** | 155.50 | | 1123.94 | |
| **Hypothesized Mean Difference** | 0 | | 0 | |
| **df** | 286 | | 198 | |
| **t Stat** | -0.77 | | -0.29 | |
| **P(T<=t) one-tail** | 0.22 | | 0.38 | |
| **t Critical one-tail** | 1.65 | | 1.65 | |
| **P(T<=t) two-tail** | 0.44 | | 0.77 | |
| **t Critical two-tail** | 1.97 | | 1.97 | |